Nicotinic Acetylcholine Receptor Chimaer

Sebastian Kračun

A thesis presented for the degree of Doctor of Philosophy to the University London

January 2008

Department of Pharmacology
UCL
London
WC1E 6BT

ProQuest LLC
789 East Eisenhower Parkway
P.O. Box 1346
Ann Arbor, MI 48106-1346

Molecular and Functional Characterisation of Nicotinic Acetylcholine Receptor Chimaeras

I, **Sebastian Kračun,** confirm that the work presented in this thesis is my own. Where information has been derived from other sources, I confirm that this has been indicated in the thesis.

Signature

Date

7.04.08

Abstract

Nicotinic acetylcholine receptors (nAChRs) are ligand-gated ion channels which exhibit considerable subunit diversity. They have been implicated in processes including synaptic transmission and modulation of neurotransmitter release. They also have a significant role in several pathological disorders as well as nicotine addiction, which makes nAChRs important targets for therapeutic drug discovery.

One of the aims of this study was to investigate the influence of the intracellular domain of nAChR subunits upon receptor assembly, targeting and functional properties. A series of subunit chimaeras was constructed, each containing the intracellular loop region, located between transmembrane (TM) domains M3 and M4, from nAChR subunits α1-α10 or β1-β4 and from the 5-hydroxytryptamine type 3 receptor (5-HT_3R) subunits 3A and 3B. Evidence has been obtained which demonstrates that the large intracellular loop exerts a significant influence upon the levels of both cell-surface and intracellular assembled receptors. Comparisons of functional ion-channel properties revealed a significant influence upon both single-channel conductance and receptor desensitisation. Experiments conducted in polarised epithelial cells demonstrate that the nAChR loop can also influence receptor targeting.

In a further study, the influence of the recently identified nAChR molecular chaperone, RIC-3 (*r*esistance to *i*nhibitors of *c*holinesterase), on receptor maturation was investigated. The influence of subunit domains upon the RIC-3's chaperone activity was investigated by co-expression with subunit chimaeras.

Finally, α9/5-HT_{3A} and α10/5-HT_{3A} subunit chimeras were used to investigate the pharmacological properties of α9α10 nAChRs, a receptor subtype expressed in hair cells of the auditory system. Physiologically relevant concentrations of the anti-malarial compounds, quinine, quinidine and chloroquine were shown to act as competitive inhibitors, whereas the NMDA receptor antagonist, neramexane, blocked α9α10 nAChR mediated responses via a non-competitive mechanism.

Acknowledgements

First of all I would like to thank Professor Neil Millar, for allowing me to conduct my PhD research, on the humble nicotinic acetylcholine receptor, in his wonderful laboratory. I was very lucky to have been supplied with what can only be described as ample bench and office space; the latter which doubled as an all important sandwich preparation area. For these 'laboratory comforts' I am truly grateful. More importantly, Neil has supported me throughout all stages of my PhD, allowing me independence and guidance whenever needed. In particular, I would like to thank him for helping me cope with the final stages of the production of this treatise. Thank you Neil! Huge thanks must also go to Dr Alasdair Gibb, the best secondary supervisor I could have hoped for and the least pessimistic electrophysiologist I know (a rare breed indeed). Without Ali's help much of Chapter 4 would not exist. Thank you for letting me loose on your 'rig', which I was able to use as my own for a particularly long time.

To the rest of the Millar Lab – what a joy it was to work with you all and I hope to always keep your friendship. Dr Stuart Lansdell, I am grateful to you for helping me when my molecular biology knowledge couldn't cope on its own, for never getting angry and for always supplying an alternative viewpoint on matters not only always work related – oh and just so you have it in writing, thank you for the

tea! Patricia 'The Oracle' Harkness, I am so very glad you were in the lab. Thank you for helping me with cell culture and antibodies during my PhD, thank you for being my human PubMed and thank you immensely for thinking ahead for me during those times when I could not. Gareth Young, you almost beat me to it! Cheers for the good times, the many late nights at work – and not at work – for trying to get me fit and, of course, for quite literally being my right-hand-man and one half of the 'gay-photo' duo. To all the other members of the lab, both past and present: Liz Baker, Anne Doward, Ronnie Gee and Toby Collins, – you were all great to work with and thank you all for putting up with me. Special thanks go to Ronnie for starting me off on the 'loop project' all those many moons ago.

I am grateful to the Wellcome Trust for funding my research and keeping a roof over my head in expensive London town. Thank you also to Dr Belén Elgoyhen for two collaborations that resulted in my first published data. A very deserved and special thank you goes to Tony Langford, the best lab-manager-person money can't buy. Certainly, work life would have been a much more disordered affair without your watchful eye. Thank you for your common-sense approach to the dreaded 'health and safety' side of lab life, for taking care of all my last-minute orders, for making sure the building didn't collapse and for providing me with one of the best quotes I will take away with me from my PhD; "*If you leave anything open to misinterpretation, it WILL be misinterpreted.*"

I thank the wonderful 'UCL8', who were quite simply the best group of individuals to embark on this PhD with. An extra mention must go to two of the UCL8, namely Isaac Bianco and Tiago Branco, who were brilliant flatmates for four years. I thank Isaac for being a great queen to my king during our stay in 'The Palace' and Tiago for introducing me to Portugal on so many fine occasions. I am grateful to all those in the Pharmacology Department at UCL, who made it such a wonderful place to work, learn and have fun in. Although the name will disappear, my memory of those who were a part of the department will not.

A big thank you to my parents who have always supported me in all that I have decided to do. Thanks for being patient with me for so many years. I'm not a student anymore! Thanks to my brother Benjamin, who helped a homeless when things got a little hairy.

A very, very special thank you goes to a wonderful Annette. Meine liebe Schnecke, danke, dass Du mich so oft besucht hast und immer an mich geglaubt hast, obwohl ich der grösste Meckeronkel bin. Du wirst für immer einen speziellen Platz in meinem Herzen haben.

Finally, thanks to absolutely everyone who came to one of my ceilidhs.

Publications

Some of the results presented in this thesis have been reported in the following publications:

Ballestero, J.A., Plazas, P.V., Kracun, S., Gómez-Casati, M.E., Taranda, J., Rothlin, C.V., Katz, E., Millar, N.S. and Elgoyhen, A.B. (**2005**) Effects of quinine, quinidine and chloroquine on α9α10 nicotinic cholinergic receptors. *Molecular Pharmacology* 68, 822-829.

Plazas, P.V., Savino, J., Kracun, S., Gomez-Casati, M.E., Katz, E., Parsons, C.G., Millar, N.S. and Elgoyhen, A.B. (**2007**) Inhibition of the α9α10 nicotinic cholinergic receptor by neramexane, an open channel blocker of *N*-methyl-D-aspartate receptors. *European Journal of Pharmacology* 566, 11-19.

Gee, V.G., Kracun, S., Cooper, S.T., Gibb, A.J. and Millar, N.S. (**2007**) Identification of domains influencing assembly and ion channel properties in α7 nicotinic receptor and 5-HT_3 receptor subunit chimaeras. *British Journal of Pharmacology*. 152, 501-512.

Kracun, S., Harkness, P.C., Gibb, A.J. and Millar N.S. (**2008**) Influence of M3-M4 intracellular domain upon nicotinic acetylcholine receptor assembly, targeting and function. *British Journal of Pharmacology*. 153, 1474-1484.

Contents

Figures and tables

Abbreviations

5-HT	5-hydroxytryptamine
$5\text{-HT}_3\text{R}$	5-hydroxytryptamine type 3 receptor
5-HT_{3A}	'A' subunit of the 5-hydroxytryptamine type 3 receptor
$5\text{-HT}_{3B,C...}$	'B', 'C'... subunit of the 5-hydroxytryptamine type 3 receptor
Ab	antibody
αBTX	alpha bungarotoxin
AC	alternating current
AChBP	acetylcholine binding protein
AChE	acetylcholine esterase
Alexa 488-BTX	Alexa 488-conjugated α-bungarotoxin
Arg	arginine
Asn	asparagine
Asp	aspartate
BiP	immunoglobulin binding protein
BSA	bovine serum albumin
cDNA	complimentary deoxyribonucleic acid
C-terminal	carboxy (COOH) terminal
Cys	cysteine

DC	direct current
DMEM	Dulbecco's modified Eagles' medium
DMPP	1,1-dimethyl-4-phenylpiperazinium
DMSO	dimethylsulphoxide
dNTPs	deoxynucleotide triphosphates
DTT	dithiothreitol
E18	embryonic day 18
EC_{50}	median effective concentration
EDTA	ethylenediaminetetraacetic acid
EGFP	enhanced green fluorescent protein
ER	endoplasmic reticulum
FCS	foetal calf serum
FITC	fluoroscein isothiocynate
FLIPR	fluorescence imaging plate reader
Fluo-4	Fluorescent Calcium indicator 4
GABA	gamma-aminobutyric acid
$GABA_AR$	gamma-aminobutyric acid type A receptor
$GABA_BR$	gamma-aminobutyric acid type B receptor
Glu	glutamate
HA	haemagglutinin epitope
HBSS	Hanks' buffered saline solution
$HBSS^{++}$	Hanks' buffered saline solution with 25 μM $MgCl_2$ and 25μM $CaCl_2$

HEPES	4-(2-hydroxyethyl)-1-piperazine-ethane-sulphonic acid
HEK	human embryonic kidney
HEK-293	HEK cell line 293
i	single-channel current
I	mean current
Ig	immunoglobulin
Ile	isoleucine
kDa	kilodalton
LB broth	Luria-Bertani Broth
Leu	leucine
M1/M2/M3/M4	transmembrane domains 1/2/3/4
MA-helix	membrane associated amphipathic α-helix
MDCK	Madin-Darby canine kidney
MLA	methyllycaconitine
MOPS	3-N-morpholinopropanesulphonic acid
mRNA	messenger ribonucleic acid
MQ	milli-Q
NAc	nucleus accumbens
nAChR	nicotinic acetylcholine receptor
NCB-20	murine neuroblastoma/Chinese hamster embryonic brain cell hybrid
NEM	*N*-ethylmaleimide
NMDA	N-methyl-D-aspartate

N-terminal	amino (NH_2) terminal
p	open channel probability
PBS	phosphate buffered saline
PCR	polymerase chain reaction
PEI	polyethylenimine
PFA	paraformaldehyde
Phe	phenylalanine
PLL	poly-L-Lysine
PMSF	phenylmethylsulphonyl fluoride
Poly-A	poly-adenylation
Pro	proline
pS	picosiemens
Rd-BTX	rhodamine-conjugated α-bungarotoxin
RIC-3	resistant to inhibitors of cholinesterase protein 3
rpm	revolutions per minute
σ^2_I	current variance (or standard deviation squared)
S	Svedberg unit of sedimentation coefficient
SDM	site-directed mutagenesis
SDS	sodium dodecyl sulphate
SDS-PAGE	SDS polyacrylamide gel electrophoresis
Ser	serine
SV40	simian virus 40
T-antigen	tumour antigen protein

τ_1	time constant 1
τ_2	time constant 2
τ_w	weighted mean time constant
TAE	tris-acetate with EDTA
Tet	tetracyline
Trp	tryptophan
tsA201	HEK-293 subclone (stably transfected with SV40 large T-antigen)
Tyr	tyrosine
Val	valine
VTA	ventral tegmental area

Chapter 1

Introduction

Chapter 1

Introduction

1.1 Discovery of the nicotinic acetylcholine receptor – a brief history

"I shall never bend this bow again."

These were reported as the last words of a native South American Indian, looking at his bow, immediately after accidentally shooting himself with a poison-tipped arrow while hunting (Waterton, 1879). The poison in question was 'curare', which causes death through rapid muscle paralysis leading to asphyxiation. Various South American tribes have for centuries prepared curare-containing mixtures from the vine-like plants *Strychnos toxifera, Chondrodendron tomentosum* and related species. The preparation of curare was first described by the naturalist and explorer Alexander von Humboldt (von Humboldt and Bonpland, 1807), although explorers to the New World had reported the use and deadly effects of poisoned arrows as early as the 16th century (Raleigh, 1596).

During the mid 19th century, Claude Bernard undertook a detailed scientific study of curare on samples returned to Europe and was able to determine that the poison interrupted signalling between a nerve and the striated muscle it innervated, while leaving smooth and cardiac muscle unaffected. He found that after curare-induced paralysis of a frog, the muscles could be induced to contract by direct electrical stimulation, but not through stimulation of the associated nerves (Bernard, 1850). While Bernard thought that the nerve terminal was 'paralysed' by curare, it was Arthur Vulpian who later determined that curare acted on, what he described as an 'intermediate zone' between the nerve terminal and the muscle (Vulpian, 1866), at the motor endplate region, whose morphology had by then recently been described (Kühne, 1863). Later, John Langley demonstrated using denervated muscle that curare acted on what he coined a 'receptive substance' associated with the muscle, as opposed to the nerve or the 'fundamental substance' of the muscle itself. Langley also worked with the alkaloid nicotine (from the *Solanaceae* family of plants), and discovered that both curare and nicotine acted as mutual antagonists of each other's effects on muscle contraction; nicotine stimulating (at low concentrations), and curare blocking (Langley, 1905). Around this time the immunologist Paul Erlich independently developed his 'lock and key' hypothesis to describe the action of toxins on the 'receptive side chains' of cells. Taken together with Langley's studies, and the theory of chemical transmission first proposed by Du Bois-Reymond (du Bois-Reymond, 1877), the concept of 'chemical transmitters' and 'receptors' emerged (Langley, 1906). Henry Dale later identified acetylcholine as a possible candidate molecule for a

chemical transmitter and described how the alkaloids muscarine and nicotine mimicked the effects of acetylcholine on smooth and striated muscle, respectively (Dale, 1914), which could be blocked by atropine and (+)-tubocurarine (the active component of curare), respectively. However, it was not until Otto Loewi's famously simple and elegant experiment on the autonomic innervation of two isolated beating frog hearts, that the idea of chemical transmission was decisively demonstrated (Loewi, 1921). Loewi named the chemical transmitter released upon electrical stimulation of the vagus nerve '*Vagusstoff*' (vagus substance) and demonstrated that, when transferred to a second denervated and isolated heart, it elicited the same response as observed in the donor heart – specifically, a reduction in contraction. *Vagusstoff* was later identified to be acetylcholine (Dale and Feldberg, 1934), and was also shown to be the endogenous chemical transmitter released by motor neurones innervating voluntary striated muscle, leading to muscle contraction (Dale *et al.*, 1936).

Soon after acetylcholine had been identified as the transmitter at the neuromuscular junction, the cholinergic nature of transmission in the electric organ (electroplaque tissue) of the marine ray *Torpedo marmorata* was established (Feldberg *et al.*, 1939). This tissue, embryonically derived from myoblasts, is common to all electric fish (including the electric eel, *Electrophorus electricus*). It produces an electrical discharge, in order to stun prey and deter predators, which can be blocked by the action of curare. The rich cholinergic innervation of post-synaptic membranes found in these electric organs made them

an ideal source from which to isolate and purify the acetylcholine receptor in sufficient quantities to enable further biochemical, pharmacological and structural studies. This was greatly facilitated by the discovery of the acetylcholine receptor ligand, α-bungarotoxin, which binds to the receptor practically irreversibly and with high affinity. This toxin was first isolated from the snake venom of the Formosan banded krait, *Bungarus multicinctus,* based on its ability to cause a block of neurotransmission in a manner qualitatively similar to curare poisoning (Chang and Lee, 1963). Indeed, (+)-tubocurarine protects against the blocking action of α-bungarotoxin, indicating that both compounds bind to the same site of the acetylcholine receptor found at the motor endplate (Lee and Chang, 1966).

The potent and highly selective α-bungarotoxin was used to isolate large quantities of the nicotinic acetylcholine receptor protein (Langley's "receptive substance"), from the electric organs of the electric eel, *Electrophorus electricus* (Changeux *et al.*, 1970), and the electric ray, *Torpedo marmorata* (Miledi *et al.*, 1971). The abundant source of pure receptor protein, which could now readily be studied, soon established the nicotinic acetylcholine receptor, as the prototypic ligand-gated ion channel.

It is interesting to note, as a brief aside, that during his 1799-1804 exploration of the Americas, Alexander von Humboldt encountered, and for the first time studied in detail, the anatomy and behaviour of the electric eel, *Electrophorous electricus* (von Humboldt, 1808). As discussed above, it was on the very same trip that he

also described the preparation and effects of the poison curare (von Humboldt and Bonpland, 1807). It is unlikely that he could ever have imagined that both would come together again in the future, so crucially, in isolating the nicotinic acetylcholine receptor and, as a result, encourage the many related advances in physiology and medicine that have occurred since.

1.2 The neurotransmitter acetylcholine (ACh) and its receptors

1.2.1 Acetylcholine and cholinergic transmission

Acetylcholine was the first neurotransmitter to be described (Dale, 1914), and is perhaps the best characterised neurotransmitter to date. Acetylcholine is a low-molecular weight (146.2 g/mol) chemical transmitter synthesised in neurones by the enzyme choline acetyltransferase from the compounds choline and acetyl coenzyme A. Neurones containing the enzyme choline acetyltransferase are typically termed cholinergic neurones and regulate neural transmission, through the release of ACh, in the central and peripheral nervous systems (CNS and PNS, respectively). ACh is rapidly broken down by the enzyme acetylcholine esterase, which is found in the synaptic clefts of cholinergic synapses and limits the size and duration of the postsynaptic potential.

1.2.2 Nicotinic and muscarinic acetylcholine receptors

As described above (Section 1.1), the neurotransmitter ACh acts on two main receptor subtypes which have been pharmacologically subdivided into 'nicotinic' AChRs (nAChRs) and 'muscarinic' AChRs (mAChRs); so classified due to the acetylcholine-mimicking effects of the alkaloids nicotine (from the *Solanaceae* plant family), and muscarine (first isolated from the mushroom *Amanita muscaria*), respectively. Despite a common activation by acetylcholine, both types of receptor are structurally distinct and are not closely related. The nAChRs are referred to as 'ionotropic' receptors which form an ion channel in the cell membrane and belong to the superfamily of ligand-gated ion channels (LGICs) known as Cys-loop receptors (Ortells and Lunt, 1995; Sine and Engel, 2006). The mAChRs are referred to as 'metabotropic' receptors and belong to the family of seven-transmembrane G-protein coupled receptors (GPCRs), which mediate their effects via heterotrimeric GTP-binding proteins (G-proteins; Ishii and Kurachi, 2006).

1.3 The nicotinic acetylcholine receptor (nAChR)

1.3.1 The Cys-loop superfamily of ligand gated ion channels

The nAChRs belong to a sub-family of LGICs known as Cys-loop receptors, which are characterised by a conserved Cys-loop signature motif, consisting of two disulphide-bonded cysteines separated by 13 residues within the amino (N)-terminal domain of all members of this family. The Cys-loop family of receptors includes 5-hydroxytryptamine (or serotonin) type 3 (5-HT_3) receptors, γ-aminobutyric acid type A ($GABA_A$) and type C ($GABA_C$) receptors, glycine receptors, and some invertebrate glutamate and histidine receptors (Karlin, 2002; Connolly and Wafford, 2004; Millar, 2006). All members of the Cys-loop family are thought to possess a similar structural architecture consisting of five homologous subunits arranged in a ring to form a central ion-permeable pore (Figure 1.1). Individual subunits are composed of three structurally distinct domains: a large extracellular N-terminal domain, primarily made up of β-pleated sheets, four α-helical transmembrane spanning domains (M1, M2, M3 and M4), and a large, structurally ill-defined, intracellular loop of variable length between M3 and M4 (Figure 1.1). While nAChRs and 5-HT_3Rs are cation permeable, mediating excitatory transmission, the other members of this group are anion permeable and mediate inhibitory transmission. Comparison of the nucleotide sequence of genes within the Cys-loop family of ligand-gated ion channel

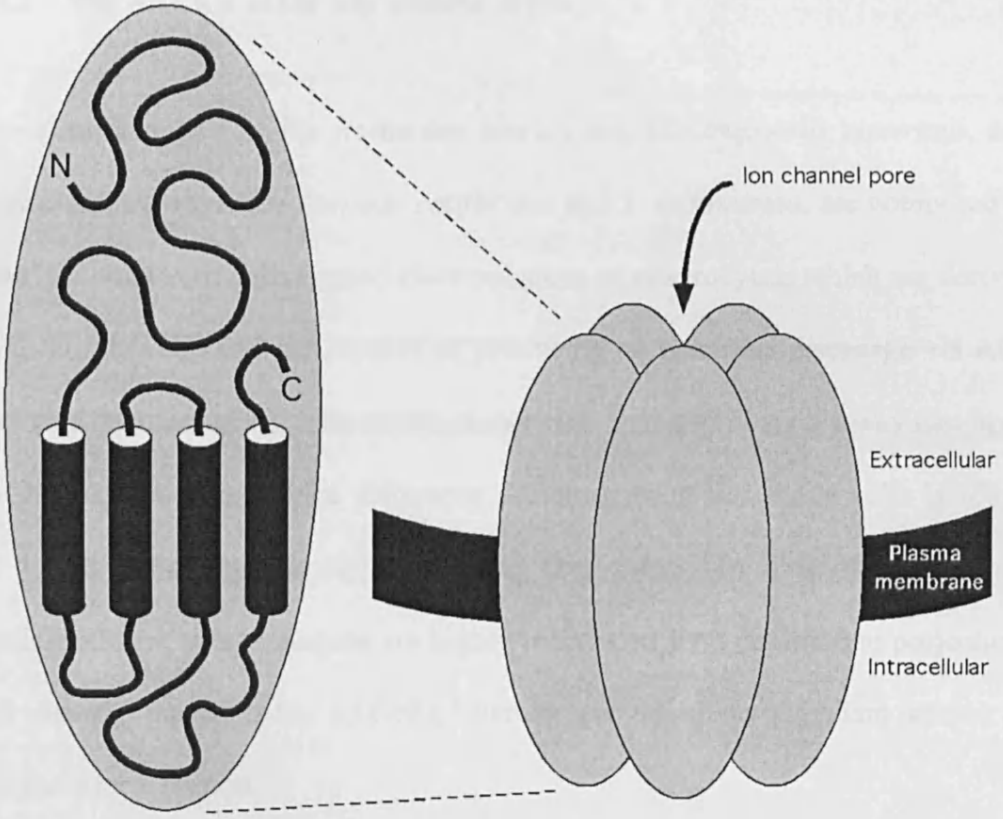

Figure 1.1 The predicted membrane topology of a Cys-loop receptor subunit and the pentameric structure of an assembled receptor. Schematic representation of the membrane topology of a subunit from the Cys-loop family of receptors (left panel), showing three distinct subunit domains: The large extracellular N-terminal domain, the four transmembrane domains (M1-M4, represented by black cylinders) and the variable length M3-M4 intracellular loop domain. The subunits are arranged in a pentamer (right panel), forming a central ion-permeable channel through the plasma membrane, allowing ions to pass from the extracellular side of the membrane to the intracellular side. The channel can conduct both cations and anions depending on the particular Cys-loop family receptor subtype in question (e.g. nAChRs and $GABA_A$Rs, respectively). Diagram reproduced with permission (Millar, 2003).

suggests that all the members originate from a common ancestral gene (Ortells and Lunt, 1995).

1.3.2 The nAChR of the fish electric organ

The electric organs of the freshwater electric eel, *Electrophorus electricus*, and marine electric rays like *Torpedo californica* and *T. marmorata*, are composed of rows or columns of cells termed electroplaques or electrocytes, which are derived from muscle cells and are capable of producing an electrical discharge via ACh mediated depolarisation. The electroplaques are arranged in such a way that upon nAChR activation a voltage difference accumulates across many cells enabling the fish to discharge enough current to stun prey. In order to fulfil their specialised role, electroplaques are highly innervated with cholinergic projections and densely packed with nAChRs, thereby providing an abundant source of receptors for isolation.

The elapid snake toxin α-bungarotoxin (αBTX), isolated from the venom of the Formosan banded krait *Bungarus multicinctus* (Chang and Lee, 1963), is a potent nicotinic receptor antagonist and was used to isolate and purify nAChRs from *Electrophorus electricus* (Changeux *et al.*, 1970). The αBTX protein is a polypeptide of 74 amino acids with a molecular weight of around 8000 Da. It consists primarily of β-sheet secondary structure and contains five disulphide bonds (Love and Stroud, 1986). The specific high affinity binding of αBTX to the

nAChR has been exploited extensively in the characterisation of the receptor and has helped to reveal many of its biochemical and pharmacological properties.

The nAChR of the fish electric organ is an integral membrane-spanning glycoprotein composed of five homologous subunits (Brisson and Unwin, 1985). The receptor can exist as a pentameric monomer of ~250 kDa and a disulphide-linked dimer of ~500 kDa, which migrate on a sucrose gradient with sedimentation coefficients of 9 S and 13 S, respectively (Gibson *et al.*, 1976; Reynolds and Karlin, 1978). The pentameric nAChR is composed of four types of subunits termed α, β, γ and δ, which were named according to their increasing apparent molecular weight of approximately 40 kDa, 48 kDa, 62 kDa and 66 kDa, respectively, as determined by SDS-PAGE of purified nAChR preparations from *Torpedo* (Hucho *et al.*, 1976). The four subunits are arranged with a stoichiometry of $\alpha_2\beta\gamma\delta$, and combine to form a ring-like structure around an axis perpendicular to the plane of the membrane, creating a central ion-conducting channel pore (Unwin, 1993).

1.3.3 The nAChR of the vertebrate neuromuscular junction

The nAChR of the vertebrate neuromuscular junction (NMJ) is, to date, one of the best characterised LGICs as regards structure and function. Electrophysiological properties such as channel gating, conductance and desensitisation have been well defined (Peper *et al.*, 1982; Sakmann and Neher, 1984; Colquhoun and Ogden, 1988). Action potentials reaching the motor nerve endings stimulate the release

of acetylcholine from the pre-synaptic membrane; these then diffuse about 50 nm across the synaptic cleft to the post-synaptic membrane. Acetylcholine in the synaptic cleft rapidly reaches concentrations in the range of 0.1-1.0 mM (Katz and Miledi, 1977). At the post-synaptic membrane two molecules of acetylcholine bind per nAChR (Adams, 1981), causing a conformational change within the receptor, allowing cations (principally sodium, but also potassium and calcium) to flow through the ion-channel pore and across the plasma membrane. The resulting depolarisation of the muscle cell results in the eventual contraction of the muscle fibre. The entire process, from activation of the motor neuron to muscle fibre contraction, occurs in less than 100 μs (Adams, 1981; Peper *et al.*, 1982). Activation of nAChRs is terminated within a few milliseconds through the natural diffusion of ACh which is then rapidly hydrolysed by acetylcholine esterase (Katz and Miledi, 1977).

It became clear that the nAChR located at the cholinergic synapse of the vertebrate neuromuscular junction was structurally related to the nAChR of the fish electric organ. In both systems, nerve transmission is blocked by the action of antagonists such as (+)-tubocurarine and αBTX. The purified mammalian muscle nAChR was found to sediment with a similar buoyant density to the nAChR from the electric organ and consist of four subunit components (Froehner *et al.*, 1977). Monoclonal antibodies raised against individual *Torpedo* nAChR subunits crossreact with mammalian muscle nAChR subunits and injection of any one of the four *Torpedo* nAChR subunits can elicit an auto-immune response in

rats against their own nAChRs (Lindstrom *et al.*, 1978; Lindstrom *et al.*, 1979). From sequence similarity, it is clear that the nAChR of the vertebrate NMJ and that of the electric fish have high structural similarity (Section 1.4). Through molecular cloning techniques (Section 1.3.7), an additional γ-like subunit (termed ε) has been identified in vertebrate muscle (Takai *et al.*, 1985) which is not present in the fish electric organ nAChR.

The nAChR in mammalian muscle exists as one of two homogeneous receptor populations, each type expressed according to the developmental stage of the animal. Both species of receptor share common α, β and δ subunits, but the γ subunit is only expressed in embryonic (and denervated) muscle and is later replaced, in a developmental switch, for the ε subunit found in adult muscle. Electrophysiological analysis of recombinant nAChRs containing α, β, γ and δ subunits expressed in *Xenopus laevis* oocytes, revealed conductance estimates (~39 pS) resembling those typical of foetal muscle; while *Xenopus* oocytes expressing α, β, δ and ε subunits formed nAChR channels with conductance estimates (~59 pS) more closely resembling the channels found at the adult NMJ (Mishina *et al.*, 1986).

1.3.4 Neuronal nAChRs

The neurotoxin αBTX, in addition to binding to the muscle nAChR, also exhibits high-affinity binding in the CNS and PNS (Greene *et al.*, 1973; Hunt and Schmidt, 1978). However, unlike the situation at the neuromuscular junction,

αBTX binding and blockade of nicotine-mediated synaptic transmission in nervous tissue are not strongly coupled events (Quik and Geertsen, 1988). It was found that in a number of cases, αBTX was unable to block nicotine-mediated transmission in vertebrate neurones and radiolabeled αBTX only partially co-localised with nicotine binding sites (Clarke *et al.*, 1985; Schuetze and Role, 1987). Antiserum raised against the nAChR of *Electrophorus electricus* was shown to block responses elicited by nicotine from the rat phaeochromocytoma (PC-12) cell line, but failed to precipitate the αBTX-binding component (Patrick and Stallcup, 1977a; Patrick and Stallcup, 1977b). In contrast αBTX does effectively block nicotine-evoked responses in vertebrate neurones (Marshall, 1981). It was thus suggested that two classes of receptors structurally homologous to the nAChR in muscle and electric fish exist in the nervous system; those that are αBTX sensitive and those that are αBTX insensitive (McGehee and Role, 1995).

Molecular cloning techniques have identified twelve vertebrate neuronal nAChRs. These have been grouped into the 'α-type' neuronal nAChR subunits (α2-α10), and the 'non α-type' neuronal nAChR subunits (β1-β4). The α subunits are so defined because they share a pair of conserved adjacent cysteine residues (equivalent to positions 192 and 193 of the *Torpedo* α subunit), which make up part of the agonist-binding site. The β subunits lack these conserved residues. Interestingly, the α8 subunit has been discovered only in chick (Schoepfer *et al.*, 1990), and appears to have no mammalian homologue. Unlike the homogeneous

receptor population of their muscle-type counterparts, neuronal nAChRs exist as a diverse group of receptors, drawing on a much larger repertoire of subunits with which to make up the receptor complex (Le Novère *et al.*, 2002; Millar, 2003).

Neuronal nAChRs exist as homomeric complexes made up of five identical subunits (e.g. α7), or as heteromeric complexes containing two or more types of subunit (e.g. α4β2 and α4α5β2). Not all subunits can co-assemble with each other to generate functional receptors, but there appears to be extensive diversity in subunit composition of neuronal nAChRs (Le Novère *et al.*, 2002; Millar, 2003).

1.3.5 Cloning of nAChRs

Soon after the first isolation and purification of nAChRs from the electric organs of the fish, *Electrophorus electricus* and *Torpedo marmorata* (Changeux *et al.*, 1970 and Miledi *et al.*, 1971, respectively), the first 54-56 amino acids from each of the purified polypeptides comprising the isolated protein complex were determined by protein sequencing (Raftery *et al.*, 1980). Using this amino acid sequence information, the first nAChR genes (encoding the subunits α, β, γ and δ) were identified and cloned from the electric organ of *Torpedo californica* and their primary structure deduced (Noda *et al.*, 1982; Noda *et al.*, 1983a; Noda *et al.*, 1983b). The cloning of the *Torpedo* nAChR subunits rapidly led to the identification of other nAChR subunits. Seventeen vertebrate nAChR subunits

have been cloned and characterised (α1-α10, β1-β4, γ, δ and ε). As described above, the α1, β1, γ and δ subunits comprise the nAChR which is found in denervated or embryonic muscle and the electric organs of fish. In the adult neuromuscular junction, the γ subunit is replaced by the ε subunit. These subunits are referred to as 'muscle-type' nAChRs (Section 1.3.3). The remaining subunits make up the 'neuronal-type' nAChRs, based on their expression profiles within the CNS and PNS. With the advent of whole genome sequencing, a large number of nAChRs have also been identified from non-vertebrate species. Ten nAChR subunits in insects, such as the fruit fly *Drosophila melanogaster* (Millar and Denholm, 2007), and 29 nAChR subunits in the nematode *Caenorhabditis elegans* (Jones *et al.*, 2007), have to date been identified.

1.4 The structure of nAChRs

1.4.1 Primary protein structure of nAChR subunits

The primary amino-acid sequences of all the nAChR subunits have approximately 40-50% amino-acid sequence similarity and all are believed to share a similar membrane topology with the other members of the Cys-loop receptor family (Lester *et al.*, 2004). Each nAChR subunit contains an N-terminal signal sequence of around 20 amino acids which is cleaved from the mature protein polypeptide. The N-terminal portion of the protein constitutes a large hydrophilic

extracellular domain containing asparagine (N)-linked glycosylation sites (See Section 1.5.2). The N-terminal domain consists largely of a β-sheet structure with interconnecting hairpin-loop turns (Unwin, 2005). It contains a conserved 15 amino-acid Cys-loop, formed by the disulphide linkage of residues which align to C^{128} and C^{142} of the *Torpedo* α1 subunit and is characteristic of all members of the receptor family (See Section 1.3.1). The N-terminal domain includes sequences which make up the ligand binding site (Sine, 2002). Sequence analysis and hydrophobicity plots indicate that there are four hydrophobic, putative transmembrane spanning domains termed M1, M2, M3 and M4, which are highly conserved throughout the subunit family and are generally accepted to adopt an α-helical structure (Unwin, 2005). The M2 α-helices of each of the five subunits which comprise the assembled nAChR line the channel pore and act as a selectivity filter and gate for ion flow through the channel (Imoto *et al.*, 1988). There is a large cytoplasmic loop between the transmembrane domains M3 and M4, which displays the greatest sequence variability between subunits and contains several potential sites of phosphorylation (Huganir and Greengard, 1990; Moss and Henley, 2002). A possible consequence of the variability of the large M3-M4 cytoplasmic loop is that intracellular molecular interactions could be specific to certain subunits and receptors. This may provide a mechanism by which receptors can be selectively modulated and targeted. Subunit protein sequences terminate with a short C-terminal domain located on the extracellular face of the membrane.

1.4.2 Stoichiometry and arrangement of subunits

The nAChR of the *Torpedo* electric organ is arranged as a pentamer with the stoichiometry $\alpha_2\beta\gamma\delta$ (Unwin, 1993). It can exist as a monomer or as a dimer in which two receptor monomers are linked via a disulphide bridge between the penultimate cysteine residues of the δ subunits (DiPaola *et al.*, 1989). Data obtained from electron diffraction studies of Torpedo nAChR have revealed that the subunits are arranged around the central ion-pore in the clockwise order, α-γ-α-β-δ, as viewed from above the plane of the membrane (Figure 1.2; Unwin, 2005).

The nAChR in murine skeletal muscle has a predicted topology similar to that of the *Torpedo* receptor (Sealock, 1982). It is highly likely that the arrangement around the ion-channel pore for the muscle nAChRs is the same as the *Torpedo* receptor (based on sequence similarity), except that in adult muscle the position of the δ subunit is replaced by the ε subunit.

In both fish electric organ and vertebrate muscle nAChRs, the agonist-binding site has been mapped to the α-γ and α-δ subunit interfaces. Affinity labelling experiments using competitive antagonists were found to label primarily the α subunits and, to a lesser extent, the γ and δ subunits (Pedersen and Cohen, 1990; Corringer *et al.*, 2000). The unequal levels of binding observed between the subunits (α1 binding > γ and δ binding) suggested an asymmetric location of the

binding site, with the α1 subunit contributing a greater effect towards binding. Thus, the α1 subunit has been termed the 'principal component' subunit, while the γ and δ were termed the 'complementary component' subunits of the ACh binding site (Corringer *et al.*, 1995; Corringer *et al.*, 2000).

Subunit stoichiometry is more complex in the heteromeric neuronal nAChRs, owing to the larger diversity of subunits available to form receptors. Two well-studied heteromeric receptors contain α4 and β2 subunits, and α3 and β4 subunits. These combinations are thought to have two α subunits and three β subunits but there is also evidence for alternative subunit stoichiometries (Zwart and Vijverberg, 1998; Nelson *et al.*, 2003). Heterologous expression studies in *Xenopus* oocytes have provided evidence for an α3β4 nAChR stoichiometry of $(\alpha3)_2(\beta4)_3$, with the arrangement αβαββ (Boorman *et al.*, 2000). However, α4β2 nAChRs can exist in two different stoichiometries in both oocytes and mammalian cells: $(\alpha4)_2(\beta2)_3$ and $(\alpha4)_3(\beta2)_2$, which exhibit differing functional properties (Zwart and Vijverberg, 1998; Nelson *et al.*, 2003). The lower-affinity (ACh EC_{50} = ~100 μM) $(\alpha4)_3(\beta2)_2$ stoichiometry predominates in mammalian cells and exposure to nicotine can up-regulate the levels of the β2 subunit and promote the expression of the higher-affinity (ACh EC_{50} = ~1 μM) $(\alpha4)_2(\beta2)_3$ stoichiomtery (Moroni *et al.*, 2006). The stoichiometry of recombinant α9α10 nAChRs has been shown in oocytes to be $(\alpha9)_2(\alpha10)_3$ (Plazas *et al.*, 2005). It has yet to be conclusively determined if the stoichiometries of recombinant receptors elucidated in heterologous expression systems truly represent those of native

receptors, a matter which is further complicated by nAChR subtypes containing more than one type of α or β subunit (Lewis *et al.*, 1997; Millar, 2003). Some nAChR subunits are capable of forming homopentameric receptors (e.g. α7 and α9; (Couturier *et al.*, 1990 and Elgoyhen *et al.*, 1994, respectively). It has been reported that homomeric α7 receptors have five binding sites for the ligand methyllycaconitine (MLA; Palma *et al.*, 1996), implying a pentameric structure. A summary of the diverse family of vertebrate nAChR subunits and the rules governing their assembly are briefly described in Table 1.1.

1.4.3 The three-dimensional structure of the nAChR

Electron microscopy studies of the *Torpedo* nAChR have yielded insights into the molecular and structural elements of the nAChR that underlie aspects of its function, such as agonist binding and gating. Tubular crystals of the postsynaptic membrane of electroplaque tissue analysed by cryo-electron microscopy have provided three-dimensional structural details of the nAChR (Figure 1.2) at a resolution of 17 Å (Toyoshima and Unwin, 1988), 9 Å (Unwin, 1993), and more recently, 4 Å (Unwin, 2005).

The receptor has a length of about 160 Å (or 16 nm), with the N-terminal domain protruding outwards from the membrane by about 80 Å. The pentameric receptor is composed of subunits which all have dimensions approximately 30 Å x 40 Å x 160 Å (Unwin, 2005). The intracellular domain is the only part of the protein which remains unresolved in the three-dimensional structure, perhaps due to this

Subtype	Family	Tribe	Subunits	Combinations
Neuronal-type (non muscle-type)	I*		α9, α10	α9α10[a,b]
	II*		α7, α8	α7[c] α8‡[d]
	III†	III.1	α2, α3, α4, α6	α2β4[e] α3α5β4[g,h]
		III.2	β2, β4	α3β4[e] α6β2β3[i,j]
		III.3	α5, β3	α4β2[f] α4α6β2β3[i,j]
Muscle-type	IV*	IV.1	α1	α1β1γδ[k]
		IV.2	γ, δ, ε	α1β1εδ[k]
		IV.3	β1	

Table 1.1 Schematic summary of vertebrate nAChR subunit diversity and assembly. Vertebrate nAChRs can be broadly classified as either 'muscle-type' or 'neuronal-type'/'non muscle-type', depending on their expression profile (see main text). The nAChRs are further divided into four 'families' (I-IV) based on their sequence similarities and gene structure. The nAChR combinations in families I, II and IV are sensitive to the snake neurotoxin αBTX (*); while those in family III are αBTX-insensitive (†). Current evidence suggests that natively, the subunits α7 and α8 appear primarily to form homopentameric receptors, although there is also evidence from chick that they can co-assemble with each other (for review see Millar, 2003). The two largest nAChR subunit families can be further subdivided into three 'tribes' (1-3; Le Novère *et al.*, 2002), depending on the role each subunit plays within the receptor complex. Subunits forming the principal and complementary components of the ligand binding site belong to the 1st and 2nd tribe, respectively. The subunits which do not participate directly in the formation of the ligand binding site belong to the 3rd tribe. The rules of nAChR assembly require that heteromeric receptors are composed of at least two subunits from each of the 1st and 2nd tribes *e.g.* $(\alpha4)_2(\beta2)_3$, as found throughout the CNS; and may contain one subunit from the 3rd tribe *e.g.* $(\alpha1)_2\beta1\varepsilon\delta$, as found at the adult NMJ or $\alpha4\alpha6(\beta2)_2\beta3$, as found in the retina and its projections. Members of the 3rd tribe (*e.g.* α5 and β3) are often referred to as 'orphan subunits', since they cannot form a functional receptor without subunits from the 1st and 2nd tribes. Note that not all of the receptor subunit combinations characterised to date are included in this table, which is intended as a simplified guide (for recent reviews see Millar, 2003; Gaimarri *et al.*, 2007; and Gotti *et al.*, 2007). ‡ The α8 subunit has been identified in avian species with no evidence for a mammalian homologue. [a, Elgoyhen *et al.*, 2001; b, Plazas, 2005; c, Couturier *et al.*, 1990; d, Gerzanich *et al.*, 1994; e, Duvoisin *et al.*, 1989; f, Papke *et al.*, 1989; g, Fucile *et al.*, 1997; h, Conroy and Berg, 1995; i, Champtiaux *et al.*, 2003; j, Zoli *et al.*, 2002; and k, Mishina *et al.*, 1986]

being a less rigid part of the receptor, resulting in a more disordered region within the crystal. The only part of the intracellular loop to be resolved is the membrane associated (MA)-helix, which adopts a rigid structure in relation to the rest of the loop and constitutes the cytoplasmic vestibules of the nAChR, protruding approximately 50 Å below the membrane (Peters *et al.*, 2005; Unwin, 2005).

Recently, a molluscan acetylcholine binding protein (AChBP), first identified in *Lymnaea stagnalis*, has been described and characterised (Brejc *et al.*, 2001). The AChBP is a water-soluble protein which has clear amino acid sequence similarity to the nAChR extracellular domain. It forms a soluble homo-pentameric protein that is thought to be involved in suppression of cholinergic transmission by binding acetylcholine. The AChBP has been crystallised and its structure determined at high resolution (2.2 Å) by X-ray crystallography (Ulens *et al.*, 2006). The three-dimensional structure of the AChBP was found to be remarkably similar to the extracellular region of the *Torpedo* nAChR. In addition to binding acetylcholine, the AChBP can also bind other nicotinic ligands such (+)-tubocurarine and αBTX, (Brejc *et al.*, 2001). The AChBP has been successfully crystallised in the presence of the nAChR agonists nicotine and carbachol (Celie *et al.*, 2004), and of the antagonists α-conotoxin (Celie *et al.*, 2005) and α-cobratoxin (Bourne *et al.*, 2005). Recently, a 1.94 Å high-resolution crystal structure of the extracellular domain of the mouse nAChR α1 subunit bound to αBTX was determined (Dellisanti *et al.*, 2007). The crystal structures have been used extensively to interpret experimental observations at the detailed

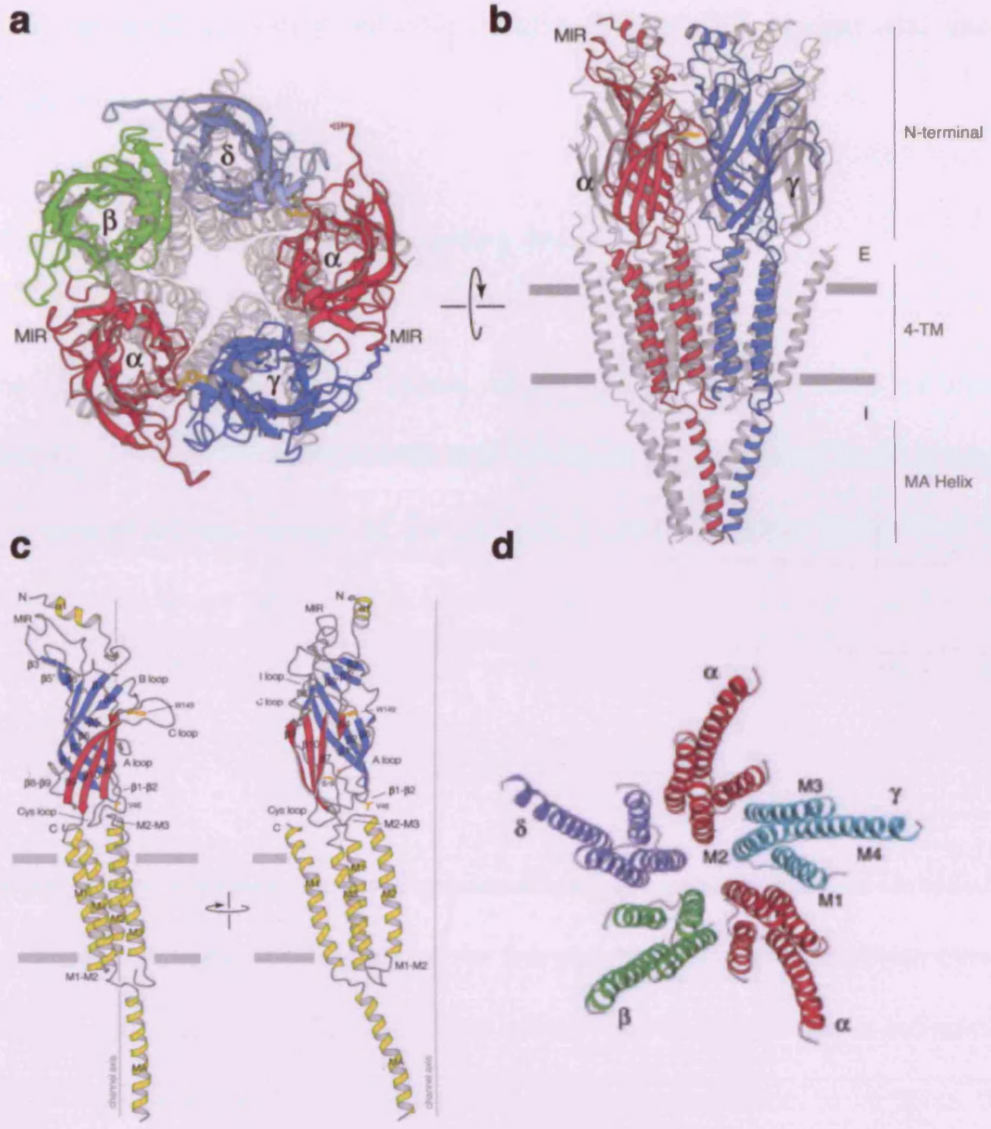

Figure 1.2 High resolution structure of the nAChR. Ribbon diagrams of the *Torpedo* nAChR amino-acid sequence (4-TM and MA domains) and the *Lymnaea* AChBP (N-terminal domain), fitted to the density map obtained by electron microscopy. **(a)** View of the whole receptor, as seen from the synaptic cleft and **(b)** when rotated through 90° and viewed parallel with the membrane plane. Subunits are labelled in red (α), green (β), blue (γ) and light-blue (δ). **(c)** For clarity, a single subunit (α) is shown viewed with the central channel axis behind (left panel) and rotated through 90° with the channel axis to the side (right panel). **(d)** View of the receptor channel domain, as seen from the synaptic cleft, showing the relative positions of the α-helices which make up the TM domain. The M2 helix of each subunit lines the channel pore, while the helices M1, M3 and M4 separate the M2 helix from the surrounding lipids of the plasma membrane. (a), (b) and (c) reprinted from Unwin 2005, with permission from Elsevier. (d) reprinted by permission from Macmillan Publishers Ltd. (Miyazawa, 2003).

molecular level, providing valuable insights into nAChR binding and gating mechanisms.

1.4.4 The extracellular ligand-binding domain

The N-terminal extracellular domain of the nAChR is responsible for ligand binding. Acetylcholine binds to the nAChR ligand binding domain which results in a conformational change of the receptor protein complex, going from the 'closed' state to an 'open' state, allowing cations to pass through the receptor channel from the extracellular side to the intracellular side of the plasma membrane.

As previously described, the binding sites of nAChR ligands have been mapped to the α-γ and α-δ subunit interfaces of the fish electric organ and vertebrate muscle nAChRs (see Section 1.4.2). Both the α subunit and associated non-α subunits (γ or δ) contribute to the ligand-binding domain. Evidence to support this conclusion has been provided by studies in which cell lines expressing α1 with only the γ or δ subunit formed a ligand binding site with pharmacological characteristics similar to that of native receptors (Blount and Merlie, 1989). In contrast, expression of the α1 subunit alone, or in combination with the β1 subunit, failed to produce a high-affinity ligand-binding site (Blount and Merlie, 1989). These data suggest that there are two agonist-binding sites in muscle nAChRs. The binding sites have been termed non-equivalent (or non-identical)

owing to the differences in binding affinities to α-γ and α-δ complexes of antagonists such as (+)-tubocurarine (Blount and Merlie, 1989) and α-conotoxin MI (Sine *et al.*, 1995). Heteromeric neuronal nAChRs containing one α-type and one β-type subunit (e.g. α4β2), and with a stoichiometry $(\alpha)_2(\beta)_3$, are believed to also form two binding sites.

The α7 subunit is expected to have five equivalent binding sites and experiments with recovery from MLA inhibition are best fitted with a five binding site model (Palma *et al.*, 1996). It is however possible that activation of the receptor may only require ligand binding to two sites (Corringer *et al.*, 1995; Servent *et al.*, 1997). The crystal structure of the related homomeric AChBP also supports five ligand binding sites per homomeric receptor. Evidence to support this conclusion has come from X-ray crystallography studies in which receptor structures exist with five ligands bound to the binding sites (Celie *et al.*, 2004).

1.5 Assembly and trafficking

1.5.1 Folding and assembly of nAChRs

The formation of functional ligand-gated ion channels such as the nAChR is a complex process involving a number of stages prior to the insertion of the final mature protein at the cell surface (Green and Millar, 1995). The nascent linear

protein sequence of each subunit must fold into the correct membrane-spanning topology and assemble with other subunits in the correct stoichiometry and arrangement. This occurs in the endoplasmic reticulum (ER), where the receptor also undergoes post-translational modifications before export through the Golgi apparatus to the plasma membrane (Green and Millar, 1995). Nicotinic receptors assemble slowly and inefficiently in comparison to other transmembrane proteins. This is thought to be due to inaccurate folding of the subunit proteins, which has been monitored by the formation of ligand binding sites and conformational epitopes for monoclonal antibodies (Merlie and Lindstrom, 1983).

The muscle-type nAChR has provided two models of nAChR assembly. In the "heterodimer" model (Blount and Merlie, 1991; Gu *et al.*, 1991), the α subunit first associates with the γ and δ subunits to form αγ and αδ heterodimers. The heterodimers then coassemble with the β subunit creating the $\alpha_2\beta\gamma\delta$ pentamer. In the "sequential" model (Green and Claudio, 1993; Green and Wanamaker, 1997, 1998), the α, β and γ subunits rapidly assemble into trimers. The trimer undergoes further post-translational folding to form an αBTX binding site, before the addition of the δ subunit into an αβγδ tetramer and the subsequent formation of an acetylcholine binding site. Finally, the second α subunit is incorporated into the tetramer creating the $\alpha_2\beta\gamma\delta$ pentamer. Currently, evidence favours the sequential model of nAChR assembly (Wanamaker *et al.*, 2003). Only fully assembled pentameric receptors are targeted for export from the ER to the Golgi apparatus (Gu *et al.*, 1991). Further post-translational modifications such as *N*-

Glycosylation and formation of the disulphide bridge to create the Cys-loop, also occur at this stage of assembly in the ER.

1.5.2 Post-translational modification of nAChRs

After translation of the mature mRNA transcript by ER-associated ribosomes, the nascent nAChR undergoes several post-translational modifications additional to those mentioned above (Section 1.5.1). These include the formation of disulphide bonds, glycosylation, palmitoylation and phosphorylation (Green and Millar, 1995).

Glycosylation, the addition of sugar units such as glycan chains to proteins, is the most common covalent protein modification which occurs in eukaryotic cells (Helenius and Aebi, 2004). Glycan chains can be added to either the amide nitrogen of asparagine (*N*-linked glycosylation), which occurs in the ER, or to the hydroxy oxygen of serine or threonine (*O*-linked glycosylation), which occurs primarily in the Golgi apparatus. Glycosylation can contribute significantly to the molecular weight of a protein and is critical in such processes as protein folding, assembly and function. The added carbohydrates serve as 'tags' for other proteins which act as chaperones in the ER. The extracellular N-terminal domain of the nAChR contains several putative sites for glycosylation. Block of *N*-linked glycosylation in mouse fibroblasts expressing the four *Torpedo* nAChR subunits inhibits the folding and subunit assembly, and severely attenuates subsequent

expression of receptors at the cell surface (Wanamaker and Green, 2005). A high resolution (1.94 Å) crystal structure of the mouse nAChR α1 subunit revealed an *N*-linked carbohydrate chain attached to residue Asn^{141} within the Cys-loop (Dellisanti *et al.*, 2007). The glycan chain makes a number of contacts with the loop regions of the nAChR α1 subunit ligand binding pocket suggesting a role for glycosylation in ligand binding. Since this specific glycosylation site (within the Cys-loop) is conserved only in muscle nAChRs and not other members of the nAChRs, it has been speculated that it may confer the ability to bind αBTX (Dellisanti *et al.*, 2007).

Palmitoylation, the covalent linkage of palmitate to a cysteine residue of proteins, is a reversible post-translational modification and has been found in over 100 proteins to date (Resh, 2006; Linder and Deschenes, 2007). Palmitate is a 16-carbon saturated fatty acid and a common acyl residue of membrane phospholipids. Palmitate, from palmitoyl-CoA, is attached to proteins via a thiester (S-acyl) linkage by membrane-associated protein acyltranferases (PATs) in the forward reaction; and cleaved by cytoplasmic acylprotein thioesterases (APTs) in the reverse reaction. Palmitoylation has been found to play an important role in trafficking of proteins to the plasma membrane, and in the case of membrane-spanning proteins, to specific plasma membrane domains such as lipid-rafts (Salaün *et al.*, 2005). Lipid rafts have been found to co-localise with α7 nAChRs and are required for the maintenance of α7 clustering in the somatic spines of ciliary neurones (Bruses *et al.*, 2001). Palmitoylation has also been

implicated as a factor important in the successful expression of α7 nAChRs at the cell surface. In cell lines such as HEK-293, which are non-permissive to α7 expression, receptors are not significantly palmitoylated. In contrast, in PC12 cells, which do allow α7 expression, receptors show significant palmitoylation (Drisdel *et al.*, 2004).

Phosphorylation, the addition of phosphate groups to hydroxyl groups of proteins on serine, threonine or tyrosine side chains, modulates the functional properties of many cellular proteins, including nAChRs (Swope *et al.*, 1999; Wiesner and Fuhrer, 2006). In particular, the M3-M4 intracellular loop domain contains potential phosphorylation sites, as determined by the presence of protein phosphorylation consensus sequences. Tyrosine kinases can phosphorylate the β, γ and δ subunits of the *Torpedo* nAChR (Huganir *et al.*, 1984), while cyclic AMP (cAMP)-dependent protein kinase A (PKA) phosophorylates γ and δ subunits (Huganir and Greengard, 1983). Protein kinase C (PKC) can phosphorylate the α and δ subunits and affect the rate of desensitisation and channel conductance properties (Eusebi *et al.*, 1987). Src-family kinases (SFK) can promote the clustering and stability of nAChRs at the neuromuscular junction, while the same kinases mediate a negative regulatory effect upon α7 cells of the CNS (Wiesner and Fuhrer, 2006).

1.6 Distribution of native nAChR subtypes

Nicotinic AChRs are widely distributed throughout the CNS and PNS and their subunit composition is region- and cell-specific. The predominant receptor subtype found in the brain is the heteromeric αBTX-insensitive α4β2* nAChR subtype (where the asterisk denotes the possible presence of an unknown subunit; Lukas *et al.*, 1999). Within the PNS, the predominant subtype is the α3β4* containing nAChR. Homomeric αBTX-sensitive α7 nAChRs are highly expressed in the cortex, hippocampus and subcortical limbic regions of the brain, and at lower levels in the thalamic regions and basal ganglia (Gaimarri *et al.*, 2007). Due to the large diversity of nAChR subunits available to form heteromeric receptors, characterising the different receptor subtypes within the brain has been problematic.

While the distribution of nAChR subunit mRNA and protein has been investigated, the subunit composition of all native receptors is as yet unknown. Some work has been done to elucidate the subunit combinations that form receptors in native cells, for example, in chick ganglion neurones there are thought to be only three populations of receptors (Conroy and Berg, 1995). *In situ* hybridisation and immunohistochemistry experiments investigated the distribution of specific subunit mRNA and protein, and demonstrated the differing expression patterns of the nAChR subunits. For example the β2 subunit mRNA is widely distributed throughout the brain (Swanson *et al.*, 1987; Paterson and Nordberg,

2000). In contrast the α2 subunit mRNA is only seen in the interpeduncular nucleus (Wada *et al.*, 1988). There is considerable overlap in the expression profile of many of the subunit mRNAs, suggesting that the proteins they encode may have the opportunity to coassemble to form a wide range of receptors.

1.6.1 Central nervous system (CNS) distribution

Ligand binding studies with [^{3}H]ACh and [^{125}I]αBTX have been performed in the brain to examine the distribution of potential neuronal nAChRs. Both these ligands bind to muscle nAChRs but show a differential binding pattern in the brain, indicating the presence of more than one distinct population of nAChR (Clarke *et al.*, 1985).

The α4 and β2 subunit mRNAs and proteins are widely expressed in the central nervous system (Goldman *et al.*, 1987; Swanson *et al.*, 1987; Deneris *et al.*, 1988). They form functional heteromeric receptors when expressed recombinantly (Boulter *et al.*, 1987; Buisson *et al.*, 1996) with high affinity to nicotine (Connolly *et al.*, 1992). Immunodepletion experiments in chick brain have shown that a large proportion of the epibatidine binding receptors contain α4 and β2 (Conroy and Berg, 1998). These two subunits probably form the primary site for high affinity nicotine binding in the central nervous system (Zoli *et al.*, 1998). Both α4 and β2 knockout mice lack high affinity [^{3}H]-nicotine binding sites (Picciotto *et al.*, 1995; Marubio *et al.*, 1999).

Additional subunits combine with the α4β2 receptor to form diverse receptors in the central nervous system. The α5 subunit has been shown to assemble with α4 subunits in the brain (Conroy *et al.*, 1992). The β3 and β4 subunits have been shown to co-assemble with α4β2 in rat cerebellum (Forsayeth and Kobrin, 1997). However, there are also nAChRs that contain no β2 subunit. When the β2 subunit is knocked out there are still high affinity [^{3}H]-epibatidine sites in the dorsocaudal medulla oblongata, pineal gland and habenula-ventral interpeduncular system, which are consistent with the pharmacology of α3β4 (Zoli *et al.*, 1998).

Radioligand binding of [^{125}I]αBTX in the brain is thought to be due to α7 nAChRs. The localization of α7 mRNA has been shown to overlap with [^{125}I]αBTX binding sites (Séguéla *et al.*, 1993) and α7 knockout mice lack αBTX binding. Nicotine induced currents in rat hippocampal slices that are blocked by αBTX and MLA are not present in the knockout mice (Orr-Urtreger *et al.*, 1997). The radioligand [^{125}I]αBTX also binds to the α8 subunit, however, this subunit has only been identified in avian species (Schoepfer *et al.*, 1990). The α7 homomeric receptors are thought to account for about 74% of αBTX binding sites in chick brain (Keyser *et al.*, 1993). A recent summary of the data on nAChR subtype location in the rodent brain is shown in Figure 1.3.

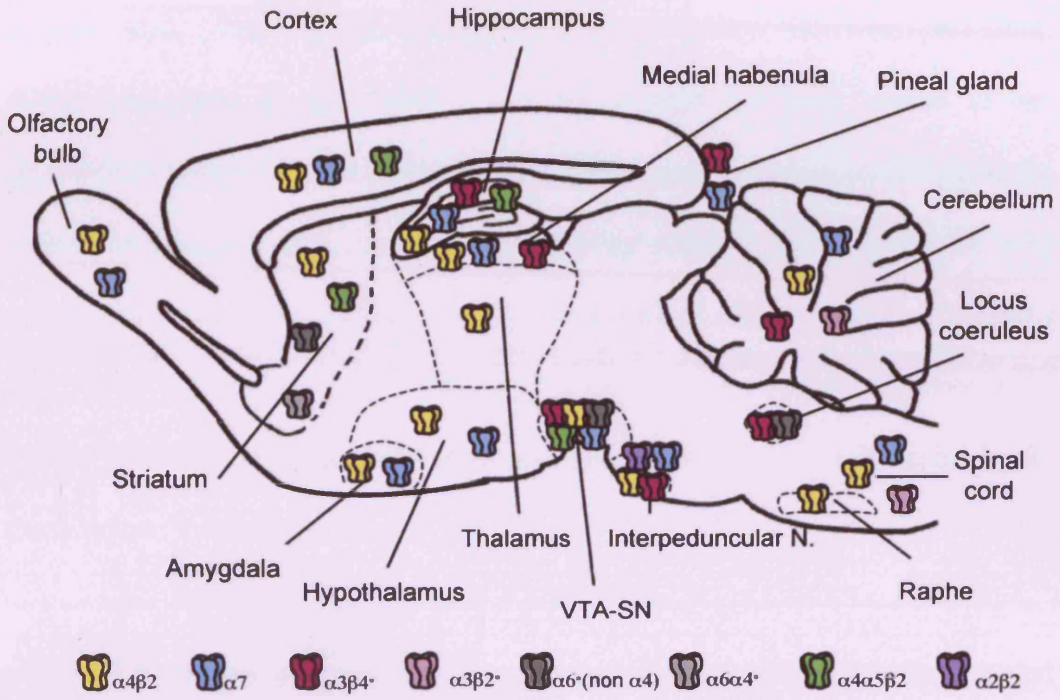

Figure 1.3 Distribution of nAChR subtypes in the rodent central nervous system. Evidence for receptor subtytpes comes from the amalgamation of data obtained from radioligand binding, immunoreactivity, *in situ* hybridisation and single-cell PCR studies, from wild-type and knockout mice. An asterisk denotes the possible presence of an unidentified subunit within the receptor. Reprinted from Gaimarri *et al.*, 2007, with permission from Elsevier.

1.6.2 Peripheral nervous system (PNS) distribution

Little or no α4 subunit is expressed in the periphery (Rust *et al.*, 1994). In contrast, the α3 and β4 transcripts are highly expressed and thought to be the primary high affinity nicotinic receptors in the periphery (Corriveau and Berg, 1993; Mandelzys *et al.*, 1994). The α3 subunit has been shown to co-immunoprecipitate with the β4 subunit in the rat trigeminal ganglion (Flores *et al.*, 1996). In addition, there is evidence that other subunits can co-assemble with some α3β4 nAChRs, including α5 and β2 in the chick ciliary ganglion (Vernallis *et al.*, 1993; Conroy and Berg, 1995) and the rat trigeminal ganglion (Flores *et al.*, 1996). The α6 and β3 subunits were also shown to assemble with α3β4 in the chick retina (Vailati *et al.*, 2000).

[^{125}I]αBTX binding sites are seen in cultured sympathetic neurones (Patrick and Stallcup, 1977b; Carbonetto *et al.*, 1978), and nAChR α7 subunit mRNA is highly expressed in the rat superior cervical ganglion and adrenal medulla (Rust *et al.*, 1994) and also in the chick ciliary ganglion (Corriveau and Berg, 1993). In both rat and chick there are thought to be at least three receptor subtypes that may contain the α7 subunit due to the distinct pharmacological subtypes that are sensitive to αBTX and MLA (Yu and Role, 1998; Cuevas *et al.*, 2000). Possible subunits that could assemble with α7 are β2 (Britto *et al.*, 1992) and β3 (Palma *et al.*, 1999). A splice variant of the α7 subunit, which forms receptors that exhibit different functional and pharmacological properties to the original homomeric α7

receptor has also been detected (Severance *et al.*, 2004). This splice-variant could account for the αBTX sensitive receptors in the PNS showing distinct properties to the typical α7 subunit found in the CNS.

1.6.3 Non-CNS or PNS distribution

Responses to ACh have been detected in cochlear hair cells (Art *et al.*, 1984), yet most nAChR subtypes are not expressed there (Hiel *et al.*, 1996). Only the α9 and α10 nAChR subunits are expressed in cochlear hair cells, with their expression generally restricted to the peripheral vestibular system and are thought to mediate the auditory response (Elgoyhen *et al.*, 1994; Elgoyhen *et al.*, 2001). The α9α10 nAChR has also been found expressed in dorsal root ganglion (DRG) neurones (Lips *et al.*, 2002). Homomeric α9 and heteromeric α9α10 nAChRs, characterised upon expression in *Xenopus* oocytes, exhibit a pharmacological profile unique among nAChRs. Consistent with their distinct localisation, nAChRs containing α9 and α10 do not fall conveniently into the conventional classification of either muscle-type or neuronal-type nAChRs (Elgoyhen *et al.*, 1994; Rothlin *et al.*, 1999; Verbitsky *et al.*, 2000; Elgoyhen *et al.*, 2001). Recently α9α10 receptors have been identified in a variety of other tissues, where their role is less well defined, such as lymphocytes, sperm, and keratinocytes, and have been implicated in mediating process such as neuropathic pain and aspects of the immune response (Vincler *et al.*, 2006). The nAChR α7 subunit has also been found in macrophage cells of the immune system where it is regulates inflammation (Wang *et al.*,

2003). Messenger RNA levels of other nAChRs subunits are present in multiple cell types of the intestine (Glushakov *et al.*, 2004), although at present, the role of nAChRs found outside the CNS and PNS remains largely unclear (Gahring and Rogers, 2005).

1.7 Aim of study

The main aim of the present study is to undertake a detailed comparison of intracellular loop domains from different nAChR subunits. This has been achieved by the construction of a series of subunit chimaeras containing a common extracellular domain (from the nAChR α7 subunit) and transmembrane domains (from the 5-HT_{3A} subunit), but with different nAChR intracellular loop domains.

Chapter 2

Materials and methods

Chapter 2

Materials and Methods

2.1 Materials

All chemicals were obtained from BDH unless otherwise specified. All restriction enzymes and restriction enzyme buffers were obtained from Promega unless otherwise stated. A Biofuge 13 (Heraeus Instruments) was used to centrifuge samples unless otherwise specified.

2.2 Plasmids

Rat α1-α7 and β1-β4 nAChR subunit cDNAs were obtained from Dr. Jim Patrick (Baylor College of Medicine, Houston, USA). The rat α7 cDNA had previously been excised and subcloned (Gee *et al.*, 2007), into the *Hind*III/*Xho*I sites of the plasmid vector pZeoSV2+ (Invitrogen). Rat α9-α10 nAChR subunit cDNAs were obtained from Dr. Belén Elgoyhen (Universidad de Buenos Aires, Buenos Aires, Argentina). Chick α8 nAChR subunit cDNA was obtained from Dr Jon Lindstrom (University of Pennsylvania, PA, USA). Chick α8 subunit cDNA was subcloned from pBluescript SK- (Stratagene) and subcloned into pcDNA3neo in

this laboratory by Dr Sandra Cooper (Cooper and Millar, 1998). The mouse 5-HT_{3A} subunit cDNA in pCDM6x1 was obtained from Dr David Julius, (University of California, CA, USA) and subcloned into pZeoSV2+ (Invitrogen) in this laboratory by Dr Sandra Cooper (Cooper and Millar, 1998). Human 5-HT_{3B} in pCDM8 was obtained from Dr Ewen Kirkness (Institute for Genomic Research, Rockville, Maryland, USA). Human RIC-3 cDNA was isolated and subcloned into pcDNA3neo in this laboratory by Dr Anne Doward (unpublished). All subunit cDNAs or chimaeric constructs in this study were in the expression vector pZeoSV2+ unless otherwise stated. Human RIC-3 constructs were in pcDNA3neo.

2.3 Molecular biological techniques

2.3.1 Construction of subunit chimaeras

The construction of a subunit chimaera ($\alpha7^{V201\text{-}5HT3A}$) containing regions of the rat nAChR α7 subunit extracellular domain and the mouse 5-HT_{3A} subunit transmembrane (TM) and intracellular domains has been described previously (Cooper and Millar, 1998), as has a related chimaera ($\alpha7^{4TM\text{-}5HT3A}$), in which the 5-$HT_{3A}$ intracellular loop domain has been replaced with the equivalent region of the α7 subunit (Gee *et al.*, 2007). Unique endonuclease restriction enzyme sites (*Not*I and *Bst*Z17I) were introduced at the N- and C-terminal ends of the large

M3-M4 intracellular loop domain of $\alpha7^{4TM\text{-}5HT3A}$ by use of the QuikChange site-directed mutagenesis, polymerase chain reaction (PCR) system (Stratagene), to create $\alpha7^{4TM\text{-}5HT3A(Not/Bst)}$. The *Not*I site was introduced at a position in $\alpha7^{4TM\text{-}5HT3A}$ equivalent to Met^{308} of *Torpedo californica* nAChR α1 subunit (as determined by protein sequence alignment using the ClustalW algorithm; MacVector, Accelrys), and numbered according to the α1 subunit sequence minus the predicted signal peptide (Noda *et al.*, 1982). Similarly, the *Bst*Z17I site was introduced to $\alpha7^{4TM\text{-}5HT3A}$ at a position equivalent to Met^{404} of the *T. californica* nAChR α1 subunit.

To generate the series of 'loop chimaeras', the M3-M4 intracellular loop domain was amplified by polymerase chain reaction (PCR) using the high-fidelity polymerase KOD (Novagen). Sequences were amplified from nAChR and 5-HT_3R subunit cDNA construcst with primers designed to introduce *Not*I and *Bst*Z17I sites. Fragments were amplified from rat nAChR subunit cDNA clones, with the exception of α8 which has not been identified in mammalian species and was amplified from chick cDNA. In the case of the 5-HT_3R subunits 3A and 3B, fragments were amplified from mouse cDNA clones. After digestion with *Not*I and *Bst*Z17I (New England Biolabs), PCR fragments were ligated into the *Not*I and *Bst*Z17I sites of $\alpha7^{4TM\text{-}5HT3A(Not/Bst)}$. All plasmid constructs (in the mammalian expression vector pZeoSV2+; Stratagene) were verified by nucleotide sequencing. The series of nAChR subunit M3-M4 intracellular loop domain chimaeras will be referred to as $\alpha7/5\text{-}HT_{3A}^{\alpha1\text{-}loop}$ (etc.) or, more simply, as 'α1 loop' chimaera (etc.).

2.3.2 Polymerase chain reaction (PCR)

One of two DNA polymerase enzymes was employed: *Taq* (Promega) was used for standard diagnostic PCR reactions and KOD (Novagen) was used for high-fidelity PCR where DNA fragments were required for further cloning (e.g. M3-M4 loop regions). PCR amplification was performed in a Peltier thermal cycler, PTC-225 (MJ Research). A typical reaction was performed in 20 µl and contained 200 ng of plasmid DNA, 0.25 µM forward and reverse synthetic oligonucleotide primers (obtained from Sigma-Genosys), 250 µM dNTPs, 1x polymerase buffer plus $MgCl_2$ (for *Taq* only) or $MgSO_4$ (for KOD only), and 2.5 U of appropriate DNA polymerase enzyme. PCR thermal conditions were defined by the respective manufacturer's instructions for each DNA polymerase enzyme.

r α1 *Not*I (+)	ATAAGAAT**GCGGCCGC**TGCCCGAGTGGGTGCGGAAGG
r α1 *Bst*Z (-)	GGGCATTC**GTATAC**AGGCGACATACTTCCACTCCTCAGACGC
r α2 *Not*I (+)	ATAAGAAT**GCGGCCGC**TGCCCAACTGGGTAAGGGTAGC
r α2 *Bst*Z (-)	GGGCATTC**GTATAC**AGGCCACATACTTCCAGTCTTCCTTCACCG
r α3 *Not*I (+)	ATAAGAAT**GCGGCCGC**TGCCCACTTGGGTCAAGGCC
r α3 *Bst*Z (-)	GGGCATTC**GTATAC**AGGCAACGTACTTCCAATCATCTTGAATC
r α4 *Not*I (+)	ATAAGAAT**GCGGCCGC**TGCCCGCCTGGGTGCGTAGAG
r α4 *Bst*Z (-)	GGGCATTC**GTATAC**AGGCCACGTATTTCCAGTCCTCCTTCAC
r α5 *Not*I (+)	ATAAGAAT**GCGGCCGC**TGGCGCCCTGGGTTCGTAAG
r α5 *Bst*Z (-)	GGGCATTC**GTATAC**AGGCTATGAATTTCCAATCTTCAACAACC
r α6 *Not*I (+)	ATAAGAAT**GCGGCCGC**TGCCCAAGTGGGTGAAGACC
r α6 *Bst*Z (-)	GGGCATTC**GTATAC**AGGCCATGTATTTCCAGTCATCTTCTACC
r α7 *Not*I (+)	ATAAGAAT**GCGGCCGC**TGCCTAAGTGGACCAGAATC
r α7 *Bst*Z (-)	GGGCATTC**GTATAC**AGGCTGCAAACTTCCATTCACTGC
r α8 *Not*I (+)	ATAAGAAT**GCGGCCGC**TGCCCAGATGGGTCCGTG
r α8 *Bst*Z (-)	GGGCATTC**GTATAC**AAGCTGCAAACTTCCACTCACTGC

r α9 *Not*I (+)	ATAAGAAT**GCGGCCGC**TGCCACACTGGGCCAAGGTG
r α9 *Bst*Z (-)	GGGCATTC**GTATAC**AGGCGACCTTCTTCCACTCGCTGCC
r α10 *Not*I (+)	ATAAGAAT**GCGGCCGC**TGCCCGCCTGGGCTCGGGTTC
r α10 *Bst*Z (-)	GGGCATTC**GTATAC**AAGCCAGACGCTTCCAATCTTCGTGGCG
r β1 *Not*I (+)	ATAAGAAT**GCGGCCGC**TGCCCTTTTGGGTCCGCC
r β1 BstZ (-)	GGGCATTC**GTATAC**AGGCGACAAACTGCCAGTCCTCC
r β2 *Not*I (+)	ATAAGAAT**GCGGCCGC**TGGCCCCCTGGGTCAAGGTG
r β2 *Bst*Z (-)	GGGCATTC**GTATAC**AGGCAACGTATTTCCAGTCCTCCCTCACAC
r β3 *Not*I (+)	ATAAGAAT**GCGGCCGC**TGGCCCCCTGGGTGAAGAGG
r β3 *Bst*Z (-)	GGGCGGGC**GTATAC**AAGCCACAAATTTCCAGTCTTGCAC
r β4 *Not*I (+)	ATAAGAAT**GCGGCCGC**TGGCATCCTGGGTCAAGGAGTG
r β4 *Bst*Z (-)	GGGCGGGCGTATACACGCGACGAACTTCCAGTCCTCG
m 5-HT_{3A} *Not*I (+)	AGAAGAAT**GCGGCCGC**TACCTGACTGGCTGAGGCACC
m 5-HT_{3A} *Bst*Z (-)	GAGCAGGC**GTATAC**ATCCCACCCGCAGCCAGTCCC
h 5-HT_{3B} *Not*I (+)	ATAAGAAT**GCGGCCGC**AGCCCTTCTTGTGCCTTCGAGGG
h 5-HT_{3B} *Bst*Z (-)	GGGCATTC**GTATAC**ACAGGAGGACCAGCCACTCTGCCTC

Table 2.1 Oligonucleotide primers used to introduce restriction sites by PCR. Primer pairs used to introduce the restriction endonuclease sites *Not*I and *Bst*Z17I to the M3 and M4 ends of the M3-M4 intracellular loop of nAChR and 5-HT_3R subunit sequences. **Bold type** indicates the introduction to the sequence of the restriction sites *Not*I (**GCGGCCGC**) and *Bst*Z17I (**GTATAC**). All primers are displayed in a 5' to 3' direction (left to right), with (+) indicating a forward-facing primer and (-) indicating a reverse-facing primer. r=rat; m=mouse; h=human.

2.3.3 Site-directed mutagenesis

Site-directed mutagenesis (SDM) was performed using the QuikChange site-directed mutagenesis kit (Stratagene) using the manufacturer's instructions. Two complementary synthetic oligonucleotide primers (typically of length 25-45 bases in length) were designed, containing the desired mutation. Oligonucleotide

primers were designed, where possible, so the GC base content (% GC) was ≥ 40% and the melting temperature (T_m) was ≥ 78 °C, as determined using MacVector software (Accelrys). Primers were designed to terminate in a 3' G or C base and were PAGE (polyacrylamide gel electrophoresis)-purified by the supplier (Sigma-Genosys).

Site-directed mutagenesis reactions were performed in a volume of 50 µl containing 50 ng of template DNA, 125 ng each of the complementary oligonucleotides, 1 µl of dNTP mix (from kit), 1x reaction buffer and 1 µl of *Pfu*Turbo DNA polymerase (2.5 U/µl). The reaction was heated to 95 °C for 30 seconds and then the thermocycling reaction was performed for 12-18 cycles (depending on the number of mutated residues), as follows:

95 °C for 30 seconds (denaturation)
55 °C for 1 minute (annealing)
68 °C for 1 minute/kilobase of plasmid length (extension).

The reaction mixture was cooled to 4 °C and 1 µl of the restriction enzyme *Dpn* I (10 U/µl) was added and transferred to 37 °C for 1 hour to digest the methylated, non-mutated parental template DNA. Bacterial cells were then transformed with the DNA product. 1 µl of digested DNA was mixed in a pre-chilled polypropylene tube (Falcon 2059, Becton Dickinson) with 50 µl supercompetent XL1-blue *E. coli* cells (Stratagene) and incubated on ice for 30 minutes. Cells were then heat

shocked at 42 °C for 45 seconds, returned to ice for 2 minutes and then incubated in 500 µl of NZY^+ broth, prepared according to the manufacturers guidelines, containing 10 g/l NZ amine (casein hydrosylate enzymatic, Invitrogen), 5 g/l yeast extract, 5 g/l NaCl (pH 7.5), 12.5 ml/l 1 M $MgCl_2$, 12.5 ml/l $MgSO_4$ and 10 ml/l 2 M glucose, for 1 hour with shaking at 225 rpm. 200 µl of the transformation mix was plated onto LB agar plates containing the appropriate antibiotic and incubated at 37 °C overnight.

$\alpha7^{4TM\text{-}5HT3A}$ *Not*I (+)	CAGGACCTACA**GCGGCCGC**TGCCTAAGTGGACC
$\alpha7^{4TM\text{-}5HT3A}$ *Not*I (-)	GGTCCACTTAGGCA**GCGGCCGC**TGTAGGTCCTG
$\alpha7^{4TM\text{-}5HT3A}$ *Bst*Z (+)	GGAAGTTTGCAGCCT**GTATAC**TGGACAGGCTGCTGTTCCGC
$\alpha7^{4TM\text{-}5HT3A}$ *Bst*Z (-)	GCGGAACAGCAGCCTGTCCA**GTATAC**AGGCTGCAAACTTCC
r β2 RXR-Del (+)	GCTCTTCCTGCAGCAGCCAGAGGGCGAGGCGGTTTTCTTCCG
r β2 RXR-Del (-)	CGGAAGAAAACCGCCTCGCCCTCTGGCTGCTGCAGGAAGAGC
m 5-HT_{3A}FLAG (+)	CATTTGGCATTATTCT**GACTACAAGGACGACGATGACAAG**TGAGTG GGCACAG
m 5-HT_{3A}FLAG (+)	CTGTGCCCACTCA**CTTGTCATCGTCGTCCTTGTAGTC**AGAATAATG CCAAATG

Table 2.2 Oligonucleotide primers used for site-directed mutagenesis. Primer pairs used for site-directed mutagenesis (SDM)-PCR reactions to introduce restriction sites, FLAG-epitope tags and to remove the RXR-motif. **Bold type** indicates the introduction to the sequence of the restriction sites *Not*I (**GCGGCCGC**) and *Bst*Z17I (**GTATAC**) to $\alpha7^{4TM\text{-}5HT3A}$, or the introduction of the FLAG-epitope tag sequence (**GACTACAAGGACGACGATGACAAG**) to the C-terminal end of the 5-HT_{3A}R subunit sequence. Nucleotide base changes to the original sequence, due to the introduction of *Not*I and *Bst*Z17I are underlined. All primers are displayed in a 5' to 3' direction (left to right), with (+) indicating a forward-facing primer and (-) indicating a reverse-facing primer. r=rat, m=mouse. The $\alpha7^{4TM\text{-}5HT3A}$ receptor subunit chimaera consists of rat and mouse cDNA

Successful mutations were verified by nucleotide sequencing, and in cases where mutagenesis created a novel restriction enzyme site, by restriction enzyme digestion also.

2.3.4 Agarose gel electrophoresis

PCR products, digested plasmid DNA fragments and excised DNA inserts were separated by molecular weight by electrophoresis through either a 1% or 1.2% agarose gel. Electrophoresis-grade agarose (Invitrogen) was dissolved by heating and vigorous swirling in TAE buffer (40 mM Tris-acetate, 0.1 mM EDTA), allowed to cool and 0.3 μg/ml of ethidium bromide added. DNA samples were run along-side DNA size markers either, 1 μg of *Hind*III digested phage λ DNA (Invitrogen) or PCR markers (Promega). This enabled estimation of the size of the sample DNA. Samples and markers were loaded in 1x blue/orange loading dye (Promega). DNA was visualized by means of a UV transilluminator (UVP).

When DNA was required for subsequent purification, low melting point agarose was used (Invitrogen) and DNA fragments were excised after electrophoresis using a sterile scalpel. DNA was extracted from the agarose gel using the Wizard DNA clean up system (Promega). The agarose gel was melted in a hot block and mixed with 1ml of Wizard DNA-binding resin. DNA was isolated from the resin using a Wizard clean up column and washed with 2 ml of 80% isopropanol. Isopropanol was removed from the column by centrifugation and evaporation.

The DNA was then eluted with 50 µl sterile pre-warmed Milli-Q (MQ) H_20 and centrifuged for 1 minute at 13,000 rpm. 5 µl of this DNA was run on a diagnostic agarose gel to estimate the yield.

2.3.5 Restriction digestion of DNA

All restriction enzymes and reaction buffers were obtained from Promega unless otherwise specified. Reactions were typically carried out in 30 µl, containing 1-2 µg of DNA, 5-10 U of restriction enzyme in the appropriated buffer. The reaction was incubated at 37 °C (unless otherwise specified) for 1-4 hours. After plasmid DNA was digested it was run on an agarose gel along side uncut DNA to ensure that the restriction enzyme had cut the DNA as expected. For double digests of plasmid vectors, plasmid DNA was digested by each enzyme singly with the same protocol and run along side on an agarose gel to ensure that both enzymes had cut the DNA as expected.

2.3.6 DNA ligation

Ligation was carried out in a volume of 10 µl, (containing a molar ratio of vector:insert of 1:3), 0.5 U of T4 DNA ligase (Roche) and 1x T4 DNA ligase buffer. Ligation reactions were incubated overnight at 14-16 °C.

2.3.7 Competent cells for transformation

XL1-blue strain of *Escherichia coli* (*E. coli*) bacteria (Stratagene) were prepared as follows: cells were streaked onto a Luria-Bertani (LB) agar plate from a frozen (-80 °C) glycerol stock and grown overnight at 37 °C. A single colony was picked and used to inoculate 20 ml of LB medium [10 g/l bacto-tryptone, 5 g/l yeast extract, 10 g/l NaCl, adjusted to pH 7.0 with NaOH] and incubated overnight at 37 °C with shaking at 225 rpm. The culture was transferred to 500 ml of SOB [20 g/l peptone (DIFCO, Becton Dickinson) 5 g/l yeast extract, 0.5 g/l NaCl, 2.5 mM KCl and 10 mM $MgCl_2$]. The culture was incubated at 37 °C with shaking at 225 rpm until the optical density, measured at 550 nm (OD_{550}), reached 0.5-0.55, indicating that bacteria were in their exponential growth phase. The culture was then centrifuged at 2500 rpm (Beckman J2-M1 centrifuge, JA-14 rotor), for 15 minutes at 4 °C. The supernatant was discarded and the cells resuspended in 20 ml ice-cold RF1 solution [100 mM RbCl (Sigma), 50 mM $MnCl_2.4H_2O$ (Sigma), 30 mM potassium acetate, 10 mM $CaCl_2.2H_2O$, 15% w/v glycerol (Sigma), adjusted to pH 5.8 with 0.2 M acetic acid, filter sterilized (0.22 μM)] and incubated on ice for a further 15 minutes. Resuspended cells were centrifuged at 2500 rpm for 9 minutes at 4 °C, the supernatant discarded, and the pellet resuspended in 3.5 ml ice-cold RF2 solution [10 mM RbCl, 10 mM MOPS (3-N-morpholinopropanesulphonic acid; Sigma), 75 mM $CaCl_2.2H_2O$, 15% w/v glycerol, adjusted to pH 6.8 with 0.2 M acetic acid and filter sterilised (0.22 μM)].

The cell solution was incubated on ice for 15 minutes before being aliquoted and snap frozen in a dry ice/ethanol bath and subsequently stored at -80 °C.

2.3.8 Bacterial transformation

Bacterial transformations were performed using 50 µl frozen stocks of competent *E.coli* cells prepared as described in Section 2.3.7. 1-20 ng of plasmid DNA, or 2-4 µl of ligation mixture was gently mixed with the cells in a Falcon 352005 polypropylene tube (Becton Dickinson) and incubated on ice for 30 minutes. The DNA-cell mixture were then subjected to a heat shock at 42 °C for 90 seconds in a water bath and placed on ice for 2 minutes. 500 µl of SOC [SOB supplemented with 20 mM glucose (Sigma)] was added and this was incubated at 37 °C with shaking at 225 rpm for 1 hour to allow expression of the antibiotic resistance gene. 200 µl aliquots were plated on to LB-agar plates containing inhibitory concentrations of the appropriate antibiotic; 50 µg/ml ampicillin (Sigma) or 25 µg/ml zeocin (Invitrogen).

2.3.9 Small scale preparation of plasmid DNA

LB medium (2 ml) containing appropriate antibiotic was inoculated with a single bacterial colony and grown overnight at 37 °C with shaking at 225 rpm. The bacterial culture was then transferred to a 1.5 ml microfuge tube, centrifuged at 13,000 rpm for 30 seconds and the supernatant aspirated off. Cell pellets were

resuspended in 100 µl ice-cold solution I, containing 50 mM glucose, 25mM Tris.HCl, pH 8.0, 10 mM EDTA (Sigma), pH 8.0, by vortexing. 200 µl Solution II, containing 0.2 mM NaOH, 1% SDS, was added and carefully mixed by inversion. 150 µl ice cold solution III, containing 3 M potassium acetate, glacial acetic acid, was added and mixed carefully by inversion and stored on ice for 5 minutes. This mixture was then centrifuged at 13,000 rpm for 5 minutes and the supernatant transferred to a fresh microfuge tube. 400 µl phenol:chlorophorm (1:1; Amresco) was added and mixed by vortexing to extract the protein from the sample. The mixture was then centrifuged at 10,000 rpm for 2 minutes. The top layer of liquid (~400 µl) was transferred into a fresh microfuge tube containing 800 µl 100% ethanol, vortexed and centrifuged at 13,000 rpm for 5 minutes. The supernatant was aspirated off and the DNA pellet washed with 70% ethanol. Any excess ethanol remaining was evaporated by placing the un-capped microfuge tube into a hot block for 5-10 minute. The DNA was then resuspended in 20 µl autoclaved MQ H_2O containing 50 µg/ml RNAse A (Roche), incubated at 37 °C for 30 minutes and frozen at -20 °C for subsequent analysis.

2.3.10 Large scale preparation of plasmid DNA

The plasmid purification kit, HiSpeed Plasmid Midi Kit (Qiagen) was used according to the manufacturer's instructions as follows: LB medium (50 ml) containing the appropriate antibiotic was inoculated with a single colony or a stab from a glycerol stock and incubated overnight at 37 °C with shaking at 225 rpm.

Cells were harvested by centrifugation in 50 ml polypropylene tubes (Falcon, Becton Dickinson) at 6,000 x g (Beckman J2-M1 centrifuge) for 15 minutes at 4 °C. The pellet was resuspended in 6 ml ice cold buffer P1 [50 mM Tris.Cl (pH 8.0), 10 mM EDTA, 100 µg/ml RNAse A], by vortexing. 6 ml buffer P2, [200mM NaOH, 1% SDS], was added and mixed gently by inversion and incubated on ice for 5 minutes. 6 ml of chilled buffer P3, [3 M potassium acetate (pH 5.5)], was added and mixed gently by inversion, and incubated at room temperature for 10-15 minutes. The cell lysate was gently forced through a QIAfilter cartridge using a syringe plunger into a HiSpeed Tip, previously equilibrated with 4 ml QBT [750 nM NaCl, 50 mM MOPS (pH 7.0), 15% isopropanol, 0.15% Triton X-100], and allowed to pass through by gravity flow. The HiSpeed Tip was washed with 20 ml solution QC [1.0 M NaCl, 50 mM MOPS (pH 7.0), 15% isopropanol] and the DNA eluted with 5 ml solution QF [1.25 M NaCl, 50 mM Tris.Cl (pH 8.5), 15% isopropanol]. The DNA was precipitated with 0.7 volumes room temperature isopropanol and incubated at room temperature for 5 minutes. The precipitated DNA was then forced through a QIAprecipitator with a syringe, and the QIAprecipitator washed with 2 ml 70% ethanol. Air was forced through 2-3 times in succession to dry the membrane of the QIAprecipitator. The DNA was then eluted with 600 µl autoclaved MQ H_2O. The eluted DNA was then centrifuged in a heated vacuum centrifuge (DNA-mini, Heto-Holten) set at 45 °C for 30-60 minutes in order to concentrate DNA samples and ensure no isopropanol carryover, which could interfere with subsequent steps.

The yield of the DNA preparation was determined using either a SmartSpec Plus spectrophotometer (Bio-Rad), or a Beckman Coulter DU 800 spectrophotometer. The absorbance at λ=260 nm (A_{260}) and λ=280 nm (A_{280}) was measured. The DNA concentration was determined from the absorbance measured at λ=260 nm. A solution containing 50 μg/ml double-stranded DNA has an absorbance of 1 at λ=260 nm, calculated assuming that the mass of a nucleotide pair in DNA is 660 Daltons. The purity of the DNA was determined from the value of A_{260}/A_{280}, with approximately 1.8 indicating pure DNA. The DNA preparation was also run on an agarose gel for visualisation.

2.3.11 Nucleotide sequencing

Fluorescent-based capillary sequencing was carried out using the ABI Prism BigDye Terminator Cycle Sequencing Ready Reaction Kit 1.1 (ABI Applied Biosystems) according to the manufacturer's instructions: The reaction was carried out in a volume of 20 μl and contained 200-500 ng of template DNA, 3.2 pmol of sequencing primer (typically 18-22 bases in length) and 8 μl of Terminator Ready Reaction Mix (dye-labelled ddNTP terminators, unlabelled dNTPs, AmpliTaq DNA polymerase, $MgCl_2$ and buffer). The thermocycling reaction was performed for 25 cycles as follows:

96 °C for 30 seconds (denaturation)

50 °C for 15 seconds (annealing)

60 °C for 4 minutes (extension)

DNA was precipitated by the addition of 2 µl sodium acetate (pH 5.2) and 50 µl 99% ethanol per 20 µl of sample reaction. This was incubated on ice for 15 minutes and then centrifuged at 13,000 rpm for 15 minutes at room temperature. The supernatant was aspirated and the pellet washed in 500 µl 70% ethanol. Excess ethanol was removed by evaporation, by placing the un-capped microfuge tube in a hot block for 5-10 minutes. The DNA pellet was then resuspended in 10 µl of formamide. Samples were sequenced using an ABI Prism 3100-*Avant* Genetic Analyzer (ABI Applied Biosystems). Fluorescent DNA fragments were run on a 50 cm capillary array using POP 6 polymer (ABI Applied Biosystems) and the data was extracted using 3100-*Avant* Data Collection Software Version 1.0 (ABI Applied Biosystems). Sequences were analysed using MacVector 7.2.2 software (Accelrys).

2.4 Mammalian cell line culture and transfection

2.4.1 Mammalian cell-line maintenance

A subclone of human embryonic kidney (HEK)-293 cells, tsA201 cells were obtained from Dr William Green (University of Chicago, IL, USA). This HEK cell line stably expresses a temperature sensitive SV40 large T-antigen. The Madin-Darby canine kidney (MDCK) epithelial cell line was obtained from Dr Mark Marsh, University College London. Cell lines were kept in a liquid nitrogen freezer (~-150 °C) for long-term storage in screw-top cryotubes. Cells were kept in 1 ml Freezing Mix, containing 80% cell culture media, 10% heat inactivated foetal calf serum (FCS; Sigma) and 10% dimethylsulphoxide (DMSO).

2.4.2 Thawing cell lines

Cell lines were removed from long-term liquid nitrogen storage and the cryotube immediately placed at 37 °C to thaw. Cells were transferred to 15 ml polypropylene tubes (Falcon, Becton Dickinson) containing room temperature cell culture medium, mixed gently by pipette action and centrifuged at 900 rpm for 3 minutes. The medium was carefully removed by aspiration and the cell pellet carefully resuspended in a further 10 ml cell culture medium and centrifuged as above. The cell pellet was then resuspended in 37 °C cell culture medium and transferred to cell culture dishes and incubated as described (Section 3.4.3)

2.4.3 Cell culture

Mammalian tsA201 cells and MDCK cells were grown on 6 cm or 10 cm cell culture dishes (Corning) in Dulbecco's modified Eagle's medium (DMEM) containing 2 mM L-Glutamax (Gibco-Invitrogen), supplemented with 10% heat inactivated FCS, 100 units/ml penicillin/100 µg/ml streptomycin (Gibco-Invitrogen), at 37 °C in a humidified incubator containing 5% CO_2. Cells were passaged by aspiration of conditioned cell-culture medium, washing once with 4-6 ml PBS and trypsinised with 3-4 ml trypsin:PBS (1:1) solution for 30 seconds at room temperature (tsA201 cells), and 10-15 minutes at 37 °C (MDCK cells). The trypsin:PBS solution was removed and cell culture dishes tapped vigorously to dislodge cells from the culture dish. Cells were resuspended in 3-5 ml fresh room temperature culture medium and passed through the constricted tip of a 5 ml pipette several times to separate cell aggregates into a homogeneous mixture of dissociated single cells. The cells were then re-seeded into fresh culture dishes at various dilutions, depending on subsequent use, and topped up with culture medium and maintained as described above. Cells were discarded after 25-30 passages.

2.4.4 Transient transfection

Cells were transfected using the Effectene Transfection Kit (Qiagen) using a modified manufacturer's protocol: Cells were trypsinised and re-seeded in 3 ml

of medium (10 cm culture dish) 4-6 hours prior to transfection in order to achieve ~ 30% confluency at the time of transfection.

For tsA201 cell transfections in a 10 cm dish, 0.6 μg of plasmid DNA was added to 120 μl of Buffer EC in a sterile microfuge tube and allowed to equilibriate for 5 minutes. 4.8 μl of Enhancer (DNA condensing enhancer solution) was added, mixed by pipetting and incubated for 5 minutes. 13 μl of Effectene (non liposomal lipid formulation which coats condensed DNA with cationic lipids) was added, mixed by pipetting, and incubated for a further 10 minutes. 600 μl of pre-warmed (37 °C) fresh culture medium was added, mixed by pipetting, and added drop-wise onto the cells making a final volume of approximately 3.7 ml (~ 5x final dilution of transfection mix). After 16 hours, 6-10 ml growth medium was added.

For MDCK cell transfections in a 10 cm dish, the same protocol as used for tsA201 transfection was used except a higher ratio of transfection mixture to medium (2:1) was used (~ 2.5x final dilution of transfection mix).

For electrophysiological studies, tsA201 cells were plated onto 13 mm glass cover slips (VWR international) coated with 10 μg/ml collagen and 10 μg/ml poly-L-lysine (Sigma) in 3.5 cm culture dishes (Falcon, Becton Dickinson), containing 1 ml culture medium. The same transfection procedure was used as above (for

tsA201 cells) maintaining ~5x final dilution of transfection mix. Cells were used 24-72 hours post transfection.

2.5 Primary neuronal cultures and transfection

2.5.1 Primary hippocampal neuronal cultures

Primary hippocampal neuronal cultures were prepared from embryonic stage 18 (E18) Sprague Dawley rats, obtained from Biological Services (UCL). Primary cultures were maintained at 37 °C in a humidified incubator containing 5% CO_2.

2.5.2 Isolation and culture of hippocampal neurones

Pregnant E18 rats were euthanased by dislocation of the neck and the uterus sacs containing the pups quickly removed via a posterior-anterior abdominal incision and placed in a sterile Petri dish on ice. The pups were carefully exposed from their uterus sacs and quickly decapitated using sharp fine-scissors and their heads placed in ice-cold dissection media [15 ml 10x Hanks' balanced salt solution (HBSS; Gibco-Invitrogen), 1.5 ml 1 M 4-(2-hydroxyethyl)-1-piperazine-ethane-sulphonic acid (HEPES; Gibco-Invitrogen), made up to 150 ml with H_2O (Baxter) and sterile-filtered]. The brains were quickly removed, placed in fresh dissection medium, the hippocampi isolated by careful dissection to avoid tissue damage.

Isolated hippocampi were then transferred to a category 2 laminar flow hood where they were transferred to a sterile 15 ml polypropylene tubes (Falcon, Becton Dickinson) containing fresh dissection medium. The volume was adjusted to 4.5 ml and 0.5 ml 2.5% trypsin (Sigma) added, mixed by inversion and incubated at 37 °C for 15 minutes in a humidified incubator containing 5% CO_2 (with loose cap allowing access to air). The dissection medium was carefully replaced with fresh room temperature dissection medium, mixed by inversion and incubated for a further 5 minutes at room temperature. This wash step was repeated, after which the dissection medium was replaced with 1 ml attachment medium [500 ml minimum essential medium (MEM) with Earle's salts and L-glutamine supplemented with 50 ml heat inactivated horse serum, 5 ml 100 mM sodium pyruvate/MEM, 6.6 ml 45% glucose (Gibco-Invitrogen)]. The attachment media containing the hippocampi were then vigorously passed through two consecutively reduced diameter glass Pasteur pipettes with polished tips 10-15 x each to achieve a homogenous solution containing dissociated neurones. Neurone number was calculated in a hemocytometer with erythrosine B used at a 1:4 dilution to identify living cells. Six centimetre tissue culture dishes, containing 3 ml 37 °C attachment medium and 13 mm glass cover slips (Assistent), pre-baked and coated with sterile 0.1 mg/ml poly-L-lysine (PLL) were then seeded to achieve a density of ~300,000 neurones per (6 cm) dish. 6-18 hours later the attachment medium was replaced with maintenance medium [500 ml Neurobasal A medium supplemented with 10 ml B27 supplement, 5 ml L-glutamine, 5 ml 100

units/ml penicillin/100 μg/ml streptomycin and 6.6 ml 45% glucose (Gibco-Invitrogen)].

2.5.3 Transfection of hippocampal neurones

Neurones were transfected using a variation of a previously described calcium phosphate method (Jiang and Chen, 2006). Briefly, a total of 15 μg DNA was used to transfect each 6 cm dish. Two tubes were prepared: 'Tube A' containing 375 μl 2x HBSS (pH 7.05) and 'Tube B' containing 15 μg total DNA and sterile water up to a volume of 328.5 μl to which 46.5 μl 2M $CaCl_2$ solution had previously been added dropwise and mixed by gentle swirling. Tube A was gently mixed dropwise (1/8 at a time) into Tube B and the solution left to incubate at room temperature for 20 minutes. The DNA/transfection solution was added dropwise to the 6 cm dishes containing neurones in 1.5 ml fresh neuronal maintenance medium and incubated under standard conditions for 40-60 minutes. Transfection dishes were the washed 3x with 3 ml fresh maintenance media and then incubated with 3 ml pre-conditioned media until processing for immunostaining.

2.6 Radioligand binding

Radioligand binding was performed on either intact cells (to determine levels of receptor expressed on the cell surface) or permeabilised cells (to determine the level of total cellular receptor).

2.6.1 [^{125}I]α-bungarotoxin and [^{3}H]methyllycaconitine binding

Radioligands [^{125}I]α–bungarotoxin ([^{125}I]αBTX; specific activity 7.4 TBq mmol^{-1}) and [^{3}H]MLA (specific activity 2.2 TBq mmol^{-1}) were purchased from GE Healthcare and Perkin Elmer, respectively. For both intact-cell and cell membrane measurements, cell monolayers were rinsed and collected in HBSS using a cell scraper (Corning) and pelleted by gentle centrifugation. Cell membranes were prepared by freeze/thawing of cell pellets and were resuspended in phosphate buffer containing protease inhibitors (with final concentrations of 1 μg ml^{-1} pepstatin, 2 μg ml^{-1} leupeptin, 2 μg ml^{-1} aprotinin), transferred to 5 ml polystyrene assay tubes and incubated with radioligand (10 nM [^{125}I]αBTX or 10nM [^{3}H]MLA) for 2 hours, shaking, on ice. In the case of αBTX binding, 1% bovine serum albumin was added to the assay. Non-specific binding was determined with 1 mM nicotine and 1 mM carbachol. For cell-surface [^{125}I]αBTX binding, cells were prepared as above except, after pelleting, cells were resuspended by gentle agitation and pipetting, and assayed in HBSS (containing protease inhibitors, as above) at room temperature. [^{125}I]αBTX and [^{3}H]MLA

labelled samples were harvested using a Brandel cell harvester (Model M36, Semat) onto Whatman GF/A and Whatman GF/B filters, respectively, pre-soaked for at least 1 hour in 0.5% w/v polyethylene-imine. Radioactive counts were assayed in a gamma counter (Wallac 1261 Multigamma) for [^{125}I]αBTX binding and by a scintillation counter (Beckman LS 6500) for [^{3}H]MLA binding.

2.6.2 Protein assay and cell counting

The protein concentration of cell membrane preparations was determined using a Bio-Rad *DC* protein assay according to the manufacturer's instructions. Typically, 20 µl of diluted sample (1/10) or bovine serum albumin (BSA) standard was added to a semi-microcuvette (Starstedt) and mixed with 100 µl of Reagent A (alkaline copper tartrate solution). 800 µl of Reagent B (a dilute Folin Reagent) was added, the reaction mixed by vortexing and incubated at room temperature for 30 minutes. Protein concentration was determined by measurement of the absorbance at λ=750 nm with a spectrophotometer (SmartSpec Plus, Bio-Rad). Samples were compared to BSA standards at concentrations of 0.1, 0.2, 0.4, 0.8, 1.0 and 1.2 mg/ml.

2.7 Metabolic labelling and immunoprecipitation

2.7.1 Metabolic labelling

To facilitate immunoprecipitation, an eight amino acid FLAG epitope tag (DYKDDDDK) was introduced at the extreme C-terminus of the loop chimaeric constructs by site-directed mutagenesis, using the QuikChange mutagenesis system (Stratagene, Amsterdam) and primers previously described (Table 2.2). Transfected tsA201 cells were metabolically labelled as described previously (Cooper and Millar, 1997). Briefly, after growth in methionine-free medium for 15 min, cells were labelled with 9-12 MBq Pro-mix, a mixture of [^{35}S]methionine and [^{35}S]cysteine, (GE Healthcare) in 3.5 ml methionine-free medium for 3 hours. Complete medium containing 10% heat-inactivated FCS was then added and the cells incubated for a further 3 hours. Cells were washed twice with 6 ml phosphate buffered saline (PBS) and harvested into 500 µl ice-cold lysis buffer (150 mM NaCl, 50 mM Tris-HCl pH 8.0, 5 mM EDTA and 1% Triton-X100) containing protease inhibitors (0.25 mM phenylmethylsulfonyl fluoride, 1 mM *N*-ethylmaleimide and 2 µg/ml, each, of leupeptin, aprotinin and pepstatin). Solubilisation and all subsequent steps were performed at 4°C. The cell lysate was pre-cleared by incubation overnight with 35 µl protein G-Sepharose (GE Healthcare) in a 1:1 mixture with lysis buffer. Non-solubilised material was pelleted by centrifugation at 16,000 x g for 15 min. Cell lysates were incubated with primary antibody for 3 hours. The antibody-receptor complex was

immunoprecipitated by the addition of 30 µl protein G-Sepharose, incubated for a further 3 h and isolated by centrifugation. Samples were washed 4 times with 1 ml lysis buffer. Samples were examined by SDS polyacrylamide gel electrophoresis followed by autoradiography as described previously (Lansdell *et al.*, 1997).

2.7.2 SDS-polyacrylamide gel electrophoresis of proteins

Discontinuous sodium dodecyl sulphate polyacrylamide gel electrophoresis (SDS-PAGE), was carried out to separate polypeptides using an 8% resolving gel [21.1 ml H_2O, 8 ml 40% acrylamide, 10 ml 1.5M Tris (pH 8.8), 0.4 ml 10% SDS, 0.4 ml 10% ammonium persulphate and 24 µl tetramethylethylenediamine (TEMED)] with a 5% stacking gel [5.8 ml H_2O, 1 ml 40% acrylamide, 1 ml 1.5 M Tris (pH 6.8), 80 µl 10% SDS, 80 µl 10% ammonium persulphate and 8 µl TEMED]. Total gel size was 15 cm by 20 cm and 0.15 cm thick. The electrophoresis apparatus was assembled and Tris glycine running buffer (25 mM Tris, 250 mM glycine and 0.1% SDS) was added to the upper and lower reservoirs. Protein samples were resuspended with loading buffer [final concentration of constituents: 50 mM Tris-HCl (pH 6.8), 2% SDS, 0.1% bromophenol blue, 10% glycerol and 100 mM dithiothreitol for reducing conditions]. Broad range Rainbow coloured markers (Promega) and [^{14}C] methylated proteins (GE Healthcare) were used to estimate protein band sizes. The samples were loaded and passed through the stacking gel at 55 mA and then separated overnight through the resolving gel at 8 mA. The gel

was fixed (25% methanol and 10% acetic acid) for 30 minutes, washed briefly in deionised H_2O and soaked in Amplify (GE Healthcare) for 30 minutes. The gel was then transferred onto damp Whatman 3MM filter paper, covered with saran wrap and dried under vacuum at 80 °C (typically for 2-4 hours). The dried gel was then exposed to autoradiographic film.

2.8 Immunofluorescence microscopy

MDCK cells were washed three times with PBS or until loose cells and cell debris were removed from the cell monolayer. The polyester membrane was carefully excised from the surrounding support using a scalpel, marked for orientation and fixed in 3% PFA for 15-30 minutes. The membranes were then washed five times in HBSS, permeabilised with 1% Triton/HBSS, for 15-30 minutes and blocked for 30 minutes in blocking solution containing 2% BSA/5% FCS/1% Triton/HBSS. Cells were incubated for two hours at room temperature, or overnight at 4°C in blocking solution containing Alexa-488 α-bungarotoxin (Gibco-Invitrogen) and DECMA-1 rat monoclonal antibody against E-cadherin, (U3254; Sigma-Aldrich). Cells were washed five times in HBSS, re-blocked for 30 minutes, then incubated for one hour at room temperature, or overnight at 4°C in blocking solution containing rhodamine-conjugated goat-anti-rat IgG secondary antibody (31680; Pierce). Cells were washed five times in HBSS, once in water and then mounted under glass in FluoSave (Calbiochem) mounting fluid, with the apical cell surface

facing upwards. Confocal images were obtained with a Zeiss LSM 510 Meta confocal microscope and LSM acquisition software. Images were processed using Volocity image analysis software (Improvision). For immunofluorescent labelling of tsA201 cells and hippocampal neurones, treatment was the same as with MDCK cells, except as where specified, mAb 1234A (Peng and Froehner, 1985) against Rapsyn was used and Rhodamine conjugated α-bungarotoxin (Molecular Probes) was used. Hippocampal neurones were examined with a Zeiss Axiophot microscope using appropriate oil-immersion objectives.

2.9 Intracellular calcium assay

Transfected cells were re-plated onto pre-coated poly-L-lysine (PLL)-coated black-walled 96-well plates (Marathon Laboratories) 18-20 hours post transfection. Approximately 24 hours after plating, the culture medium was removed and cells washed with 1x 100 µl HBSS per well and then incubated in 50 µl of 1 µM Fluo-4-acetoxymethyl (Fluo-4-AM) ester (Invitrogen-Molecular Probes) in HBSS containing 0.02% Pluronic F-127 (Invitrogen-Molecular Probes) for 45-60 minutes at room temperature and in the dark. Cells were rinsed 2x 160 µl HBSS per well and assayed using a Fluorometric Imaging Plate Reader (FLIPR; Molecular Devices) in 160 µl high calcium buffer (HCB; HBSS supplemented with 18.8 mM $CaCl_2$, 8.8 mM sucrose and 6.3 mM HEPES). Cells were excited at λ=488 nm and the emitted fluorescence passed through a 510 to

570 nm bandpass interference filter before detection with a cooled CCD camera. A range of 1, 1-dimethyl-4-phenylpiperazinium (DMPP) agonist concentrations (5X) were prepared in HCB in a separate a 96-well plate (Sarstedt) and 40 µl delivered, via an automated 96-tip pipettor, to the corresponding well of the cell-plate containing 160 µl HCB. Different drug concentrations were typically repeated in triplicate. Fluorescence measurements were recorded simultaneously for all 96 wells at one-second intervals, for 120 seconds in total, with continuous agonist addition after 25 seconds and values expressed as arbitrary fluorescence units.

FLIPR data was analysed with Microsoft Excel and GraphPad Prism software. The value for the agonist-induced response at each time-point was divided by the lowest value before agonist application to normalise the data. Peak responses were calculated from the mean of triplicate samples and the results from mock-transfected (empty vector) cells on the same 96-well plate, which acted as a negative control, were subtracted from positively transfected cells. Results were averaged over $\geq n=3$ independent experiments. Data plots and dose-response curves were created and fitted with the appropriate equations in Graph Pad Prism software.

2.10 Electrophysiological recording

HEK tsA201 cells, grown on glass cover slips coated in collagen and poly-L-lysine, were co-transfected with pEGFP-C2 (Clontech), encoding enhanced green fluorescent protein, and plasmids containing either wild type or chimaeric subunit cDNA in the ratio of 1:10.

2.10.1 Whole-cell patch-clamp recording

Whole-cell recordings were performed at room temperature, 24-72 hours after transfection using cells that were identified as expressing GFP by fluorescence microscopy. Recording solution contained (in mM): 110 NaCl, 5.4 KCl, 0.8 $MgCl_2$, 1.8 $CaCl_2$, 25 glucose, 0.9 NaH_2PO_4, 44 $NaHCO_3$. Borosilicate electrodes (GC150F-7.5; Harvard Apparatus) of resistance 4-8 MΩ contained (in mM) 140 CsCl, 10 HEPES, 10 EGTA, 0.5 $CaCl_2$, 29.53 CsOH, pH adjusted to 7.26. The holding potential was –60 mV. Fast cell superfusion was achieved with a theta-barrelled application pipette made from 1.5 mm diameter theta tubing (AH-30-0114; Harvard Apparatus), which was moved laterally using a stepper motor. 20-second applications of 50 μM DMPP were applied and evoked currents recorded using an Axopatch 200B amplifier. These were digitised online at 10 kHz using the software WinEDR (Strathclyde Electrophysiology Software; www.strath.ac.uk/Departments/PhysPharm) after filtering and further

amplification to provide a low-gain 0 Hz–2 kHz record that was used to measure the agonist-induced mean current.

2.11 Desensitisation analysis

The kinetics of desensitisation were analysed on 20 second agonist applications. Responses were inverted and fitted with a single exponential or the sum of two exponential functions:

$$I(t)=SS+I_{max} \cdot e^{-(t/\tau)} \text{ [single] or } I(t)=SS+I_{max1} \cdot e^{-(t/\tau 1)} + I_{max2} \cdot e^{-(t/\tau 2)} \text{ [double]}$$

Where t is the whole cell current, I_{max} is the peak of the whole cell current, SS is the steady state current, t is the time after the peak of the whole cell current and τ is the time constant of desensitisation. The fit of a single or double exponential was performed by inverting the current and fitting to the appropriate function using Prism software (GraphPad). Thus the time constants (τ) and relative amplitudes for double exponential function and the steady state desensitisation were obtained. Where a double exponential fit was used, a weighted time constant was calculated by multiplying each time constant by the proportion of its starting amplitude.

2.12 Conductance estimation from noise analysis

A high-gain bandpass (2 Hz–2 kHz butterworth filter) recording was used for variance and spectral density analysis. The recording was divided into segments of 0.82 seconds duration and edited to remove any segments with obvious artefacts.

2.12.1 Noise variance analysis

The relationship between the variance and the single-channel current can be derived from the binomial theorem, assuming that channels open independently from one another (Traynelis and Jaramillo, 1998). For a cell with N channels that have a single-channel current of i, the mean current (I) is equal to:

$$I=iNp$$

where p is the probability that the channel is open. The current variance (σ^2_I) is equal to:

$$\sigma^2_I=i^2Np(1-p)$$

When this is rearranged and N is substituted for:

$$\sigma^2_I=iI(1-p)$$

This means that when p is small (<0.1) then the variance is directly proportional to the mean current, with the single-channel current as the constant of proportion. The variance (after subtraction of baseline variance) of each high gain AC segment was determined and plotted against the mean current (after subtraction of baseline current) of the equivalent low gain DC segment. This was then fitted with a straight line (y=ix+c; where c was constrained to 0) by linear regression, and the single-channel conductance derived from the slope of the line (i), divided by the holding potential of the recording (-60 mV in this case).

2.12.2 Noise power spectral density analysis

The relationship between the variance of the current fluctuations and the kinetics of receptor activation was examined by generating a power spectrum. The objective was to show how energy (amplitude squared per frequency) is distributed across the frequencies of the variance.

A 10% cosine taper window was applied to each segment and the single-sided spectral density computed by fast Fourier transform and averaged over 96 logarithmically spread frequency ranges. The mean background spectrum was subtracted from the mean spectrum in the presence of the agonist to give the net agonist-induced noise spectrum. The single channel conductance was calculated from the variance of the noise and from integration of the net power spectrum

fitted with a single or the sum of two Lorentzian components as appropriate (Dempster, 2001):

$$G(f)=S_{(0)}/1+(f/f_c)^2 \text{ [single]} \text{ or } G(f)= S_{(0)1}/1+(f/f_{c1})^2+ S_{(0)2}/1+(f/f_{c2})^2$$

Where t is the spectral density, $S_{(0)}$ is the asymptotic spectral density at zero frequency, f is frequency and f_c is half power frequency. The time constant $\tau=1/(2\pi f_c)$ is an estimate of the mean single channel burst length (reviewed by Traynelis and Jaramillo, 1998). For two-component spectra a weighted noise time constant was calculated from $\tau_w = \tau_1 A_1 + \tau_2 A_2$ where A_1 and A_2 are the relative areas of each Lorentzian component. The number of Lorentzian equations used to fit the data does not reflect the number of conductance states or the likely number of kinetic states in the receptor activation mechanism. The single channel conductance, γ, was calculated from:

$$\gamma=S_{(0)}/ 4I_m(V-V_{rev})$$

Where I_m is the mean current, V is the holding potential and V_{rev} is the reversal potential of the receptor.

2.13 Data manipulation and statistical analysis

All statistical analysis was performed in Microsoft Excel and GraphPad Prism software, with a minimum significance level of $p<0.05$. For multiple comparisons, ANOVA (analysis of variance) was used and significances calculated using the Tukey-Kramer post-test allowing for unequal sample sizes. As ANOVA assumes equal variances, Bartlett's test was employed to determine if differences in variances between groups of data were significant. In those cases where significant differences were observed, the raw data was transformed by converting values to their logarithms to equalise the variances and make the distribution more Gaussian. ANOVA is less robust when analysing non-Gaussian distributed values from small sample sizes (<12 or so) and with unequal number of samples, which was the case here.

Chapter 3

Characterisation of nAChR loop chimaeras

Chapter 3

Characterisation of nAChR loop chimaeras

3.1 Introduction

As discussed in the Introduction (Chapter 1), individual nAChR subunits adopt a complex membrane topology, comprising a large extracellular N-terminal agonist-binding domain, four α-helical transmembrane domains (M1-M4), and a large intracellular loop of variable length between M3 and M4 (Green and Millar, 1995). Previous studies have indicated that this intracellular loop domain of nAChRs is important for interaction with intracellular proteins (Jeanclos *et al.*, 2001; Huebsch and Maimone, 2003), receptor targeting (Williams *et al.*, 1998; Xu *et al.*, 2006) and ion channel properties (Kelley *et al.*, 2003; Hales *et al.*, 2006; Gee *et al.*, 2007).

Most nAChR subunits form only heteromeric complexes in which α subunits must co-assemble with at least one other type of subunit to generate a functional receptor. A well-characterised example is the nAChR expressed in the adult neuromuscular junction which is assembled from four different subunits (two copies of the α1 subunit co-assembled with a single copy of each of the β1, δ and

ε subunits). Similarly, most nAChRs expressed in the nervous system (neuronal nAChRs) are heteromeric complexes (Le Novère and Changeux, 1995; Millar, 2003; Alexander *et al.*, 2007). There are a few examples of nAChR subunits which are able to generate functional homomeric receptors, notably α7, α8 and α9 (Couturier *et al.*, 1990; Elgoyhen *et al.*, 1994; Gerzanich *et al.*, 1994). However, in each case, there is evidence that these subunits are also able to form heteromeric complexes in at least some species (Keyser *et al.*, 1993; Gotti *et al.*, 1994; Elgoyhen *et al.*, 2001). As a consequence of the propensity of nAChR subunits to assemble into heteromeric complexes, it can be difficult to examine the influence of individual subunits (or individual subunit domains) in isolation. To examine the influence of intracellular loop domains from individual subunits independently, a series of subunit chimaeras has been constructed and characterised.

Subunit chimaeras have been constructed, each containing a common extracellular, agonist/antagonist binding domain from the nAChR α7 subunit and the transmembrane domains of the 5-HT_{3A} subunit, and the variable intracellular (M3-M4) loop domain from all vertebrate neuronal nAChR subunits (α2-α10 and β2-β4) and from the muscle nAChR α1 and β1 subunits. By constructing an extensive series of related subunit chimaeras containing a variety of different intracellular loop domains, it has been possible to examine the influence of this domain upon aspects of receptor assembly, targeting and function. This was achieved using a variety of experimental techniques including radioligand

binding, immunoprecipitation, fluorescence confocal microscopy and whole-cell electrophysiology.

3.2 Design and construction of loop chimaeras

The starting point for constructing the series of 'loop chimaeras' (Figure 3.1) was a previously described nAChR/5-HT_3R subunit chimaera, $\alpha7^{4TM\text{-}5HT3A}$ (Gee *et al.*, 2007). The $\alpha7^{4TM\text{-}5HT3A}$ chimaera contains the extracellular N-terminal agonist/antagonist binding domain and the M3-M4 intracellular loop domain of the rat nAChR α7 subunit; and the four transmembrane domains (4-TM) of the mouse 5-HT_{3A} subunit. This receptor construct was in turn modelled upon the previously described nAChR/5-HT_3R chimaera, $\alpha7^{V201\text{-}5HT3A}$ (Eiselé *et al.*, 1993; Cooper and Millar, 1998). The $\alpha7^{V201\text{-}5HT3A}$ chimaera contains the N-terminal extracellular domain of the rat nAChR α7 subunit and the remaining C-terminal domain (4-TM domain including the M3-M4 loop domain) of the mouse 5-HT_{3A} subunit. The sequences were spliced together at position Val^{201} (numbered according to the *Torpedo* α1 subunit). Like the native nAChR α7 and 5-HT_{3A}R subunits, both $\alpha7^{V201\text{-}5HT3A}$ and $\alpha7^{4TM\text{-}5HT3A}$ are able to form functional homomeric ion channels (Eiselé *et al.*, 1993; Cooper and Millar, 1998; Gee *et al.*, 2007). In contrast to the considerable problems which have been encountered in expression of the nAChR α7 subunit in several mammalian cell lines (Cooper and Millar, 1997; Kassner and Berg, 1997; Rangwala *et al.*, 1997), a major advantage of the

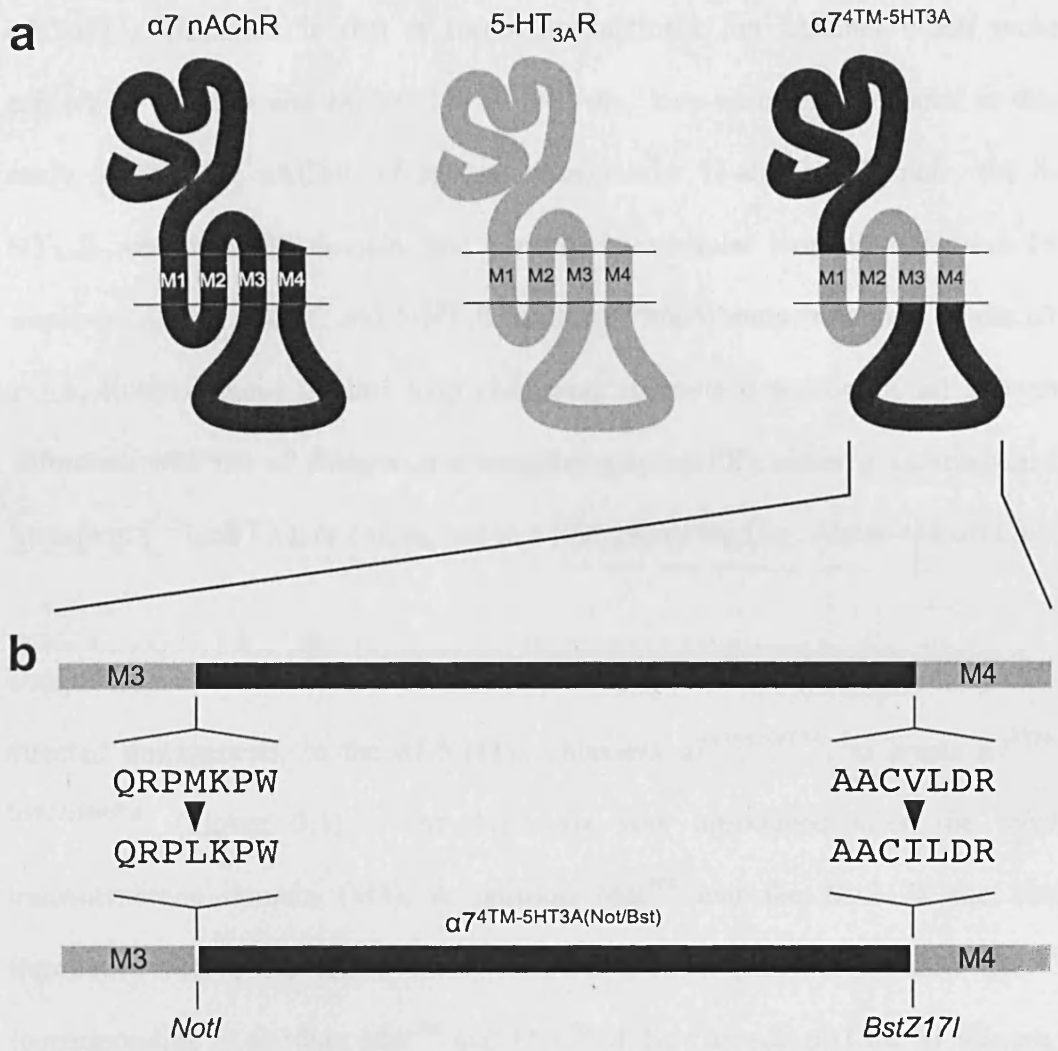

Figure 3.1 Cloning strategy and creation of $\alpha7^{4TM\text{-}5HT3A(Not/Bst)}$ chimaera. **(a)** Schematic representation showing the membrane topology of the nicotinic acetylcholine receptor α7 subunit (left panel) and related Cys-loop receptor family member the 5-HT_{3A} subunit (middle panel) used to create the chimaeric receptor, $\alpha7^{4TM\text{-}5HT3A}$ (right panel). Note that $\alpha7^{4TM\text{-}5HT3A}$ contains the extracellular N-terminal domain and intracellular M3-M4 loop domain from the α7 nAChR, while the transmembrane regions (M1-M3 and M4) originate from the 5-HT_{3A}R. **(b)** Cloning strategy used to create $\alpha7^{4TM\text{-}5HT3A(Not/Bst)}$. Site-directed mutagenesis was used to insert *Not*I and *Bst*Z17I restriction sites flanking the M3-M4 intracellular loop of $\alpha7/^{4TM\text{-}5HT3A}$ to create $\alpha7^{4TM\text{-}5HT3A(Not/Bst)}$. Note the two amino acid changes, $Met^{308}\rightarrow Lys^{308}$ and $Val^{405}\rightarrow Iso^{405}$, resulting from the insertion of the *Not*I and *Bst*Z17I sites, respectively.

α7/5-HT_{3A} chimaera is that it forms a functional ion channel much more efficiently (Cooper and Millar, 1998). All the 'loop chimaeras' created in this study contain the nAChR α7 subunit extracellular N-terminal domain, the 5-HT_{3A}R subunit 4-TM domain, and variable intracellular loop domain from 16 members of the nAChR and 5-HT_3R families. Importantly, retention of the α7 extracellular domain in the 'loop chimaeras' permits detection of all subunit chimaeras with the α7 antagonist α-bungarotoxin (αBTX); either in radiolabelled form (e.g. [^{125}I]αBTX), or conjugated to a fluorescent tag (e.g. Alexa-488 αBTX).

Unique *Not*I and *Bst*Z17I restriction endonuclease sites were introduced, by site-directed mutagenesis, to the α7/5-HT_{3A} chimaera $\alpha7^{4TM\text{-}5HT3A}$, to create $\alpha7^{4TM\text{-}5HT3A(Not/Bst)}$ (Figure 3.1). The *Not*I site was introduced after the third transmembrane domain (M3), at position Met^{308} and the *Bst*Z17I site was introduced before the fourth transmembrane domain (M4) at position Cys^{404} (corresponding to residues Met^{308} and Met^{404} of the *Torpedo* nAChR α1 subunit, respectively; Noda *et al.*, 1982). The restriction sites were selected based on the positional requirements (flanking the loop), while keeping the number of nucleotides altered to a minimum and avoiding any residue changes that could be predicted to alter the protein drastically.

Compatible *Not*I and *Bst*Z17I restriction sites were introduced to the equivalent sites (determined by protein sequence alignment), either side of M3-M4 intracellular loop region, of the vertebrate neuronal type nAChR subunits (α2-α10

and β2-β4), the muscle type nAChR subunits (α1 and β1), and of the 5-HT_{3B} subunit. The *Not*I and *Bst*Z17I restriction sites were incorporated to the oligonucleotide primers used to amplify the M3-M4 intracellular loop segments during a standard high-fidelity polymerase chain reaction (PCR). All the loop segments were amplified from rat cDNA clones, except in the case of the nAChR α8 subunit, which was amplified from chick cDNA and the 5-HT_{3B} subunit which was amplified from human cDNA. The relative lengths of the M3-M4 intracellular loop domain is highly variable between subunits and consists of between 78 and 143 amino acids in most cases, except for the nAChR α4 subunit which is 259 amino acids in length (Figure 3.2). The intracellular loops were then ligated into the $\alpha7^{4TM\text{-}5HT3A(Not/Bst)}$ construct following appropriate digestion with *NotI* and *Bst*Z17I restriction enzymes. The series of nAChR and 5-HT_3R subunit M3-M4 intracellular loop domain chimaeras will be referred to as $\alpha7/5\text{-}HT_{3A}^{\alpha1\text{-}loop}$ (etc.) or, more simply, as 'α1 loop' chimaera (etc.). All loop chimaeras were cloned into the pZeoSV2+ mammalian expression vector containing a constitutive SV40 promoter region and zeocin antibiotic selection.

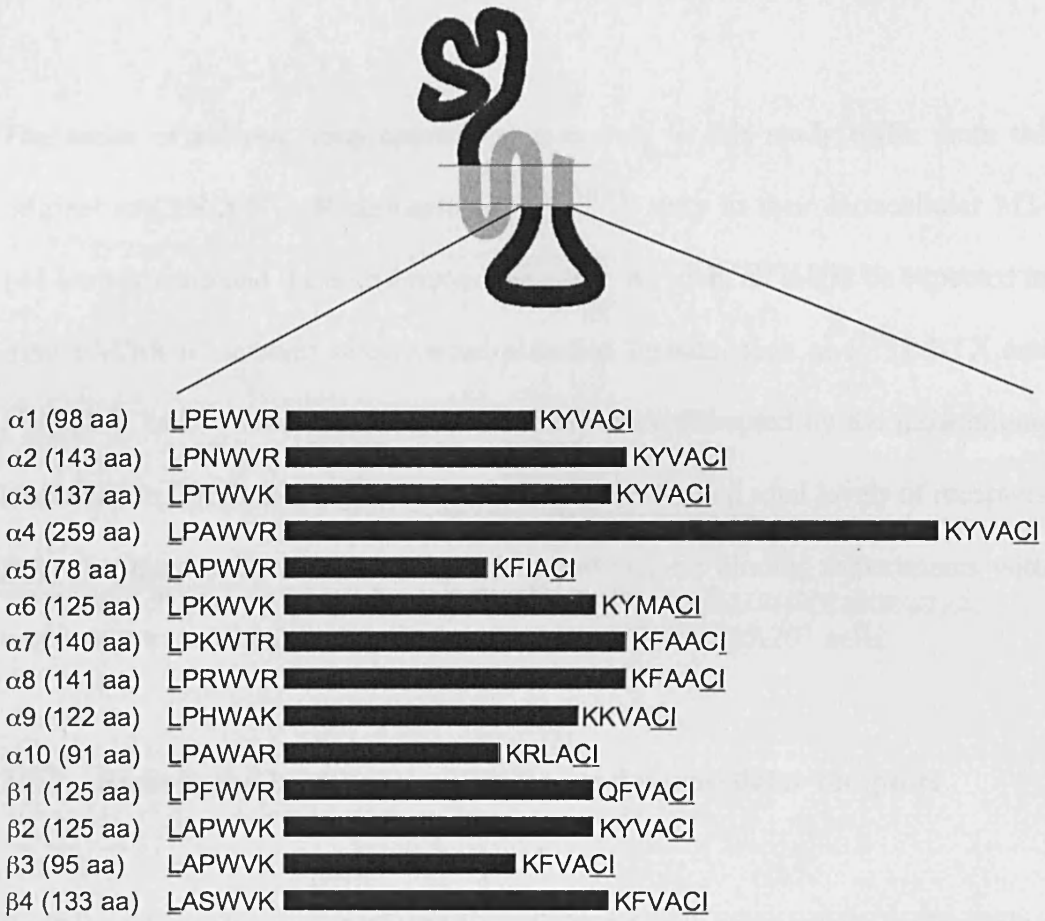

Figure 3.2 Intracellular (M3-M4) loop chimaeras. A series of subunit chimaeras was constructed containing the intracellular M3-M4 loop domain from all vertebrate nAChR α and β subunits (α1-α10 and β1-β4). All subunit chimaeras contained a common extracellular domain (from the nAChR α7 subunit) and common transmembrane domains (from the 5-HT_{3A} subunit). Horizontal lines represent the approximate relative length of the various intracellular loop domains of each subunit. The exact number of amino acids (aa) within each of these subunit domains is indicated next to the subunit name. To illustrate more clearly the location of the loop domains examined, the six N- and C-terminal amino acids of each domain are indicated. Amino acids which were altered by the introduction of *Not*I and *Bst*Z17I restriction enzyme sites are underlined.

3.3 Characterisation of loop chimaeras by radioligand binding

The series of subunit 'loop chimaeras' examined in this study differ from the original nAChR/5-HT_{3A}R chimaera ($\alpha7^{4TM\text{-}5HT3A}$) only in their intracellular M3-M4 loop domain and the added restriction sites. As such, all might be expected to bind nAChR α7 subunit selective radiolabelled ligands, such as [^{125}I]αBTX and [^{3}H]MLA, unless subunit folding or assembly were disrupted by the intracellular loop domain. Both the levels of cell-surface receptors and total levels of receptors from disrupted cells were investigated by radioligand binding experiments with transiently transfected human embryonic kidney (HEK) tsA201 cells.

3.3.1 Radioligand binding to cell-surface and intracellular receptors

Radioligand binding was performed on disrupted cell preparations to determine levels of total-membrane binding. Initial radioligand binding studies were performed with [^{125}I]αBTX, but results were inconsistent and difficult to interpret due to high levels of non-specific binding in disrupted cell preparations (data not shown). To reduce problems associated with non-specific binding, studies with disrupted cells were performed with tritiated methyllycaconitine ([^{3}H]MLA), rather than [^{125}I]αBTX. For all loop chimaeras, specific binding of [^{3}H]MLA was detected, indicating that all loop constructs were able to fold into receptors capable of forming a ligand binding site (Figure 3.3). Despite evidence for specific radioligand binding to all loop chimaeras, significant differences were

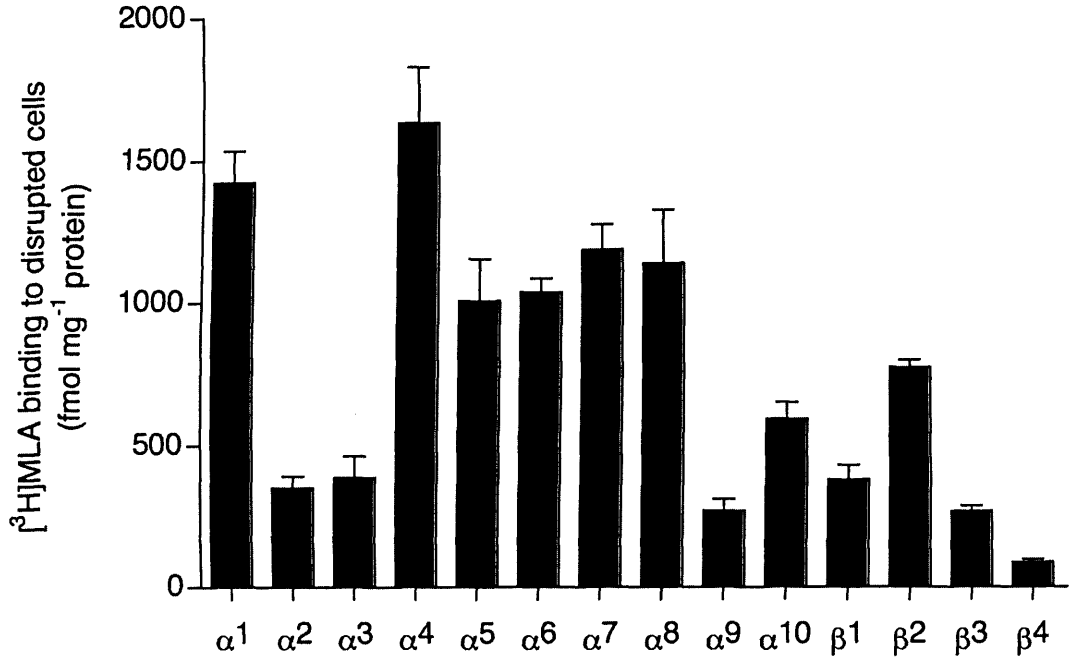

Figure 3.3 [^{3}H]MLA binding to loop chimaeras expressed in tsA201 cells. Human embryonic kidney tsA201 cells were transfected with 'loop chimaeric' DNA and assayed for [^{3}H]MLA binding 42-54 hours post transfection. Total-membrane [^{3}H]MLA binding as determined by assaying disrupted cells using a single saturating concentration of 10 nM [^{3}H]MLA. Data are presented as fmol/mg protein and are means of n=5 independent transfections, with each individual binding assay performed in triplicate. Error bars represent SEM.

observed in the level of binding (Table 3.1). Since there is extensive evidence that unassembled subunits do not form a high affinity nicotinic ligand binding site, the differences in levels of [^{3}H]MLA binding suggest that the M3-M4 intracellular loop domain can exert a profound influence on subunit folding and assembly.

3.3.2 Radioligand binding to cell-surface receptors

Intact transfected tsA201 cells were examined by cell-surface iodinated α-bungarotoxin ([^{125}I]αBTX) binding. Radioligand binding was performed with [^{125}I]αBTX (a membrane-impermeant ligand), rather than with [^{3}H]MLA, to prevent detection of intracellular receptors. Significant differences were observed in the level of specific cell-surface [^{125}I]αBTX binding with different loop chimaeras (Figure 3.4; Table 3.1). The highest levels of cell-surface [^{125}I]αBTX binding were detected with chimaeras containing the α1, α4, α7 and α8 loop domains (~1400-1800 fmol/mg protein). Intermediate levels of cell-surface [^{125}I]αBTX binding (~500-750 fmol/mg protein) were detected with chimaeras containing the α3, α6 and 5-HT$_{3B}$ loop domains (Figure 3.4). In contrast, specific cell-surface binding of [^{125}I]αBTX was low or absent with chimaeras containing α2, α5, α9, α10, β1, β2, β3 and β4 loop domains (Figure 3.4). Levels of [^{125}I]αBTX binding to loop chimaeras are summarised in Table 3.1. For several loop chimaeras, differences are apparent between the level of cell-surface binding compared with the level of radioligand binding detected in disrupted cells. This is

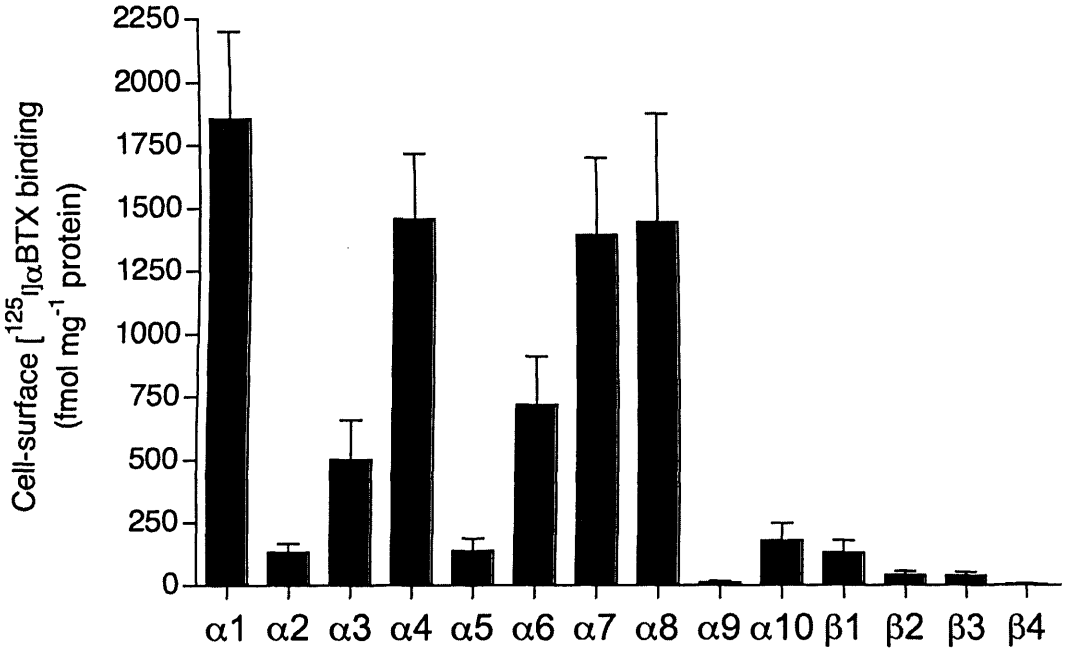

Figure 3.4 [^{125}I]αBTX binding to loop chimaeras expressed in tsA201 cells. Human embryonic kidney tsA201 cells were transfected with 'loop chimaeric' DNA and assayed for [^{125}I]αBTX binding 42-54 hours post transfection. Cell-surface [^{125}I]αBTX binding as determined by assaying intact cells using a single saturating concentration of 10 nM [^{125}I]αBTX. Data are presented as fmol/mg protein and are means of n=3-7 independent transfections, with each individual binding assay performed in triplicate. Error bars represent SEM.

particularly notable for loop chimaeras such as β2, for which moderate to high levels of radioligand binding was detected in disrupted cells but little or no binding was detected on the cell surface. It appears, therefore, that the M3-M4 loop domain can exert an influence upon the efficiency with which assembled receptors are transported to the cell surface.

3.4 Characteristion of loop chimaeras by immunoblotting

In order to detect levels of total subunit protein an 'epitope tag' was introduced into loop chimaera cDNAs by site-directed mutagenesis (Figure 3.5). An eight amino acid (DYKDDDDK) recombinant FLAG epitope tag (Brizzard *et al.*, 1994), was added to the extreme C-terminal end of the loop chimaeras (Figure 3.5) to facilitate immunoblotting. This was done primarily to examine whether differences in levels of radioligand binding could be attributed to differences in levels of subunit expression.

FLAG-tagged subunit chimaeras were expressed in HEK tsA201 cells and metabolically radiolabelled (with [^{35}S]methionine and [^{35}S]cysteine). Tagged subunits were immunoprecipitated with the commercially available monoclonal anti-FLAG antibody (mAb FLAG-M2) and examined by SDS-PAGE, followed by autoradiography (Figure 3.6).

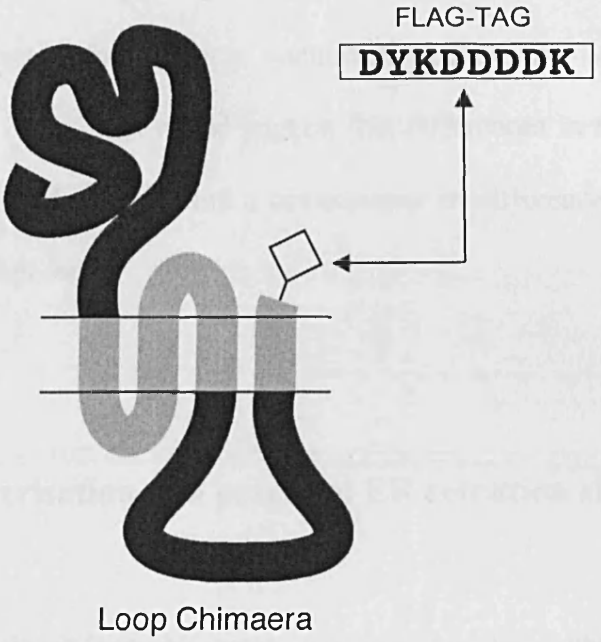

Figure 3.5 Introduction of a FLAG epitope tag into 'loop chimaeras'. Schematic representation showing the membrane topology of a loop chimaera receptor subunit and the position of the inserted eight amino-acid FLAG epitope tag (DYKDDDDK). The FLAG-tag was introduced to the extreme C-terminal end of the protein, immediately prior to the stop codon.

The α4, α5 and α6 loop constructs were selected for immunoblotting studies (as examples of constructs displaying high, low and intermediate levels of cell-surface [^{125}I]αBTX binding, respectively. Bands of the expected molecular weight were detected for all three subunit chimaeras and were of a similar intensity (Figure 3.6). This would suggest that differences in the levels of cell-surface [^{125}I]αBTX binding are not a consequence of differences in the levels of expressed subunit protein.

3.5 Characterisation of a potential ER retention signal

All the receptor subunit loop chimaeras investigated in this study share a common N-terminal domain of the α7 nAChR subunit and the 4-transmembrane domain from the 5-HT_{3A}R subunit. They differ only in the sequence of the M3-M4 intracellular loop. The sequences of the cytoplasmic loop are the least conserved part of the protein molecule between family members and exhibit considerable diversity between each other. It is possible that sequences found within this region of the protein are determinants of receptor maturation and/or transport to the cell surface. Various sequence motifs have been identified within the cytoplasmic regions of ion-channels which can regulate intracellular trafficking (Moss and Henley, 2002; Michelsen *et al.*, 2005). A possible explanation for the low levels of cell surface receptor, such as those displayed by the chimaeric loop constructs α2, α5, α9, α10, β1, β2, β3 and β4, as assayed by [^{125}I]αBTX binding

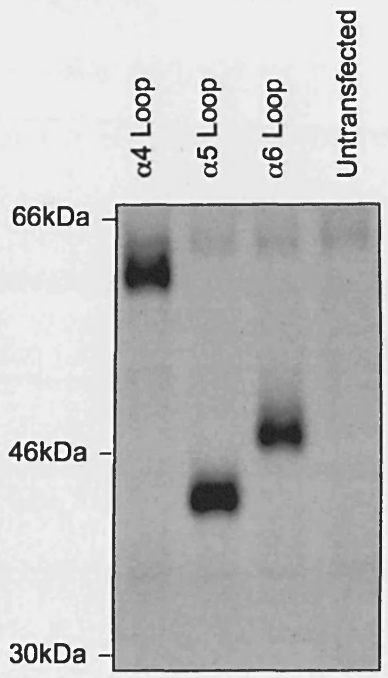

Figure 3.6 Immunoprecipitation of FLAG-tagged loop chimaeras. Tagged chimaeras were immunoprecipitated from metabolically-labelled human tsA201 cells and examined by SDS-PAGE. Immunoprecipitation showing the FLAG-tagged chimaeras containing the loops from nAChR subunits α4, α5 and α6, as examples of loops that display high, low and intermediate [^{125}I]αBTX cell-surface binding, respectively. The figure shown is representative of n=3 independent experiments. The positions of the molecular weight markers are shown on the left.

(Figure 3.3), could be the so called ER retention signal (Michelsen *et al.*, 2005). The ER is an important quality control checkpoint within the cell and protein subunits must be correctly folded and assembled in order to exit. The masking of ER retention motifs by assembly with another subunit, interactions with other proteins or phosphorylation may regulate the forward trafficking of such proteins (Michelsen *et al.*, 2005). Indeed, studies of nAChR assembly suggest that exit from the ER is an important checkpoint for controlling receptor stoichiometry (Blount *et al.*, 1990).

As discussed earlier (Section 3.3), the β2 loop chimaera is notable in forming relatively high levels of intracellular radioligand binding but very low levels of cell-surface binding sites. Analysis of the M3-M4 loop domain of the β2 subunit identified an 18 amino-acid arginine-rich region (Figure 3.7). This sequence contains a repetitive string of seven 'RXR' motifs (where 'R' represents an arginine residue and 'X' represents any amino-acid). The amino-acid sequence 'RXR' has previously been reported to play a role in the ER retention of a number of receptors (Michelsen *et al.*, 2005), including K_{ATP} channels (Zerangue *et al.*, 1999), $GABA_B$ (Margeta-Mitrovic *et al.*, 2000), NMDA (Standley *et al.*, 2000; Scott *et al.*, 2001), $5\text{-}HT_{3B}$ (Boyd *et al.*, 2003) and Kainate receptors (Nasu-Nishimura *et al.*, 2006). Because the β2 loop chimaera displayed very low levels of cell-surface receptor when expressed in HEK cells (Figure 3.3), it was reasoned that the deletion of the 18 amino-acid RXR motif containing sequence might lead to an increase in the cell-surface levels of the chimaeric receptor.

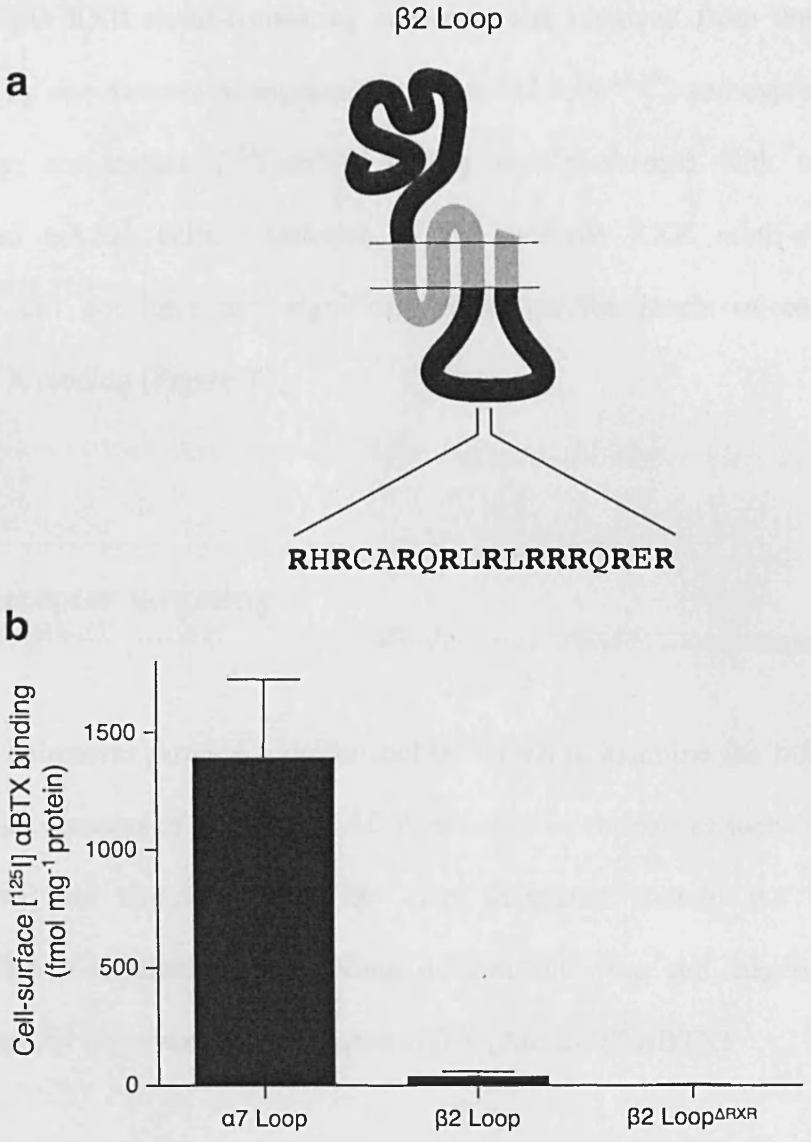

Figure 3.7 Deletion of an RXR-motif in the β2 loop chimaera and influence on cell-surface [^{125}I]αBTX binding. Site-directed mutagenesis was used to delete the 18 amino-acid long RXR-motif **(a)**, present within the intracellular M3-M4 loop sequence of the nAChR β2 subunit, from the β2 Loop chimaera to create β2 Loop$^{\Delta RXR}$ chimaera. **(b)** Cell-surface [^{125}I] αBTX binding conducted in tsA201 human embryonic kidney cells to determine the effect of the RXR-motif deletion on the number of cell-surface β2 Loop receptors. Receptor binding was assayed using a single saturating concentration of 10 nM [^{125}I]αBTX. The α7 Loop chimaera, which normally displays high cell-surface binding, was used as a positive control. Data are presented as fmol/mg protein and are means of n=3 independent transfections, with each individual binding assay performed in triplicate. Error bars represent SEM.

The multiple RXR motif-containing sequence was removed from the β2 loop chimaera by site-directed mutagenesis to create 'β2 loop$^{\Delta RXR}$' and expressed. As previously, cell-surface [^{125}I]αBTX binding was performed with transiently transfected tsA201 cells. Deletion of the multiple RXR motif-containing sequence did not have any significant effect on the levels of cell-surface [^{125}I]αBTX binding (Figure 3.7).

3.6 Receptor targeting

The loop chimaeras provide a useful tool by which to examine the influence of intracellular domains of individual nAChR subunits on properties such as receptor distribution and targeting. All the loop chimaeras contain the same α7 extracellular N-terminal αBTX binding domain, allowing cell targeting to be investigated by fluorescently conjugated αBTX (Alexa-488 αBTX).

3.6.1 Receptor targeting in MDCK cells

Madin-Darby canine kidney (MDCK) cells have been used extensively to examine the targeting of transmembrane proteins (Mellman, 1995; Nelson and Yeaman, 2001) and have also been used to demonstrate the influence of subunit composition upon the targeting of $GABA_A$ receptors (Connolly *et al.*, 1996). Cultured MDCK cells establish clearly defined and easily identifiable polarised

membranes. In addition, there is evidence to indicate that sorting of transmembrane proteins to epithelial apical and basolateral membranes is a useful model for axonal and dendritic sorting in neurones (de Hoop and Dotti, 1993).

The influence of intracellular loop domains upon receptor targeting was examined by expression of loop chimaeras in polarised epithelial MDCK cells. Fluorescence confocal microscopy was used to detect the distribution of subunit chimaeras labelled with Alexa-488 αBTX (Figure 3.8a and 3.8c). For comparison, staining of endogenous E-cadherin, which is expressed exclusively on basolateral membranes (Mays *et al.*, 1995), was examined (Figure 3.8b and 3.8c). Since the selective targeting of E-cadherin to the basolateral membrane is dependent on MDCK polarisation (van Beest *et al.*, 2006), this also provides a means of confirming cells are polarised.

Loop chimaeras which displayed high levels of specific [^{125}I]αBTX binding (α1, α4, α7 and α8 loop chimaeras) were expressed in polarised MDCK cells. Fluorescence confocal microscopy revealed predominantly apical staining for chimaeras containing the α4, α7 and α8 loop domains. In contrast, the α1 loop chimaera displayed a non-polarised (apical and basolateral) distribution (Figure 3.8a and 3.8c).

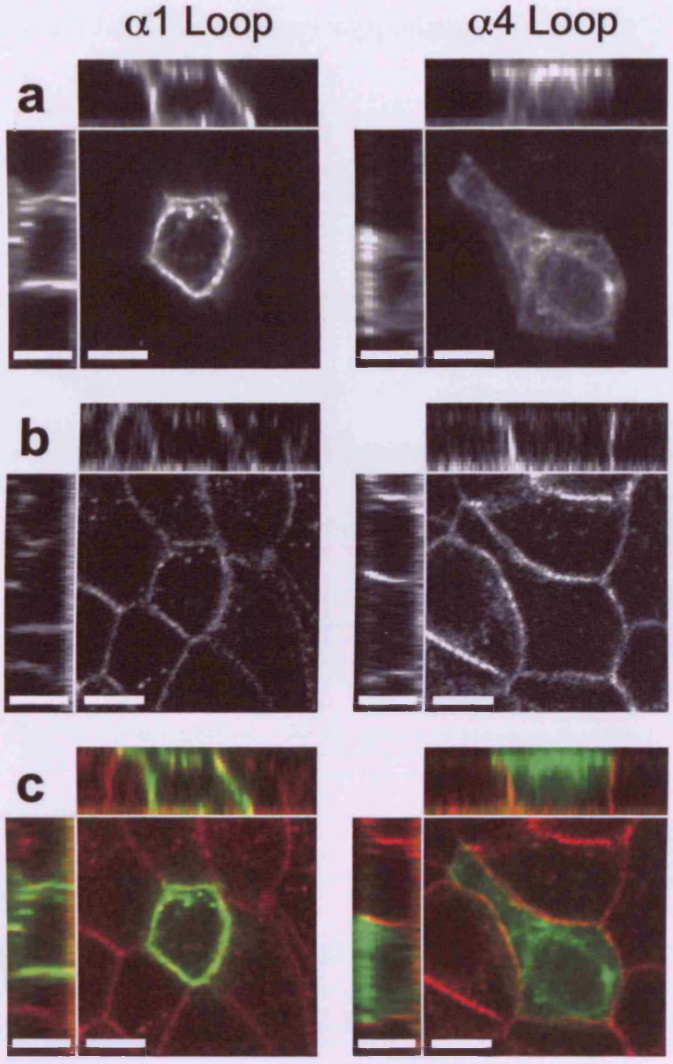

Figure 3.8 Targeting of loop chimaeras examined in polarised epithelial (MDCK) cells. Confocal images are shown illustrating a non-polarised distribution of the α1 loop chimaera (left hand panels) and a polarised (apical) distribution of the α4 loop chimaera (right hand panels). The main images are single confocal section from 15-17 separate 0.5 μm sections. Above and to the left of the main images are representative X-Z and Y-Z confocal sections from each image in which the apical cell surface is located at the top and to the left, respectively. (**a**) Labelling of subunit chimaeras with Alexa-488 αBTX. (**b**) Antibody (rhodamine) staining of endogenous E-cadherin, which is located on the basolateral membrane of MDCK cells. (**c**) Merged images from **a** and **b** in which Alexa-488 αBTX staining is shown in green and antibody staining of endogenous E-cadherin is shown in red. Results are representative of n=3 independent experiments. Scale bars = 7 μm.

3.6.2 Receptor targeting in primary hippocampal neurones

Primary hippocampal neurons have frequently been used to investigate aspects such as axonal and dendritic sorting as well as intra- and extra-synaptic sorting. However, neurones express αBTX sensitive nAChRs endogenously, complicating the use of this toxin to assay targeting and expression without a method to discriminate between native receptor subunits and the loop chimaeric subunits. The FLAG epitope-tagged loop constructs (See Section 3.5) provide a means to discriminate between endogenous αBTX sensitive nAChRs. Preliminary studies were performed with cultured rat hippocampal neurones to examine their suitability for studies of intracellular trafficking of loop chimaeras.

Rat hippocampal cells were cultured and transfected with loop chimaeras using a calcium phosphate based transfection protocol. Neurones were co-transfected with FLAG-tagged loop chimaeras and an EGFP encoding plasmid to aid identification of positively transfected cells. Hippocampal neurones were successfully isolated and cultured (Figure 3.9). In addition, specific staining of endogenous nAChRs was detected in untransfected neurones with rhodamine-αBTX (Figure 3.9). Experiments aimed at transient expression of loop chimaeras were performed and evidence for successful transfection of neurones with EGFP was obtained (data not shown). However, attempts to detect loop chimaeras in transfected hippocampal neurones were not pursued due to a shortage of time.

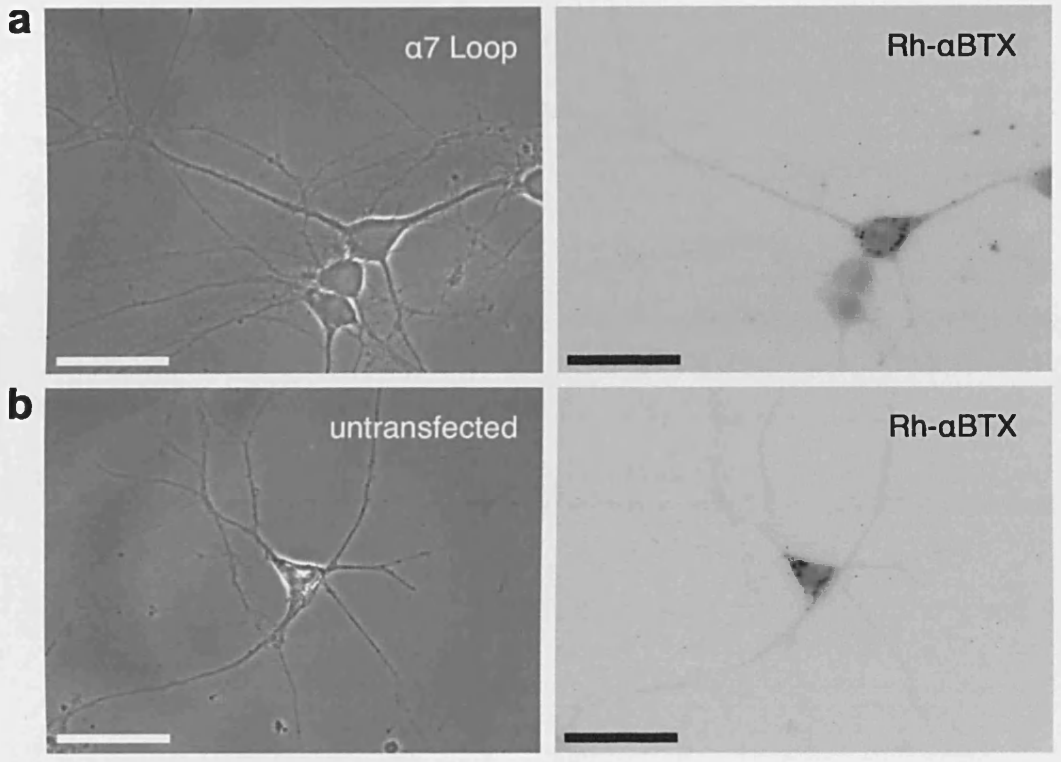

Figure 3.9 Cultured hippocampal neurones transfected with α7 loop chimaera, displaying αBTX-sensitive staining. Preliminary experiments showing hippocampal neurones, isolated from E18 rats and cultured for ~7 days prior to transfection using the calcium phosphate method. Neurones were processed for immunostaining 2-3 days post transfection. Neurones were transfected with FLAG-tagged α7 loop chimaera **(a)**, or vector control **(b)**, and viewed under bright-field optics (left panels). The same neurones were imaged under fluorescence optics showing Rh-αBTX staining and viewed here as negatives (right panels). Scale bar = 50 μm.

3.7 Rapsyn-induced clustering of nAChRs

Rapsyn (receptor associated protein at the synapse), also known as 43K, is a cytoplasmic protein which aggregates with the muscle-type nAChR and is essential for the high-density (~10,000 receptors/μm^2) clustering of the receptor at the vertebrate neuromuscular junction (Witzemann, 2006). Rapsyn-deficient mice fail to form nAChR clusters and show severe neuromuscular dysfunction (Gautam *et al.*, 1995). It has been established that rapsyn mediates the clustering of muscle nAChRs via interaction with the M3-M4 intracellular loop domain (Huebsch and Maimone, 2003).

In a pilot experiment rapsyn was co-expressed with the α1 loop chimaera and HEK tsA201 cells studied for evidence of receptor clustering by immunofluorecence microscopy (Figure 3.10). In the absence of rapsyn, α1 loop staining appears diffuse and uniformly spread throughout the cell surface. There is evidence for the existence of small receptor clusters, as indicated by the presence of punctate staining (arrows in 3.10a). Co-expression with rapsyn however, leads to a marked difference in the α1 loop staining. The receptor no longer appears diffuse and uniformly spread throughout the cell surface but is instead heavily concentrated in large aggregates, many times larger than the small punctae observed in the absence of rapsyn (arrowheads 3.10b). The α1 loop-staining pattern co-localises well with that of rapsyn, indicating co-localisation of both proteins, which is indicative of a protein-protein interaction.

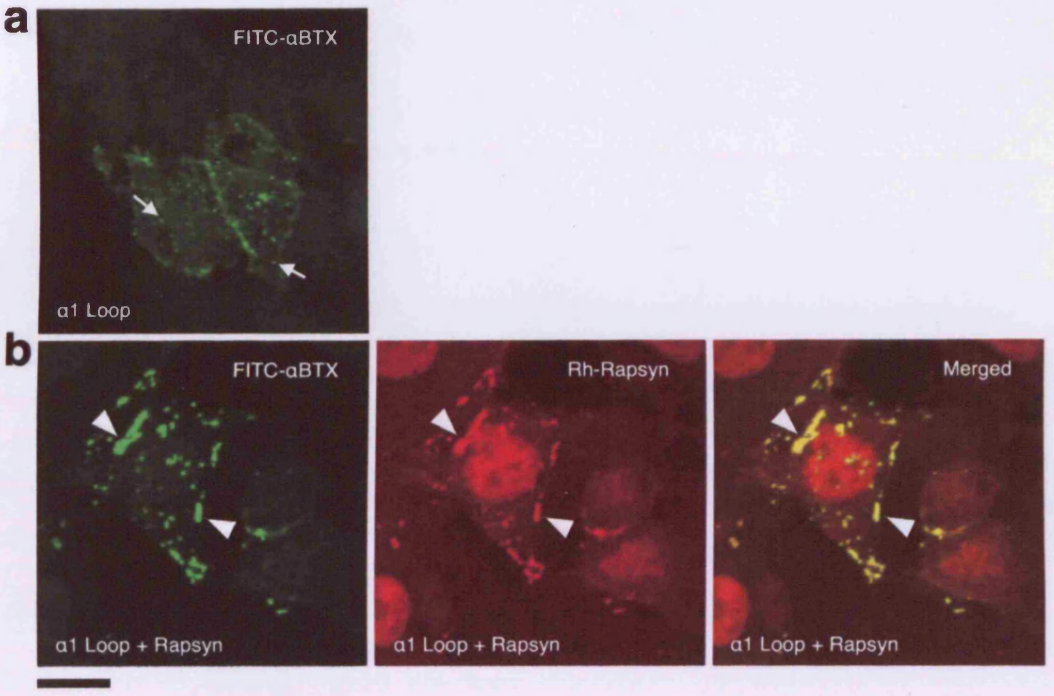

Figure 3.10 Rapsyn (43K protein)-induced receptor clustering in tsA201 cells examined by immunofluorescence microscopy. Human embryonic kidney tsA201 cells were transiently transfected with the α1 loop chimaera either alone **(a)**, or together with rapsyn **(b)**. Cells were permeabilised and processed for immunofluorescence ~48 hours post transfection. Figures show confocal microscope sections displayed here as a stack projection overlay. Cells were labelled with αBTX (green; left panel) and rapsyn (red; middle panel). Both channels were merged (right panel), to show co-clustering. Arrows indicate small punctate staining and arrowheads indicate large clusters of protein aggregates. Results are representative of n=3 independent experiments. Scale bar = 10 μm.

3.8 The influence of RIC-3 on loop chimaeras

Recent data suggests that the transmembrane chaperone protein, RIC-3, can influence the maturation (folding and assembly) of neuronal nACh and 5-HT_3 receptors (reviewed by Millar, 2008). RIC-3 was originally identified in a genetic screen in the nematode worm *Caenorhabditis elegans* as the protein encoded by the gene, *r*esistance to *i*nhibitors of *c*holinesterase (*ric-3*; Nguyen *et al.*, 1995). Interestingly, RIC-3 appears to be specific in its chaperone activity; while modulating aspects of nACh and 5-HT_3 receptor maturation, it fails to affect other neurotransmitter-gated ion channels, including the closely related Cys-loop receptor $GABA_A$ (Miller *et al.*, 1996; Halevi *et al.*, 2002; Halevi *et al.*, 2003; Lansdell *et al.*, 2005). RIC-3 has been demonstrated to facilitate the functional expression of the homomeric nAChR α7 subunit in 'non-permissive' mammalian cell lines such as HEK cells (Lansdell *et al.*, 2005; Williams *et al.*, 2005). When co-expressed in *Xenopus* oocytes, RIC-3 enhances the functional expression of the α7 nAChRs (Halevi *et al.*, 2002; Halevi *et al.*, 2003). RIC-3 has also been shown to regulate functional expression of heteromeric nAChRs such as α3β4 and α4β2, and the related Cys-loop receptor 5-HT_{3A} subunit when co-expressed in HEK cells (Cheng *et al.*, 2005; Lansdell *et al.*, 2005; Cheng *et al.*, 2007). However, unlike with the α7 nAChR, conflicting data has been reported for the regulation of heteromeric nAChRs and 5-HT_{3A} receptors by RIC-3. Whereas in mammalian HEK cells RIC-3 leads to an enhancement of functional expression of α3β4 and α4β2 nAChRs and of 5-HT_{3A}Rs, in oocytes expression is suppressed. It is

possible that the apparent inconsistencies reported are due to the heterologous expression systems employed in each study (Millar, 2008).

Cell-surface [^{125}I]αBTX binding to loop chimaeras was examined in HEK tsA201 cells co-transfected with human RIC-3 (hRIC-3). In contrast to the dramatic facilitation of [^{125}I]αBTX binding to the α7 subunit (Lansdell *et al.*, 2005), preliminary data indicated no increase on the levels of cell-surface binding with any of the loop chimaeras (data not shown). On the contrary, those loop chimaeras which exhibited high levels of cell-surface binding in the absence of hRIC-3 were down-regulated when co-expressed with hRIC-3. Five nAChR subunit loop chimaeras which exhibited high levels of [^{125}I]αBTX surface binding (α1, α4, α6, α7 and α8; Figure 3.4), in addition to the 5-HT$_{3A}$ loop chimaera, were selected for further analysis to confirm the above observation (Figure 3.11). Co-expression with hRIC-3 led to a dramatic decrease in the levels of [^{125}I]αBTX cell-surface binding of around 70-90% (Figure 3.11). The differences observed between loop chimaeras were not found to be significant when tested by ANOVA, suggesting that variation within the M3-M4 loop domain did not contribute to the observed reduction in the levels of cell surface receptor mediated by co-expression with hRIC-3.

Interestingly, RIC-3 has been found to consistently decrease the levels of expression of α7/5-HT$_{3A}$ subunit chimaeras in both oocytes and mammalian cell expression systems (Millar, 2008). It would appear from these experiments that

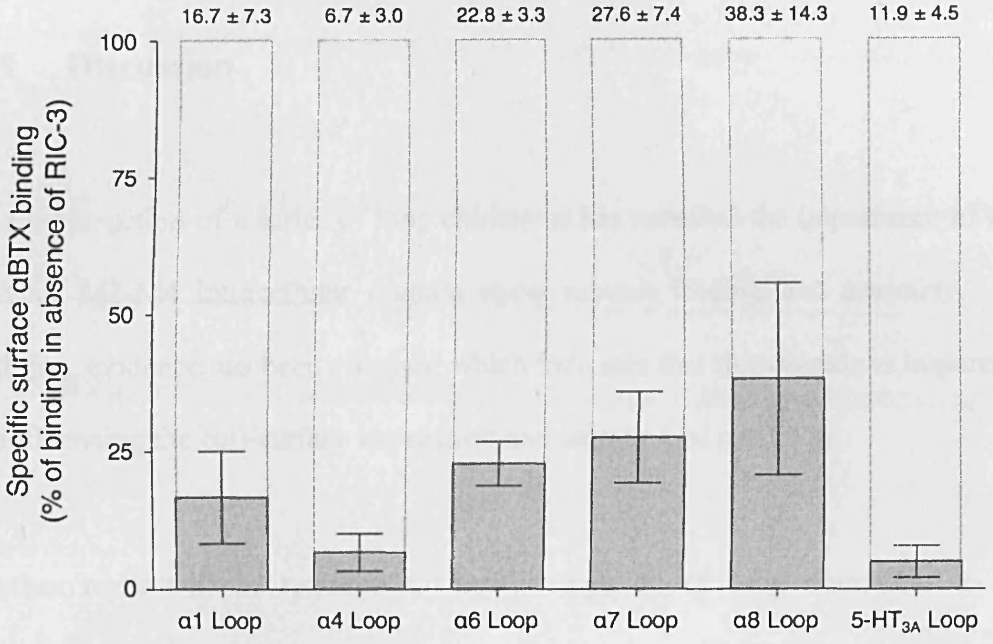

Figure 3.11 Influence of RIC-3 on the cell-surface expression of M3-M4 loop chimaeras in tsA201 cells. Human embryonic kidney tsA201 cells were transiently transfected with loop chimaeras alone or co-expressed with RIC-3. Cell-surface [^{125}I]αBTX binding as determined by assaying intact cells using a single saturating concentration of 10 nM [^{125}I]αBTX. Results are presented as a percentage of specific cell-surface binding in the absence of RIC-3 (100%). In the presence of RIC-3, cell-surface [^{125}I]αBTX binding is reduced by ~70-90% between the different loop constructs shown. No significant differences were found between the different loop constructs examined. Data are means of n=3-5 independent transfections, with each individual binding assay performed in triplicate. Error bars represent SEM.

variation between the M3-M4 intracellular loops does not influence the effect of hRIC-3 on α7/5-HT_{3A} chimaeric subunits expressed in HEK cells.

3.9 Discussion

The construction of a series of loop chimaeras has revealed the importance of the nAChR M3-M4 intracellular domain upon subunit folding and assembly. In addition, evidence has been obtained which indicates that this domain is important in influencing the cell-surface expression and targeting of nAChRs.

Further work will be required to enable targeting of loop chimaeras to be examined in primary hippocampal neurones, but this will be a longer-term goal for the laboratory. It is likely that the loop chimaeras will provide a useful tool with which to examine the M3-M4 loop domain with intracellular proteins. Initial studies have been conducted with rapsyn, a protein associated with muscle-type nAChRs, but this is potentially an important area for further research. It would be interesting, for example to examine protein-protein interactions by techniques such as immunoprecipitation. By use of techniques such as site-directed mutagenesis, it is possible that the influence of discrete regions and specific sequence motifs within the M3-M4 loop domain may be identified.

Table 3.1 Characterisation of loop chimaeras

Loop chimaera	[^{125}I]αBTX binding (fmol mg^{-1}) (n=4-7)	[^{3}H]MLA binding (fmol mg^{-1}) (n=5)	Targeting (MDCK cells)
α1 loop (α7/5-HT$_{3A}^{\alpha1\text{-loop}}$)	1857±346 [a]	1424±111 [c]	Non-polarised
α2 loop (α7/5-HT$_{3A}^{\alpha2\text{-loop}}$)	132±34 [b]	353±39 [d]	ND
α3 loop (α7/5-HT$_{3A}^{\alpha3\text{-loop}}$)	502±158	388±75 [d]	ND
α4 loop (α7/5-HT$_{3A}^{\alpha4\text{-loop}}$)	1457±259 [a]	1635±197 [c]	Apical
α5 loop (α7/5-HT$_{3A}^{\alpha5\text{-loop}}$)	139±48 [b]	1008±148 [c]	ND
α6 loop (α7/5-HT$_{3A}^{\alpha6\text{-loop}}$)	718±193	1037±50 [c]	ND
α7 loop (α7/5-HT$_{3A}^{\alpha7\text{-loop}}$)	1391±307 [a]	1187±89 [c]	Apical
α8 loop (α7/5-HT$_{3A}^{\alpha8\text{-loop}}$)	1442±429 [a]	1139±189 [c]	Apical
α9 loop (α7/5-HT$_{3A}^{\alpha9\text{-loop}}$)	13±5 [b]	272±41 [d]	ND
α10 loop (α7/5-HT$_{3A}^{\alpha10\text{-loop}}$)	179±69 [b]	592±60	ND
β1 loop (α7/5-HT$_{3A}^{\beta1\text{-loop}}$)	129±48 [b]	381±50 [d]	ND
β2 loop (α7/5-HT$_{3A}^{\beta2\text{-loop}}$)	41±16 [b]	775±24	ND
β3 loop (α7/5-HT$_{3A}^{\beta3\text{-loop}}$)	40±12 [b]	269±18 [d]	ND
β4 loop (α7/5-HT$_{3A}^{\beta4\text{-loop}}$)	5±2 [b]	88±10 [d]	ND

Binding data are ±SEM from experiments conducted in either intact cells or disrupted cell membrane preparations using a single saturating concentration of 10 nM [^{125}I]αBTX or 10 nM [^{3}H]MLA, respectively. Statistical significance: [a] vs [b] $P<0.05$, [c] vs [d] $P<0.05$. ND = not determined.

Chapter 4

Functional characterisation of nAChR loop chimaeras

Chapter 4

Functional characterisation of nAChR loop chimaeras

4.1 Introduction

The experiments described in the previous chapter provide evidence that the M3-M4 intracellular loop domain can influence the ability of nAChR subunits to form correctly folded ligand-binding sites expressed on the cell surface (Sections 3.3 and 3.4). In addition, evidence has been found to support a role of the intracellular loop in trafficking of receptors to discrete subcellular domains (Section 3.6). However, the studies described in the previous chapter do not address the question of whether these subunit chimaeras are able to generate functional agonist-gated ion channels. To examine this question, all loop chimaeras were initially assayed for function using an intracellular calcium assay in transfected mammalian cells. Based on these results, the functional properties of various loop chimaeras were investigated further by whole-cell electrophysiological recording.

4.2 Intracellular calcium assay (FLIPR)

Human embryonic kidney (tsA201) cells were transiently transfected with the M3-M4 intracellular loop chimaeras. Transiently transfected cells were re-plated into 96-well plates and loaded with the fluorescent calcium-sensitive dye Fluo-4 (Section 2.9). A fluorometric imaging plate reader (FLIPR) was used to measure the influx of calcium in response to agonist application (Figure 4.1). A baseline was established and, after 25 seconds, agonist was added simultaneously to all wells of the 96 well plate.

Previous work has shown that the nAChR agonist 1,1-dimethyl-4-phenylpiperazinium (DMPP) leads to an increased level of intracellular Ca^{2+} in cells transfected with the $\alpha7^{4TM\text{-}5HT3A}$ chimaera, as demonstrated by the use the intracellular Ca^{2+}-dependent fluorescent dye, Fluo-4, and assayed by FLIPR (Gee *et al.*, 2007). A concentration-dependent agonist-induced increase in intracellular Ca^{2+} concentration was also observed with $\alpha7^{4TM\text{-}5HT3A(Not/Bst)}$ (Figure 4.1), the chimaera from which the loop chimaeras were constructed (Section 3.2).

Agonist-induced elevations of intracellular calcium were detected in cells transfected with some, but not all of the loop chimaeras (Figure 4.2). Surprisingly, a number of loop constructs which demonstrated high levels of cell-surface [^{125}I]αBTX binding (e.g. α1 and α4 loop, Figure3.4), did not exhibit any

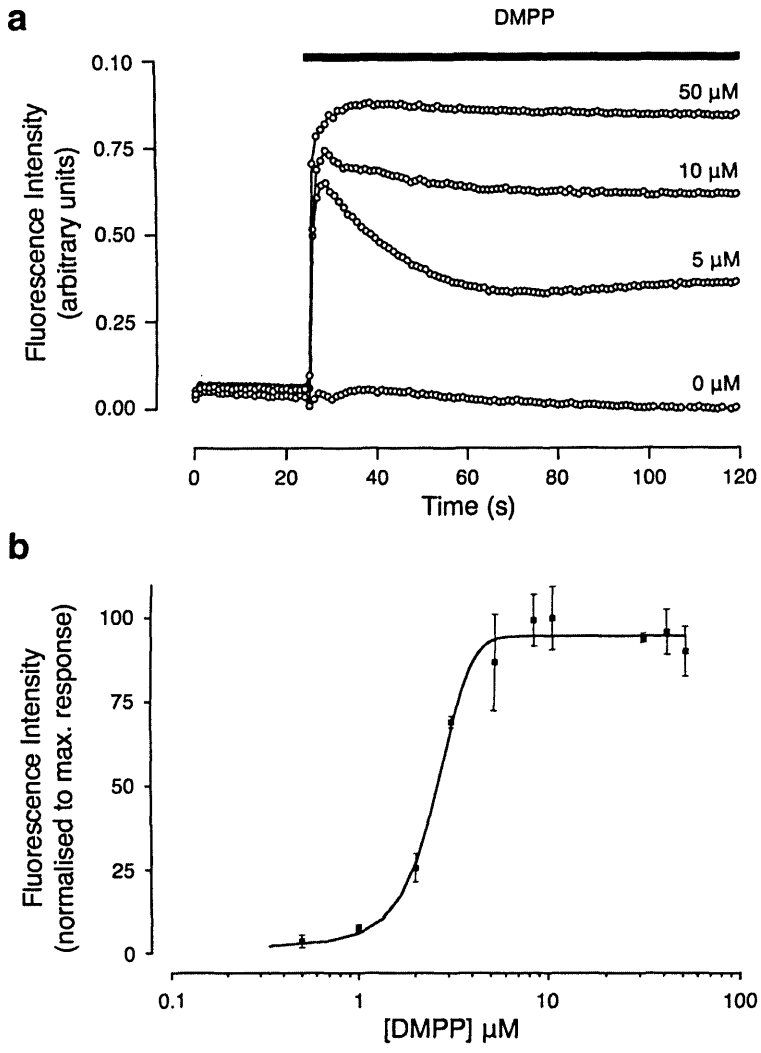

Figure 4.1 Agonist-induced dose-dependent calcium response, as determined by FLIPR in tsA201 cells transfected with α7 loop chimaeras. (a) The chimaeric α7 loop construct was expressed in tsA201 cells and calcium influx, in response to applied DMPP, measured using a fluorescence imaging plate reader (FLIPR), as an assay for function of the loop construct. Black scale bar represents the time and duration of agonist application. **(b)** Concentration-response relationship obtained from analysing calcium influx FLIPR responses at various concentrations of applied DMPP. Scale bars represent SEM of triplicate responses obtained from a single experiment. Both panels are representative examples of the typical responses observed over n = 3-5 experiments.

functional response in the FLIPR assay (data not shown). Moreover, evidence of functional expression was detected for subunits that demonstrated little, or very low surface binding (e.g. α3 and α10 loop, Figure 4.2). These constructs, which would perhaps be expected to show little or no function, did exhibit convincing and reproducible responses using the FLIPR assay (Figure 4.2). In addition, the functional responses did not appear different to those obtained from loop chimaeras which demonstrated high surface expression, as determined by surface binding (e.g. compare α8 loop versus α10 loop; Figure 4.2). The α7 loop chimaera was the only construct where the FLIPR response traces were much larger than the other functional loop chimaeras; reaching a normalised response more than double that of any other loop chimaera which exhibited a FLIPR response (Figure 4.2).

In the present study, the FLIPR-based assay has been used primarily as a screening tool to identify loop chimaeras which are able to generate functional receptors. To an extent, it may be possible to conclude from this data the relative efficiency with which the chimaeras generate functional receptors, although no information is available about the relative calcium permeability of the different loop chimaeras.

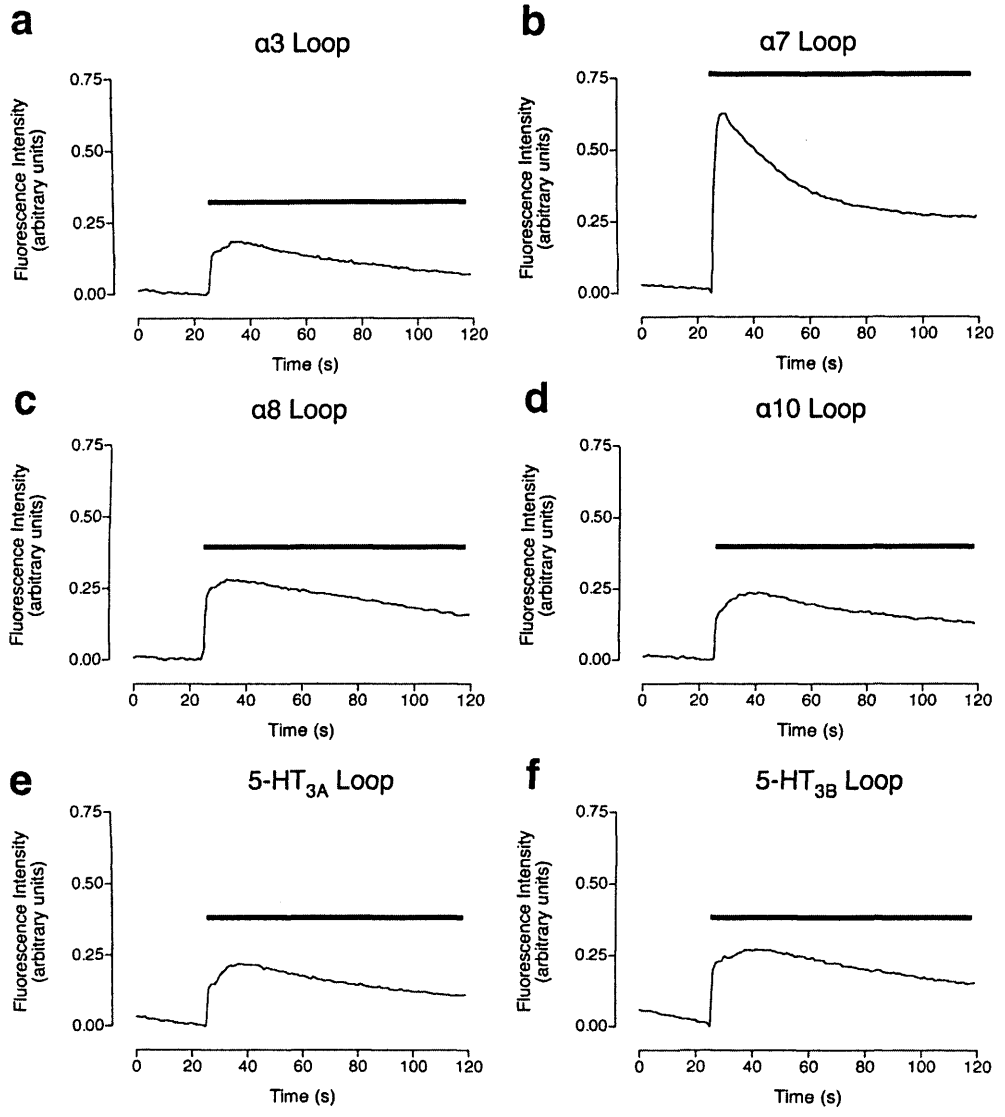

Figure 4.2 Agonist-induced calcium response, as determined by FLIPR in tsA201 cells transfected with loop chimaeras. Loop chimaeric constructs were expressed in tsA201 cells and calcium influx, in response to 50 μM applied DMPP, measured using a fluorescence imaging plate reader (FLIPR), as an assay for function of the loop construct. **(a)** rat α3 loop, **(b)** rat α7 loop, **(c)** chick α8 loop, **(d)** rat α10 loop, **(e)** mouse 5-HT_{3A} and **(f)** human 5-HT_{3B} loop. Black scale bar represents the time and duration of agonist application. Results are representative examples of n=3-10 independent experiments conducted in triplicate.

4.3 Characterisation of loop chimaeras by whole-cell recordings

All six loop-constructs that demonstrated functional responses as determined by the FLIPR assay (α3, α7, α8, α10, 5-HT_{3A} and 5-HT_{3B}) were also examined by whole-cell patch-clamp recording. The purpose of these experiments was to examine in more detail the functional properties in single cells, as opposed to a population of cells and to allow rapid agonist application to single cells to provide a much higher time resolution of the time course of the response to agonist application than is possible using the FLIPR. Receptor properties such as single channel conductance and desensitisation were investigated. Human embryonic kidney tsA201 cells were co-transfected with the loop chimaeras and a plasmid expressing enhanced green fluorescent protein (EGFP). This permitted identification of cells successfully transfected, by means of immunofluorescent microscopy. An impetus for these studies was recent evidence that the M3-M4 intracellular loop domain can exert a dramatic influence upon single channel conductance of members of the Cys-loop receptor family (Kelley *et al.*, 2003; Hales *et al.*, 2006; Gee *et al.*, 2007).

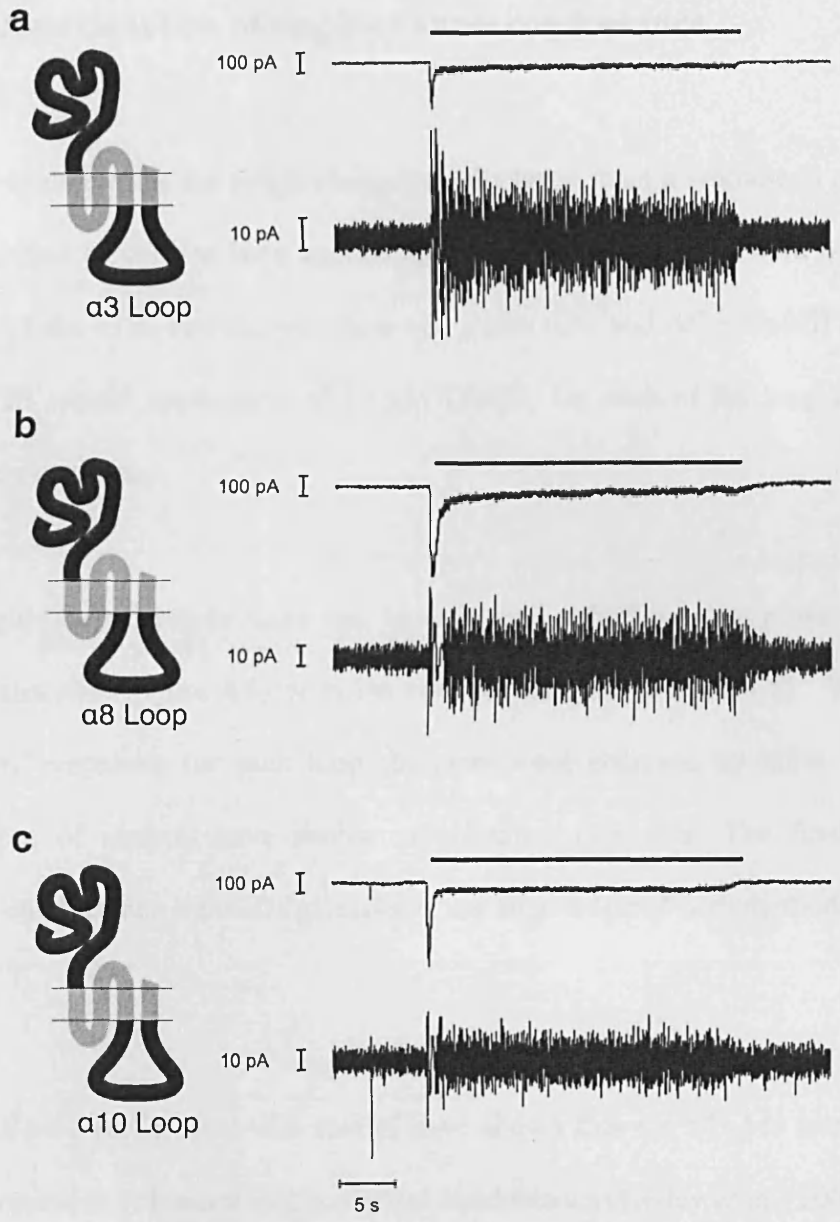

Figure 4.3 Influence of nAChR subunit loop domains upon single channel conductance. Chimaeric subunits containing the M3–M4 intracellular loop domain from the α3 subunit (**a**), α8 subunit (**b**) or α10 subunit (**c**) were expressed in tsA201 cells and analysed by whole-cell recording. Representative whole-cell responses were obtained by a 20 second application (thick horizontal scale bar) of 50 mM DMPP. Vertical scale bars = 100 pA. Below each whole-cell response is shown a high-gain band-pass filtered (2Hz – 2kHz) record illustrating the increase in noise variance associated with each response. Vertical scale bars = 10 pA.

4.4 Determination of single-channel conductance

In order to determine the single-channel conductance from a whole-cell response, the responses of cells to long agonist applications (20 seconds) were measured. Figure 4.3 shows representative whole-cell traces (DC and AC coupled) obtained from a 20 second application of 50 μM DMPP, for each of the loop chimaera constructs examined.

The single-channel conductance can be estimated either by noise power spectral density analysis (Figure 4.4) or noise variance analysis (Figure 4.5). When the whole-cell responses for each loop chimaera were analysed by noise analysis, both types of method gave similar conductance estimates. The final single-channel conductance estimates given here, are an average of both methods (Figure 4.6)

As mentioned earlier, previous studies have shown that the M3-M4 intracellular loop domain can influence single channel conductance (Kelley *et al.*, 2003; Hales *et al.*, 2006; Gee *et al.*, 2007). Whole-cell recordings have previously been used in this laboratory to examine the influence of receptor domains upon single-channel conductance, estimated by noise-analysis (Gee *et al.*, 2007). These studies revealed that $\alpha7^{V201\text{-}5HT3A}$ (which contains a 5-HT_{3A} intracellular loop) generated receptors with a single channel conductance of 0.8±0.1 pS, which is not significantly different from the sub-pS conductance observed with the 5-HT_{3A}

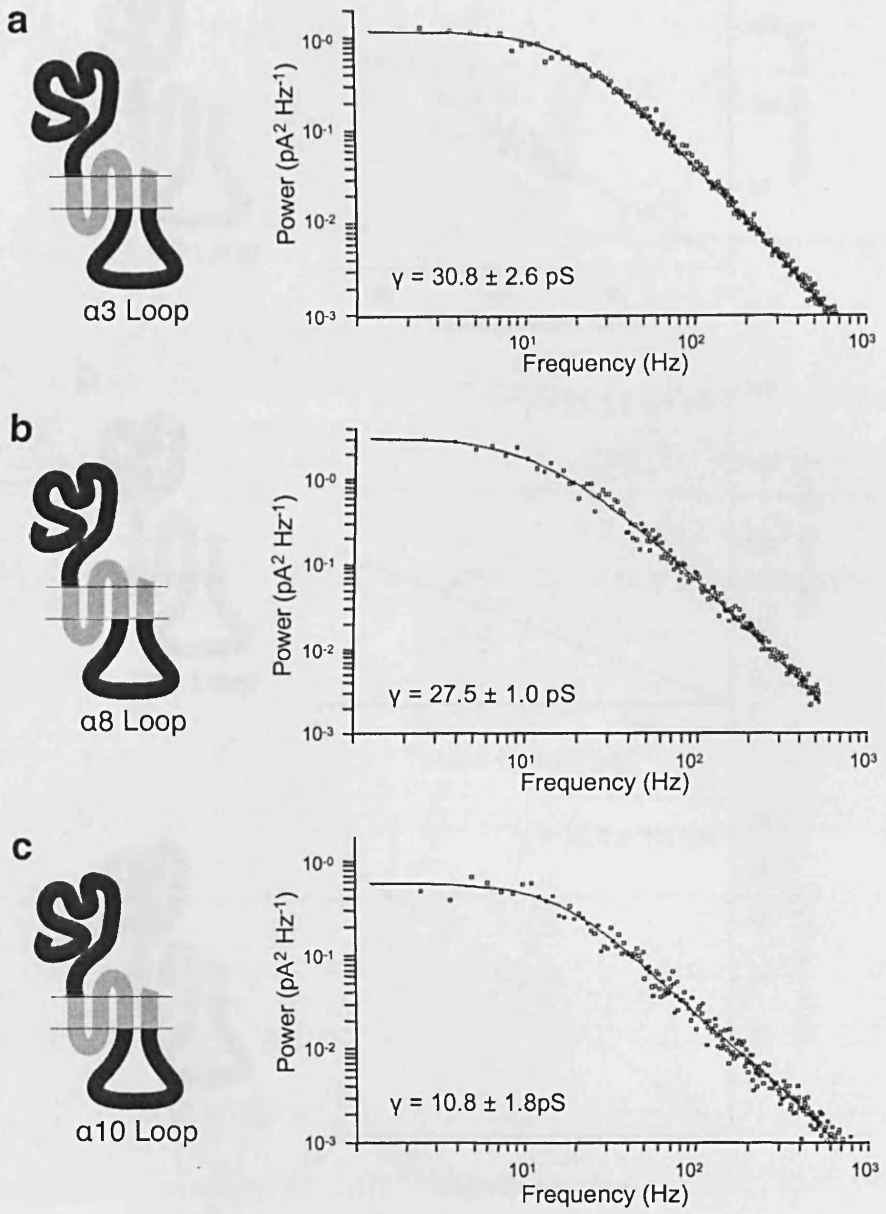

Figure 4.4 Estimation of single-channel conductance using the noise power spectral density method. Subunit chimaeras containing the M3–M4 intracellular loop domain from the α3 subunit (**a**), α8 subunit (**b**) or α10 subunit (**c**) were expressed in tsA201 cells. Whole-cell recordings obtained by applying 50 μM DMPP for 20 seconds were analysed to obtain the single channel conductance (γ).

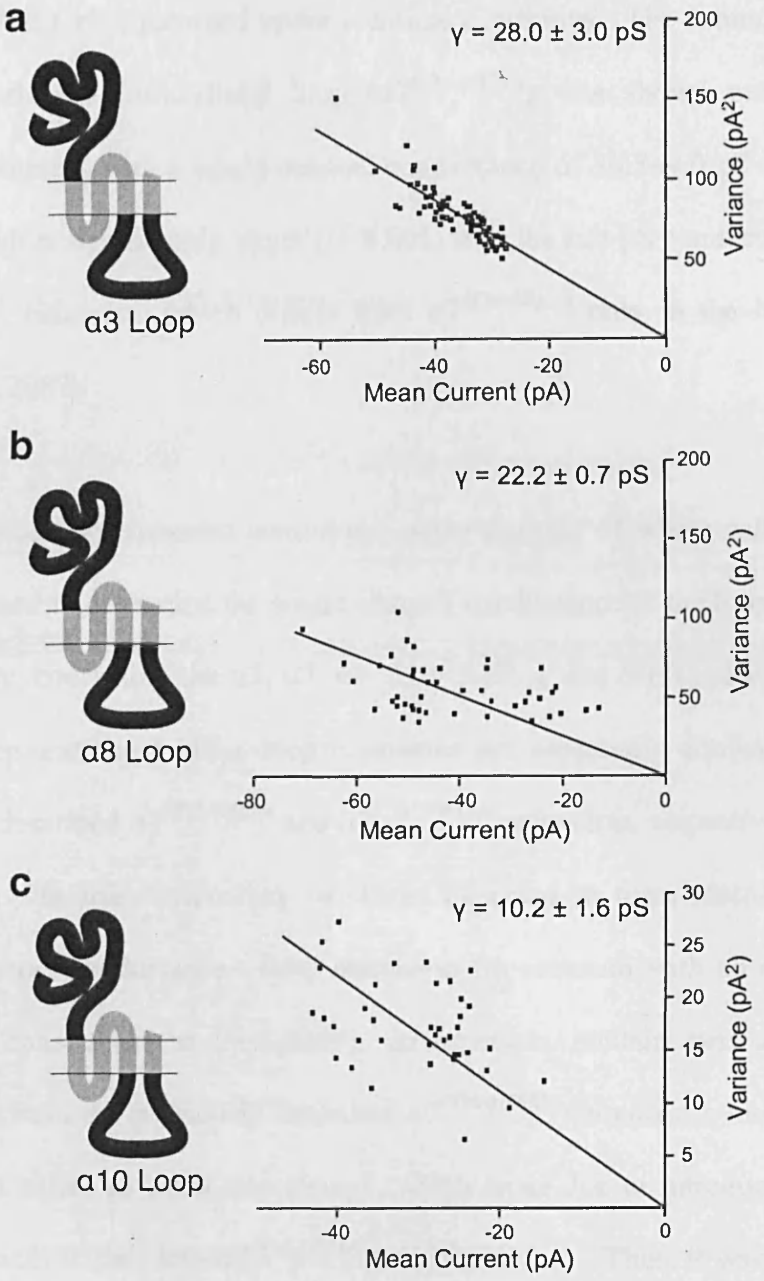

Figure 4.5 Estimation of single-channel conductance using the noise variance method. Subunit chimaeras containing the M3–M4 intracellular loop domain from the α3 subunit (**a**), α8 subunit (**b**) or α10 subunit (**c**) were expressed in tsA201 cells. Whole-cell recordings, obtained by applying 50 μM DMPP for 20 seconds, were analysed to obtain the single channel conductance (γ).

subunit (0.7±0.1 pS), recorded under identical conditions. The subunit chimaera containing the α7 intracellular loop ($\alpha7^{4TM\text{-}5HT3A}$) was shown previously to generate receptors with a single-channel conductance of 30.5±4.0 pS (Gee *et al.*, 2007), which is significantly larger ($P<0.001$) than the sub-pS conductance of the $\alpha7^{V201\text{-}5HT3A}$ chimaera, which differs from $\alpha7^{4TM\text{-}5HT3A}$ only in the loop region (Gee *et al.*, 2007).

Using identical experimental conditions, noise analysis of whole-cell responses was performed to determine the single channel conductance of the loop chimaeras in this study, containing the α3, α7, α8, α10, 5-HT_{3A} and 5-HT_{3B} loop domains. The α7 loop and the 5-HT_{3A} loop chimaeras are essentially equivalent to the previously described $\alpha7^{4TM\text{-}5HT3A}$ and $\alpha7^{V201\text{-}5HT3A}$ chimaeras, respectively (Gee *et al.*, 2007). For this reason they would be expected to form receptors with a similar channel conductance. Both chimaeras (in common with all of the loop chimaeras constructed in this study), do however, contain two amino acid differences from the previously described $\alpha7^{4TM\text{-}5HT3A}$ chimaera; a methionine to leucine and valine to isoleucine change, which arose due to introduction of the *Not*I and *Bst*Z17I sites into $\alpha7^{4TM\text{-}5HT3A}$ (see Figure 3.1). Thus, it was decided to determine the single channel conductance of all the new loop chimaeras described in this study (including the α7 loop and 5-HT_{3A} loop chimaeras).

The single channel conductances determined in this study for the α7 loop chimaera (36.1±3.2 pS, n=8) and the 5-HT_{3A} loop chimaera (0.48±0.04 pS, n=5),

were not significantly different to those determined previously for the $\alpha7^{4TM\text{-}5HT3A}$ (30.5±4.0 pS) and the $\alpha7^{V201\text{-}5HT3A}$ (0.8±0.1 pS) chimaeras (Gee *et al.*, 2007). Reassuringly, these and other data, help support the conclusion that introduction of the *Not*I and *Bst*Z17I restriction sites do not significantly alter the properties of the chimaeric receptor.

Of the nAChR loop chimaeras examined (α3, α7, α8, α10, 5-HT_{3A} and 5-HT_{3B}; Figure 4.6), four loop chimaeras generated receptors with high single-channel conductances; α3 loop (29.4±2.8 pS, n=9), α7 loop (36.1±3.2 pS, n=8), α8 loop (24.9±0.8 pS, n=5), and 5-HT_{3B} loop (34.0±6.6 pS, n=5). These single-channel conductances were not significantly different from one another (Table 4.1), as determined by analysis of variance (ANOVA, with Tukey's post test). The receptor exhibiting the lowest single-channel conductance was that containing the 5-HT_{3A} loop (0.48±0.04 pS, n=5). This was significantly lower than all other loop chimaeras investigated (P<0.001). The α10 loop chimaera displayed an intermediate single-channel conductance (10.5±1.7, n=5), which was both significantly smaller (P<0.001) than that observed with the high conductance chimaeras (α3, α7, α8 and 5-HT_{3B} loop); and significantly larger (P<0.001) than that observed with the 5-HT_{3A} loop chimaera.

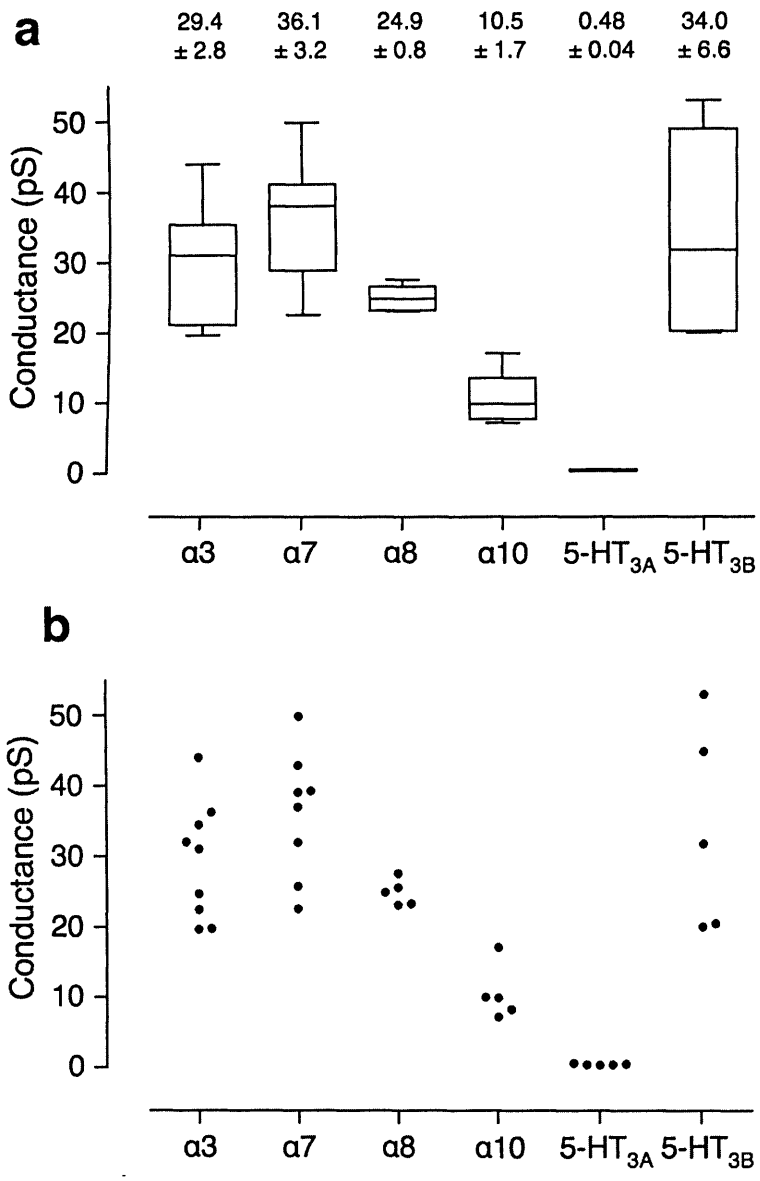

Figure 4.6 Single-channel conductance of loop chimaeras. The single-channel conductance values were obtained as an average from both the power specral desity method and the noise variance method for analysing whole-cell noise traces. The data are presented here in the form of a boxplot **(a)**, and as a scatterplot of observations **(b)**. The mean conductance values (± SEM; n = 5-9) for each construct are presented above each respective column.

4.5 Desensitisation properties

The influence of the intracellular loop upon desensitisation was also examined. All loop chimaeras tested showed extensive desensitisation (~90%), the extent of which did not differ significantly between the constructs (Figure 4.7 and 4.8). However, significant differences were detected in the time constant for desensitisation for different loop chimaeras (Figure 4.7 and 4.9). The desensitisation time constants for chimaeras containing the α7 (1334±141 ms, n=21), α8 (966±184 ms, n=6), and 5-HT_{3B} loop domains (1200±70 ms, n=3), were significantly larger ($P<0.001$) than those determined with chimaeras containing the α3 (278±23 ms, n12) and α10 loop domains (217±16 ms, n=8). Unfortunately, desensitisation properties could not be investigated in detail for the responses obtained from the 5-HT_{3A} loop chimaera, as only two responses were suitable for analysis. However, the preliminary desensitisation time constant obtained for the 5-HT_{3A} loop (111.6±38 ms, n=2), is in good agreement with previously published results for $\alpha7^{V201\text{-}5HT3A}$ (223±32) (Gee *et al.*, 2007) and indicate a desensitisation time constant for the 5-HT_{3A} loop, similar to those obtained for the α3 and α10 loops.

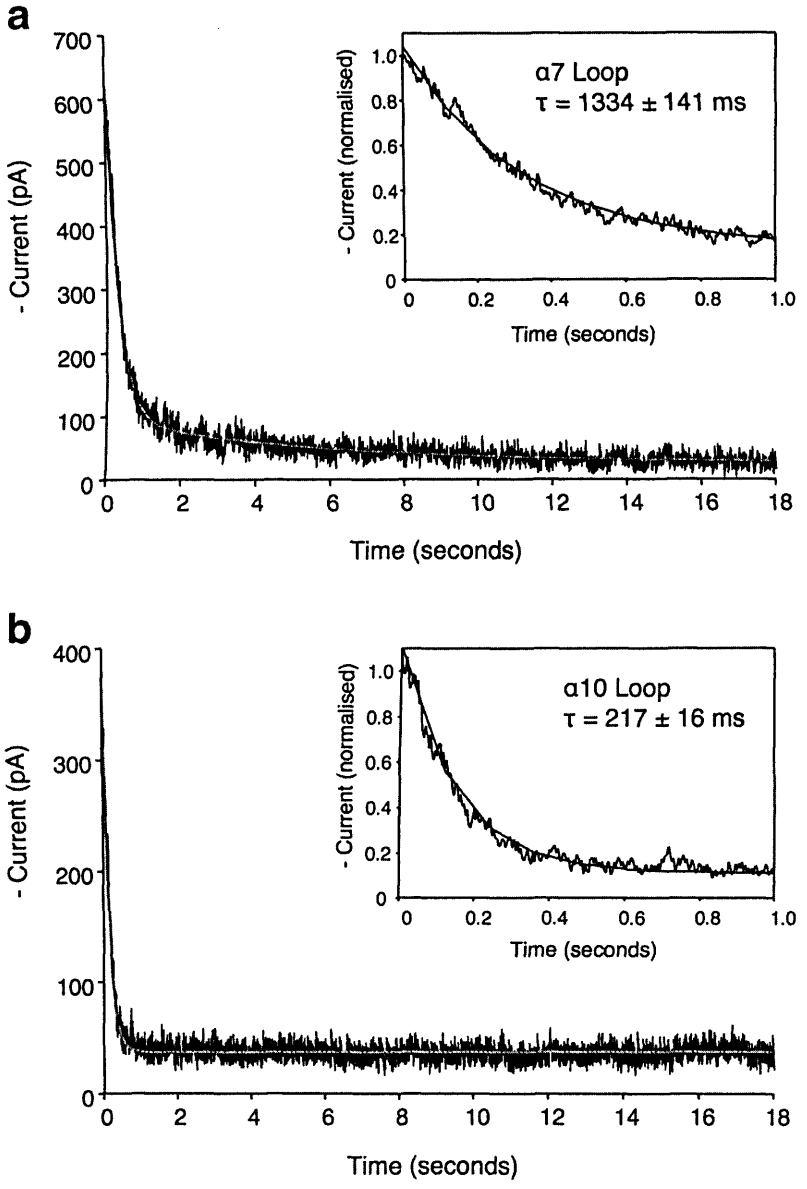

Figure 4.7 Influence of nAChR intracellular domain upon the kinetics of desensitisation. The α7 loop (**a**) and α10 loop (**b**) are shown as examples of chimaeras with slow and fast desensitisation, respectively. Subunit chimaeras were expressed in tsA201 cells and whole-cell responses obtained by 20 second applications of 50 μM DMPP. These were inverted and fitted with one or the sum of two exponential functions of the form $I = I_{ss}+I_{max}*e^{(-t/\tau)}$, where I_{ss} = steady state current, I_{max} = peak steady state current, τ = time constant. The inserts show, on an expanded timescale, the fit to the initial part of the response. Traces are representative examples of n = 8-21 responses from 3-12 cells.

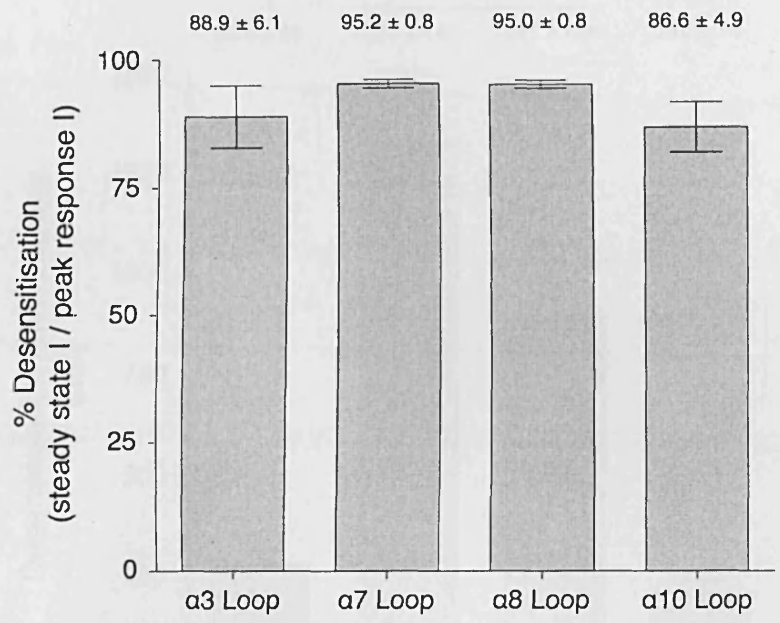

Figure 4.8 Percentage desensitisation of whole-cell responses from tsA201 cells transiently transfected with loop chimaeras. The mean percentage desensitisation of whole-cell responses obtained by applying 50 μM DMPP for 20 seconds. The responses were inverted and fitted as described in the legend for Figure 4.7. From this, the steady state current / peak response current was determined. The values of each response obtained per cell were averaged and presented as n= 3-8 cells.

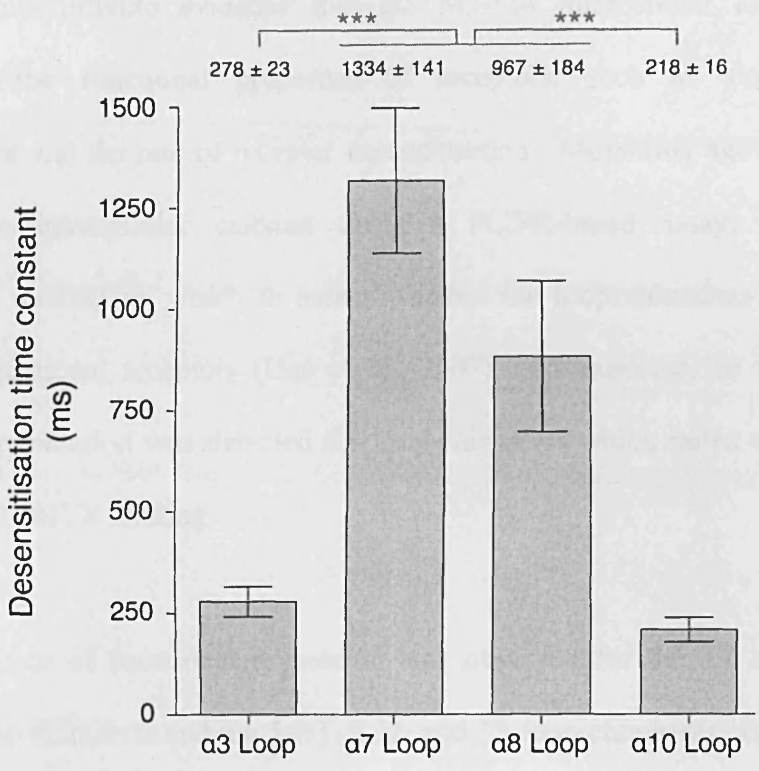

Figure 4.9 Desensitisation time constant analysis of whole-cell responses from tsA201 cells transiently transfected with loop chimaeras. The mean time constant of desensitisation of whole-cell responses obtained by applying 50 μM DMPP for 20 seconds. The responses were inverted and fitted as described in the legend for Figure 4.7 and the time constant determined. The values of each response obtained per cell were averaged and presented as n= 3-8 cells. Error bars are SEM. The differences between groups were tested for significance using ANOVA with Tukey's multiple comparison post-test. *** indicates $P<0.001$.

4.6 Discussion

These results provide evidence that the M3-M4 intracellular loop domain influences the functional properties of receptors, such as single-channel conductance and the rate of receptor desensitisation. Measuring agonist-induced changes in intracellular calcium using a FLIPR-based assay, provides a convenient method by which to assess whether the loop chimaeras are able to generate functional receptors (Gee *et al.*, 2007). As expected, no evidence of functional expression was detected for loop chimaeras which failed to give cell-surface [^{125}I]αBTX binding.

Clear evidence of functional expression was observed for the α3, α7, α8, α10 nAChR loop chimaeras and the 5-HT$_3$R 3A and 3B loop chimaeras. Interestingly, there was not a good correlation between those chimaeras which displayed high levels of cell-surface [^{125}I]αBTX binding and the size of the response for those for which clear evidence of functional expression could be detected. The α1 and α4 loop chimaeras, for example, give high levels of cell-surface [^{125}I]αBTX binding but no evidence of functional expression. The α3 and α10 loop chimaeras gave relatively low levels of cell-surface [^{125}I]αBTX binding, but clear evidence of functional expression. It appears, therefore, that the nAChR intracellular loop domain can also exert a profound influence upon the ability of subunits, once assembled, to generate functional receptors. Similar discrepancies between levels of radioligand binding and function have been reported in studies with other types

of nAChR subunit chimaeras and with subunits altered by site-directed mutagenesis (García-Guzmán *et al.*, 1994; Valor *et al.*, 2002; Castelan *et al.*, 2007; Gee *et al.*, 2007).

Despite the well established evidence that the conductance of Cys-loop type ligand-gated ion channels is influenced by amino acids located within the second transmembrane domain (Imoto *et al.*, 1988), there is now strong evidence to indicate that channel conductance is also influenced by other subunit domains, including the M3-M4 intracellular loop (Kelley *et al.*, 2003; Hales *et al.*, 2006; Gee *et al.*, 2007). The noise analysis of the loop chimaera responses, presented in this study, is entirely consistent with previous data implicating the intracellular loop in modulating channel conductance (Kelley *et al.*, 2003; Hales *et al.*, 2006; Gee *et al.*, 2007). It has been proposed that the influence of the intracellular loop domain is a consequence of positively charged amino acids found in the MA region of the subunit intracellular loop (Kelley *et al.*, 2003; Hales *et al.*, 2006). It has been demonstrated that the replacement of three arginine residues within the MA region of the 5-HT_{3A} subunit with the equivalent residues found in the 5-HT_{3B} subunit, results in a dramatic increase in single channel conductance (Kelley *et al.*, 2003). This increase has been confirmed in this study with the 5-HT_{3A} subunit loop displaying a sub-pS single-channel conductance (0.5 pS), and the 5-HT_{3B} subunit loop displaying a conductance considerably higher (34 pS). In addition, differences in single-channel conductance have been described here

showing that the loop domain of nAChRs can also dramatically influence single-channel conductance.

Inspection of the MA region of the subunit loops examined in this study (α3, α7, α8, α10 from nAChRs and 3A and 3B from the the 5-HT_3Rs) indicates that these findings are in general agreement with the proposal that positively charged amino acids in this region are important (Figure 4.10). It is possible, however, that charged amino acids other than the three arginines mutated by Kelley *et al.* are able to exert an additional influence on single channel conductance of the loop chimaeras. There appears to be a trend, whereby loop chimaeras containing more positively charged residues and/or fewer negatively charged residues within the MA region of the M3-M4 loop display lower single-channel conductance (Figure 4.10). The number of positively charged residues is greater and the overall net charge is more positive in the MA region of the nAChR loop chimaera with the lowest conductance (α10) than in those with the highest conductance (α3, α7 and α8), although there appears to be no direct relationship between net charge and conductance as is observed for the M2 domain rings of negative charge of the muscle nAChR (Imoto *et al.*, 1988). The difference in conductance between the 5-HT_{3A} loop (0.48 pS) and the 5-HT_{3B} loop (34 pS) observed here, is in agreement with previous studies where the MA-helix region in the human 5-HT_{3A}R (0.76 pS) was replaced with the same region from the 5-HT_{3B}R (22.24 pS) and expressed in HEK tsA201 cells (Kelley *et al.*, 2003).

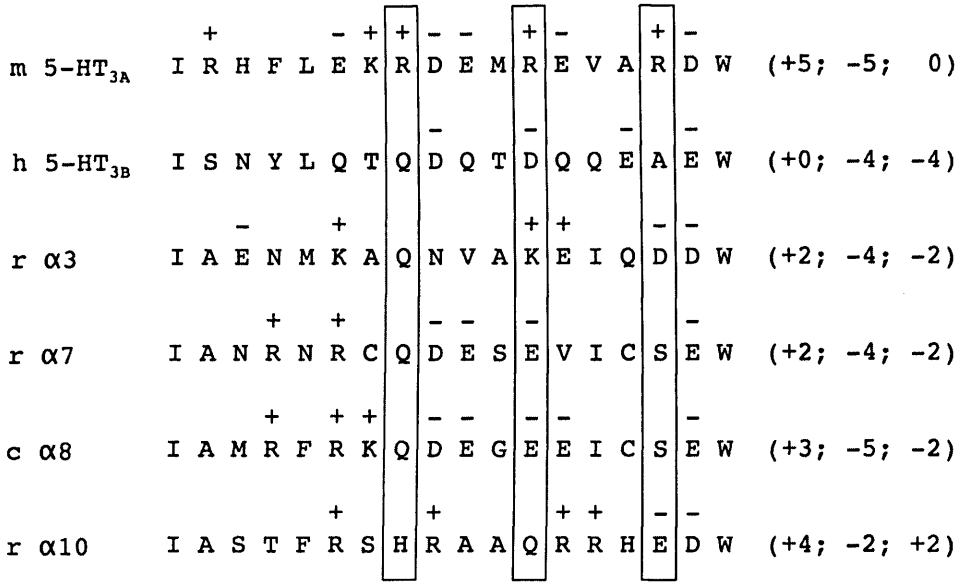

Figure 4.10 Amino acid sequence alignment of the MA region of nAChR and 5-HT$_3$R subunits. Sequences are shown for all loop chimaeras for which single channel conductance was determined by noise analysis. Amino acids with positively and negatively charged side chains are indicated (by + and -, respectively). The total number of positively charged residues, negatively charged amino acids and the overall net charge within the MA region is indicated (within parentheses, on the right hand side). The species of each subunit used for construction of the loop chimaeras is shown next to the subunit name (c, chick; h, human; m, mouse; r, rat).

A possible explanation for the differences in conductance observed is that when the MA-helix region is more positively charged (e.g. 5-HT_{3A}R and nAChR α10), the intracellular loop domain is providing the region of the protein that is rate-limiting for ion permeation, or is allosterically influencing the conduction path of the channel. In contrast, when the MA-helix region is more negatively charged (e.g. 5-HT_{3B}R, nAChR α3, α7 and α8), the subunit loop is not rate-limiting for ion permeation and so some other region of the protein then determines the overall single channel conductance. The high-resolution structure of the nAChR lends support to this hypothesis (Unwin, 2005). The MA-helix region is thought to contribute to the "vestibule-like" structure protruding from the membrane bilayer into to the cytoplasm of the cell. It has been postulated that this portion of the receptor acts as a further filter to ions passing though the ion-channel pore (Peters *et al.*, 2005; Unwin, 2005).

It has also been found that the M3-M4 intracellular domain influences the rate of receptor desensitisation (Figure 4.9). This is perhaps a surprising finding, given that residues within the M2 transmembrane domain of nAChRs were previously shown to be major determinants of the rates of receptor desensitisation (Revah *et al.*, 1991). There is, however, evidence that subunit domains other than M2 can influence desensitisation. Recent studies with nAChR/5-HT_3R subunit chimaeras have demonstrated that the N-terminal extracellular domain can influence receptor desensitisation (Gee *et al.*, 2007), as might be expected given that receptor desensitisation is coupled to receptor activation, and that the N-terminal domain

must be where receptor activation is initiated. Taken together, these results indicate that receptor desensitisation can be influenced by a variety of subunit domains.

Given the predicted conservation of structural elements throughout the Cys-loop family of receptors, it is likely that the intracellular loop will influence functional properties, such as conductance and desensitisation, not only of the nAChR and 5-HT_3R members but of glycine and GABA receptors too.

Table 4.1 Functional characterisation of loop chimaeras

Loop chimaera	Functional expression*	Conductance (pS) (n=5-9)	Time constant for desensitisation (ms) (n=6-21)
α1 loop (α7/5-$HT_{3A}^{\alpha1\text{-loop}}$)	No	ND	ND
α2 loop (α7/5-$HT_{3A}^{\alpha2\text{-loop}}$)	No	ND	ND
α3 loop (α7/5-$HT_{3A}^{\alpha3\text{-loop}}$)	Yes	29.4±2.8 [a]	278±23 [d]
α4 loop (α7/5-$HT_{3A}^{\alpha4\text{-loop}}$)	No	ND	ND
α5 loop (α7/5-$HT_{3A}^{\alpha5\text{-loop}}$)	No	ND	ND
α6 loop (α7/5-$HT_{3A}^{\alpha6\text{-loop}}$)	No	ND	ND
α7 loop (α7/5-$HT_{3A}^{\alpha7\text{-loop}}$)	Yes	36.1±3.2 [a]	1334±141 [e]
α8 loop (α7/5-$HT_{3A}^{\alpha8\text{-loop}}$)	Yes	24.9±0.8 [a]	967±184 [e]
α9 loop (α7/5-$HT_{3A}^{\alpha9\text{-loop}}$)	No	ND	ND
α10 loop (α7/5-$HT_{3A}^{\alpha10\text{-loop}}$)	Yes	10.5±1.7 [b]	218±16 [d]
β1 loop (α7/5-$HT_{3A}^{\beta1\text{-loop}}$)	No	ND	ND
β2 loop (α7/5-$HT_{3A}^{\beta2\text{-loop}}$)	No	ND	ND
β3 loop (α7/5-$HT_{3A}^{\beta3\text{-loop}}$)	No	ND	ND
β4 loop (α7/5-$HT_{3A}^{\beta4\text{-loop}}$)	No	ND	ND
5-HT_{3A} loop (α7/5-$HT_{3A}^{5HT3A\text{-loop}}$)	Yes	0.48±0.04 [c]	ND
5-HT_{3B} loop (α7/5-$HT_{3A}^{5HT3B\text{-loop}}$)	Yes	34.0±6.6 [a]	ND

* Functional expression determined by FLIPR-based intracellular calcium assay

Data are ±SEM

Statistical significance: [a] vs [b c] ; [b] vs [c] $P<0.001$, [d] vs [e] $P<0.001$

ND = not determined

Chapter 5

Characterisation of α9α10 nAChRs

Chapter 5

Characterisation of α9α10 nAChRs

5.1 Introduction

In collaboration with Dr Belen Elgoyhen's laboratory (Buenos Aires, Argentina), two studies were undertaken which made use of existing nAChR/5-HT_{3A} chimaeric subunits, to determine the effect of a series of compounds on α9α10 nAChRs. The first study concerned the effects of three quinoline derivatives quinine, quinidine and chloroquine; (Ballestero *et al.*, 2005), while the second study focused on the NMDA receptor antagonists, neramexane and memantine (Plazas *et al.*, 2007).

5.2 α9α10 nAChRs

The α9 and α10 subunits are the most recently cloned vertebrate nAChR subunits (Elgoyhen *et al.*, 1994; Elgoyhen *et al.*, 2001). As discussed previously (Chapter 1), the α9 and α10 nAChR subunits are unusual, in that they exhibit a very specialised expression profile and thus do not fall conveniently into the

conventional classification of either 'muscle-type' or 'neuronal-type' nAChRs. The α9 and α10 subunits are expressed primarily in cochlear and vestibular hair cells. Recombinant receptors assembled from α9 and α10 subunits exhibit functional and pharmacological properties that are similar to native hair cell cholinergic receptors. Recombinant α9α10 nAChR expressed in *Xenopus* oocytes show sensitivity to αBTX and a high conductance for Ca^{2+} (Elgoyhen *et al.*, 2001). These similarities to the native receptor strongly suggest that heteromeric α9α10 nAChRs mediate cholinergic dependent auditory nerve responses. While α9 subunits can form functional nAChRs when expressed in oocytes, α10 subunits on their own cannot. Indeed, α10 coexpressed in pairwise combinations with any other nAChR subunit capable of forming heteromeric receptors (α2-α6 or β2-β4) failed to elicit any functional responses. Only when coexpressed with α9 are functional receptors detected whose biophysical and pharmacological properties are similar to those detected from native hair cell nAChRs (Elgoyhen *et al.*, 2001; Gomez-Casati *et al.*, 2005). *In situ* hybridisation studies have shown that mRNA transcripts for both α9 and α10 nAChR subunits are present in the outer hair cells (OHCs) of the developing and adult cochlea, while in inner hair cells (IHCs) both subunit types are coexpressed from late embryogenesis until approximately the second postnatal week, when α10 gene expression undergoes a developmental switch and disappears (Katz *et al.*, 2004). While α9 mRNA continues to be expressed, both mRNA and protein levels of α10 are down-regulated to undetectable levels which correlates with the corresponding loss of functional responses to acetylcholine in these cells (Katz *et al.*, 2004). These data, along

with studies conducted in α9 knockout mice showing that the α9 nAChR subunit is required for the physiological responses mediated by OHCs (Vetter *et al.*, 1999), strongly suggest that α9 and α10 nAChR subunits form heteromeric receptors. Recently, the stoichiometry of the recombinant α9α10 nAChR has been elucidated in *Xenopus* oocytes, using a subunit-specific reporter mutation approach (Plazas *et al.*, 2005). From these studies, it has been concluded that the α9α10 nAChR has a pentameric structure of $(\alpha9)_2(\alpha10)_3$ (Plazas *et al.*, 2005).

In addition to their expression in the inner ear, α9α10 nAChRs have been found to be expressed in dorsal root ganglion (DRG) neurones, where they may play a role in pain processing (Lips *et al.*, 2002). They have also been identified in a variety of other tissues, where their role is less well defined, such as lymphocytes, sperm, and keratinocytes, and have been implicated in mediating process such as neuropathic pain and aspects of the immune response (Vincler *et al.*, 2006).

5.3 Expression of α9α10 nAChRs in HEK cells

As with the homomeric α7 nAChR, considerable problems have been reported with the expression of α9α10 receptors in mammalian expression systems (Millar, 1999). While α9 and α10 nAChRs can generate functional heteromeric receptors when reconstituted in frog oocytes (Elgoyhen *et al.*, 2001), and functional homomers in the case of α9 alone (Elgoyhen *et al.*, 1994), expression in common

mammalian cell lines has so far proved unsuccessful. Although much can be achieved by characterisation of oocyte-expressed nAChRs, some approaches to the pharmacological characterisation of α9α10 nAChRs (e.g. equilibrium binding studies) have been hindered by the lack of a suitable cultured cell-based expression system (Baker *et al.*, 2004). Previous studies have failed to detect functional nAChRs in mammalian cells transfected with nAChRs α9 and α10 subunits (Lustig *et al.*, 2001). When recombinant α9 and α10 nAChR subunit DNAs were introduced by transient transfection into cultured mammalian HEK tsA201 cells, either alone or in a pairwise combination, no evidence for specific high affinity [^{3}H]MLA binding was found (Baker *et al.*, 2004).

In a previous study in this laboratory, an influenza haemagglutinin (HA) epitope tag was added to the α9 and α10 subunits (Baker *et al.*, 2004). Immunoblotting studies with HA-tagged α9 and α10 subunits identified protein bands of a similar size to those expected for full-length α9 and α10 subunits (Baker *et al.*, 2004). These data suggest that the absence of specific nicotinic radioligand binding is a consequence of inappropriate subunit folding and/or assembly, rather than due to problems of inefficient protein synthesis.

Similar problems with receptor expression in transfected mammalian cell lines have been encountered with the homomeric α7 nAChR subunit and have been attributed to inappropriate folding and/or assembly (Cooper and Millar, 1997). Coexpression of the α7 subunit with the nAChR interacting chaperone protein

RIC-3 alleviates this problem and facilitates efficient expression of α7 nAChRs at the cell surface (Lansdell *et al.*, 2005; Williams *et al.*, 2005). RIC-3 has also been found to up-regulate cell-surface expression of other nAChR subtypes in mammalian cell lines, such as α3β4 and α4β2 (Lansdell *et al.*, 2005). However, coexpression of RIC-3 with α9 and α10 nAChR subunits, either alone or together, fails to produce any functionally and pharmacologically detectable cell surface nAChRs in mammalian cell lines such as HEK tsA201 (Lansdell *et al.*, 2005).

5.4 The interaction of wild-type α9α10 nAChRs with RIC-3

To investigate the influence of RIC-3 upon α9α10 nAChRs further, HEK tsA201 cells were transiently cotransfected with α9α10 nAChR subunit cDNAs and epitope tagged RIC-3 cDNA. Metabolic radio-labelling and co-immunoprecipitaton (Section 2.7) were employed to determine whether or not the α9α10 nAChR and RIC-3 show protein-protein association (Figure 5.1). As a control, the FLAG-tagged RIC-3 was also co-expressed with the rat β2 nAChR subunit, which has previously been shown to associate with RIC-3 in this type of assay (Lansdell *et al.*, 2005). Evidence was obtained for an interaction between the FLAG-tagged RIC-3 and β2 nAChR subunit, as expected (Figure 5.1). In contrast, little or no co-association was observed with the α9 subunit and much

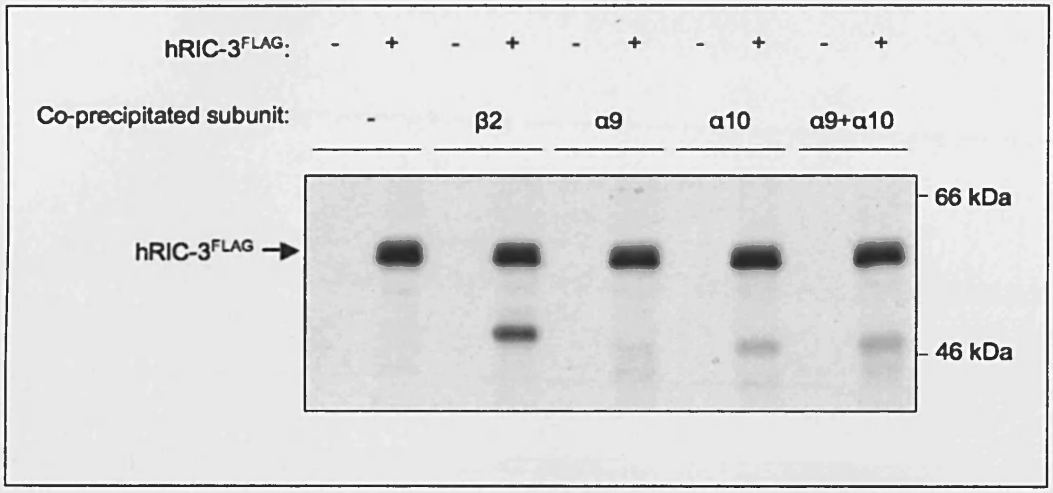

Figure 5.1 Co-immunoprecipitation of wild-type rat nAChR subunits with FLAG epitope tagged hRIC-3 (hRIC-3^{FLAG}). Human embryonic kidney tsA201 cells were transiently transfected with the nAChR subunits β2, α9, α10 or α9 and α10 together, with hRIC-3^{FLAG} (+), or empty vector (-). The cells were then metabolically radiolabeled and cell lysates incubated with the monoclonal M2 anti-FLAG antibody. The samples were resolved by SDS-PAGE and the relative levels of proteins detected by autoradiography. Results are from a single experiment.

reduced levels with the α10 subunit, when expressed individually. When coexpressed the amount of nAChR subunit protein immunoprecipitated was much lower than observed with the β2 nAChR subunit control lane but comparable to the α10 subunit alone (Figure 5.1). It is possible that this evidence for a weaker interaction between RIC-3 and the α9 or α10 subunits may explain why RIC-3 fails to facilitate maturation of these nAChRs subunits.

5.5 Characterisation of α9/5-HT_{3A} and α10/5-HT_{3A}R chimaeras

In an effort to overcome problems associated with heterologous expression of α9/α10 nAChRs in mammalian cells, a chimaeric receptor approach has been used primarily to investigate various pharmacological and molecular characteristics of the α9 and α10 receptors (Baker *et al.*, 2004). Chimaeras were created ($\alpha9^{(L209)}$/5-HT_{3A}; α9χ and $\alpha10^{(L206)}$/5-HT_{3A}; α10χ), in which the extracellular N-terminal domain of the α9 or α10 subunits were fused to the transmembrane and intracellular domains of the 5-hydroxytryptamine-3A (5-HT_{3A}) subunit (Baker *et al.*, 2004). These chimaeras successfully form functional receptors when reconstituted in oocytes (Baker *et al.*, 2004). This approach has successfully permitted the pharmacological characterisation of recombinant α9/α10 nAChR in cultured cell lines. Radioligand binding experiments give a good specific to non-specific signal, and the chimaeric receptors retain the same pharmacological

profile when compared to wild-type receptors expressed in *Xenopus* oocytes (Baker *et al.*, 2004). As described previously, [^{3}H]methyllycaconitine binds with high affinity (K_d = 7.5 ± 1.2 nM) to cells coexpressing the α9 and α10 subunit chimaeras (Baker *et al.*, 2004).

5.6 Effects of quinine, quinidine, and chloroquine on α9α10 nAChRs

In this study, the effects of three quinoline derivatives (quinine, quinidine and chloroquine) on α9α10 nAChRs was investigated (Ballestero *et al.*, 2005).

5.6.1 Introduction

For centuries, the alkaloid quinine, obtained from the bark of the *Cinchona* tree has been the traditional cure against malaria which is caused by members of the *Plasmodium* family of protozoans. In more recent times, synthetically produced compounds (e.g. quinoline derivatives) have replaced naturally occurring quinine. Data has been obtained to show that the anti-malarial quinoline derivatives quinine, quinidine and chloroquine (Figure 5.2) act as antagonists of α9α10 nAChRs (Ballestero *et al.*, 2005). Side effects of these compounds include reversible (but sometimes permanent) sensorineural hearing loss, tinnitus and vertigo (Jung *et al.*, 1993). Evidence suggests these compounds mediate their

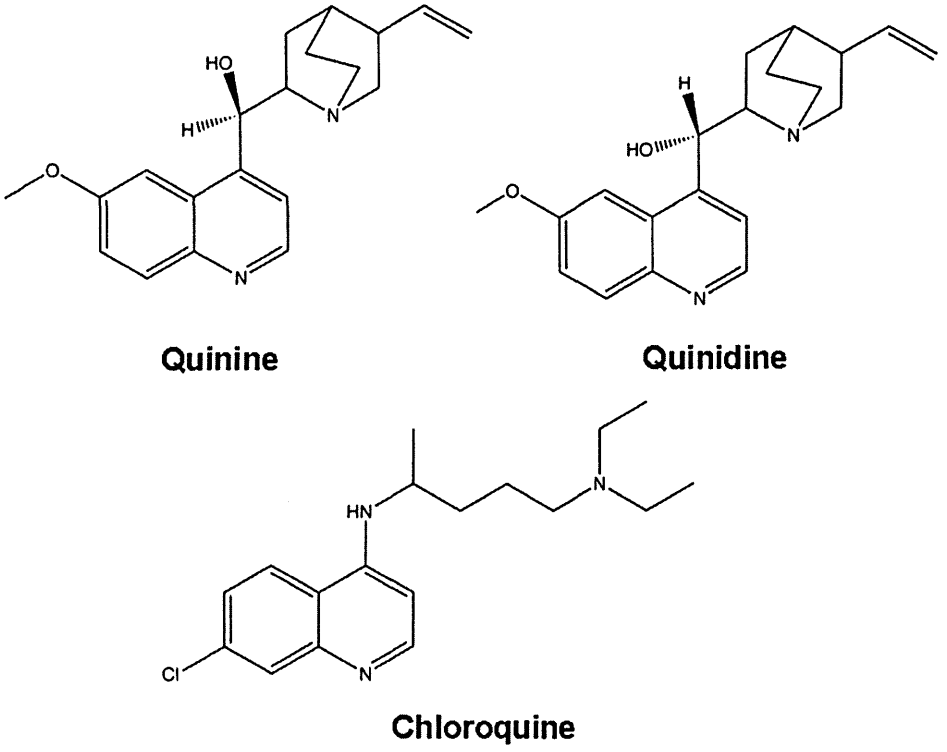

Figure 5.2 Chemical structures of quinine, quinidine, and chloroquine. All the structures share a common aromatic quinoline moiety (C_9H_7N) with a methoxy substituent. Quinine and quinidine are optical isomers and contain a quinuclidine ring.

effects via α9α10 nAChRs, further supporting a role for these receptors in mediating auditory responses and/or possible auditory protection mechanisms (see above).

Functional data from experiments on recombinant α9α10 nAChRs reconstituted in *Xenopus* oocytes, show that quinine, quinidine and chloroquine all block acetylcholine evoked responses at micromolar concentrations in a concentration dependent manner. Inhibition curves in oocytes have been used to determine the rank order of potency: chloroquine, IC_{50} = 0.39 ± 0.08 μM > quinine, IC_{50} = 0.97 ± 0.07 μM > quinidine IC_{50} = 1.28 ± 0.05 μM (Ballestero *et al.*, 2005). Further data indicated that the mechanism of block was competitive in nature, as determined by concentration-response curves in the presence or absence of differing antagonist drug concentrations. The block was fully competitive for chloroquine, and at least partially competitive, at lower concentrations, for quinine and quinidine. At higher concentrations, it appeared the mode of action was also non-competitive for quinine and quinidine (Ballestero *et al.*, 2005).

To further analyse the nature of the competitive antagonism observed in *Xenopus* oocytes, equilibrium competition radioligand binding studies were performed to examine whether chloroquine, quinine and quinidine were able to displace binding of the high-affinity nicotinic antagonist, [^{3}H]MLA. Experiments were performed to address the nature of the competitive antagonism by carrying out

displacement binding assays in the mammalian HEK cell line tsA201, transiently transfected with α9χ and α10χ receptor.

5.6.2 Competition radioligand binding

As described previously, [^{3}H]MLA binds with high nanomolar affinity (K_d = 7.5 ± 1.2 nM) to cells coexpressing the α9 and α10 subunit chimaeras (Baker *et al.*, 2004). Equilibrium competition binding studies were performed with chloroquine, quinine and quinidine to determine their affinity for the α9α10 receptor (Figure 5.3). In all cases (chloroquine, quinine and quinidine), complete displacement of bound [^{3}H]MLA was observed, providing evidence of competitive binding to a single high-affinity site. Binding affinities (K_i values) and the rank order of potency determined from three independent experiments were as follows: chloroquine, 2.3 ± 0.5 μM > quinine, 5.5 ± 0.7 μM > quinidine, 13.0 ± 2.9 μM. Thus, the rank order of potency was in agreement with that obtained from functional data in *Xenopus* oocytes.

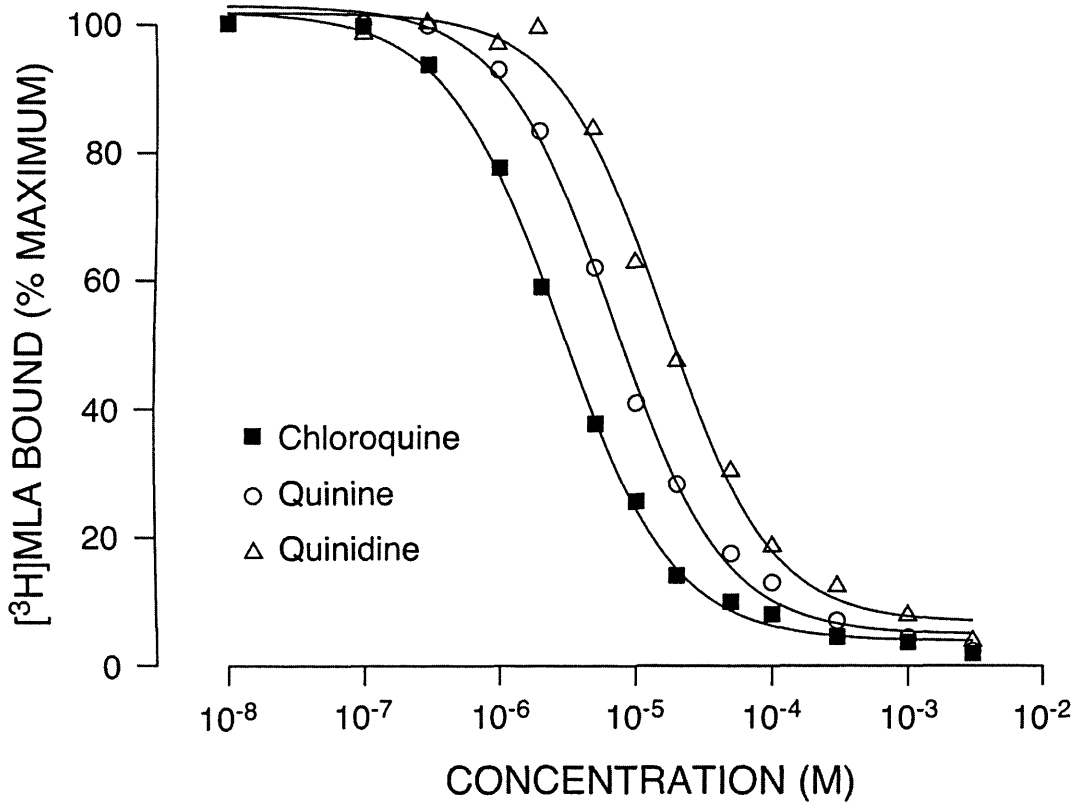

Figure 5.3 Competition radioligand binding to transfected mammalian cells. Cultured mammalian tsA201 cells were cotransfected with subunit chimaeras $\alpha9^{(L209)}$/5-HT_{3A} and $\alpha10^{(L206)}$/5-HT_{3A} (in which the extracellular N-terminal domain of the α9 or α10 subunits are fused to the transmembrane and intracellular domain of the mouse 5-HT_{3A} subunit). Competition-binding data with chloroquine, quinine, and quinidine is presented as a percentage of [^{3}H]MLA binding obtained in the absence of competing ligand. The curves are from a single experiment but are typical of three independent experiments.

5.6.3 Discussion

As described previously, chimaeric α9χα10χ receptors were successfully transiently transfected into the mammalian tsA201 cell line (Baker *et al.*, 2004). Radioligand displacement binding assays with [^{3}H]MLA were carried out to verify the competitive nature of the block established through functional experiments, and to determine the K_i of chloroquine, quinine and quinidine on α9α10 receptors. As shown (Figure 5.3), all three compounds were able to fully displace the bound [^{3}H]MLA with low micromolar affinities, confirming a competitive nature to their blocking action. Combined with the data from functional studies, in the case of chloroquine, it appears that the blocking action on acetylcholine responses is entirely mediated by a competitive mechanism. In α9α10 nAChR expressing oocytes, increasing concentrations of chloroquine shifted the acetylcholine concentration-response curve to the right, with no reduction in the maximal evoked acetylcholine response (behaviour typical of a competitive antagonist). In the case of quinine and quinidine, their block appears to be mediated by a mixed competitive and non-competitive mechanism. Whilst at low concentration of agonist, a rightward shift of the acetylcholine concentration-response curve with no reduction in the maximal evoked acetylcholine response does occur; at higher concentrations, a rightward shift of the concentration-response curve with additional concomitant insurmountable antagonism resulted (behaviour typical of a non-competitive antagonist).

It is noteworthy that the IC_{50} values calculated from the functional data in the presence of acetylcholine (chloroquine, 0.39 μM; quinine, 0.97 μM and quinidine, 1.37 μM) are lower than the calculated K_i affinities (2.3 μM; 5.5 μM and 13.0 μM, respectively; Figure 5.3). These results, at first appear to support a mechanism other than purely competitive antagonism. Thus, this observation is at odds with the hypothesis that chloroquine acts solely as a competitive antagonist on α9α10 nAChRs, as described above, since it might be expected that the IC_{50} value to be higher than the K_i for a purely competitive antagonist. An alternative explanation, which would account for this difference, is that the functional data was obtained in a frog oocyte expression system using α9α10 nAChRs; whereas the K_i values were calculated from experiments conducted in a mammalian expression system (tsA201 cells), using chimaeric α9χα10χ receptors. Reassuringly, both sets of values are in the same low micromolar range.

5.7 Inhibition of the α9α10 nAChR by neramexane

In a second related study, the effects on α9α10 nAChRs of neramexane, a novel amino-alkyl-cyclohexane derivative that is a non-competitive N-methyl-D-aspartate (NMDA) receptor antagonist, were investigated (Plazas *et al.*, 2007).

5.7.1 Introduction

Neramexane (MRZ 2/579, 1-amino-1,3,3,5,5-pentamethyl-cyclohexane), a new NMDA receptor antagonist developed by Merz and Co. (Danysz *et al.*, 2002), is currently in phase II of clinical trails for various conditions including Alzheimer's disease and chronic pain. Neramexane was developed as a therapeutic agent due to its similarities to the previously discovered channel blocker, memantine (3,5-dimethyl-1-adamantane; Figure 5.4). Memantine is an adamantine derivative, and a well established blocker of ligand-gated ion channels permeable to Ca^{2+} such as the NMDA type glutamate receptor (Chen *et al.*, 1992; Parsons *et al.*, 1993; Bresink *et al.*, 1996) or nicotinic acetylcholine receptors including α9α10 (Buisson and Bertrand, 1998; Oliver *et al.*, 2001).

Memantine has successfully been used in the treatment of dementia and spasticity for over a decade and further clinical and pre-clinical studies indicate a far greater therapeutic potential for the drug (Parsons *et al.*, 1999b). Indeed, the potential therapeutic application of agents interacting with the glutamatergic system in the CNS is enormous and ranges from neuroprotection through pain to psychiatric diseases such as schizophrenia and depression (Parsons *et al.*, 1998; Oliver *et al.*, 2001). Typically, it has been problematic to develop NMDA receptor antagonists with a satisfactory side effect to benefit ratio, so memantine has been used as a model agent to screen for novel drugs. Neramexane was selected for further study as an NMDA antagonist based on its similarity to memantine, with respect to

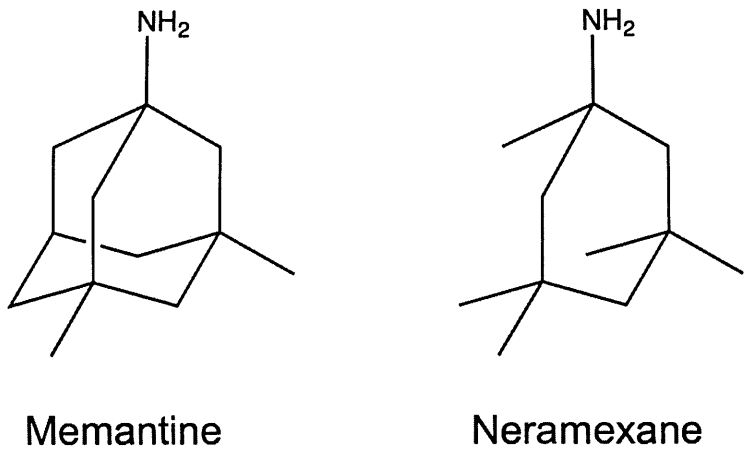

Figure 5.4 Chemical structures of neramexane and memantine. Memantine (1-amino-3,5-Dimytheyl-adamantane), is an adamantane derivative and is characterised by its carbon cage structure. Neramexane (1-amino-1,3,3,5,5-pentamethyl-cyclohexane), is an amino-alkyl-cyclohexane derivative and is characterised by its 6-carbon ring structure.

channel blocking kinetics, voltage dependency and affinity (Danysz *et al.*, 2002).

Data from *Xenopus* oocytes and *in vivo* recordings from hair cells have demonstrated that, as reported for memantine (Oliver *et al.*, 2001), clinically relevant concentrations of neramexane block recombinant α9α10 nicotinic acetylcholine receptors in a voltage-independent, non-competitive manner. These data therefore support a possible role for neramexane *in vivo*, in potentially unexplored therapeutic areas, via blockade of α9α10-containing nAChRs of cochlear hair cells.

5.7.2 Competition radioligand binding

Competition radioligand binding experiments were carried out to determine the presence or lack of an interaction between neramexane and the ligand binding domain of the receptor, in HEK tsA201 cells transfected with the α9/5-HT_{3A} ($\alpha9^{(L209)}$/5-HT_{3A}; α9χ), and the α10/5-HT_{3A} ($\alpha10^{(L206)}$/5-HT_{3A}; α10χ) receptor chimaeras. Complete displacement of bound [^{3}H]MLA was observed for both neramexane and memantine (Figure 5.5), but only at very high concentrations of competing ligand (K_i = 2.7 ± 0.5 mM; n=5, for neramexane and K_i = 0.8 ± 0.2 mM; *n*=3, for memantine). In comparison to the IC_{50} values for the antagonist activity of neramexane and memantine derived from oocyte experiments (0.30 ± 0.03 μM and 1.2 ± 0.4 μM, respectively), the K_i values determined from competition

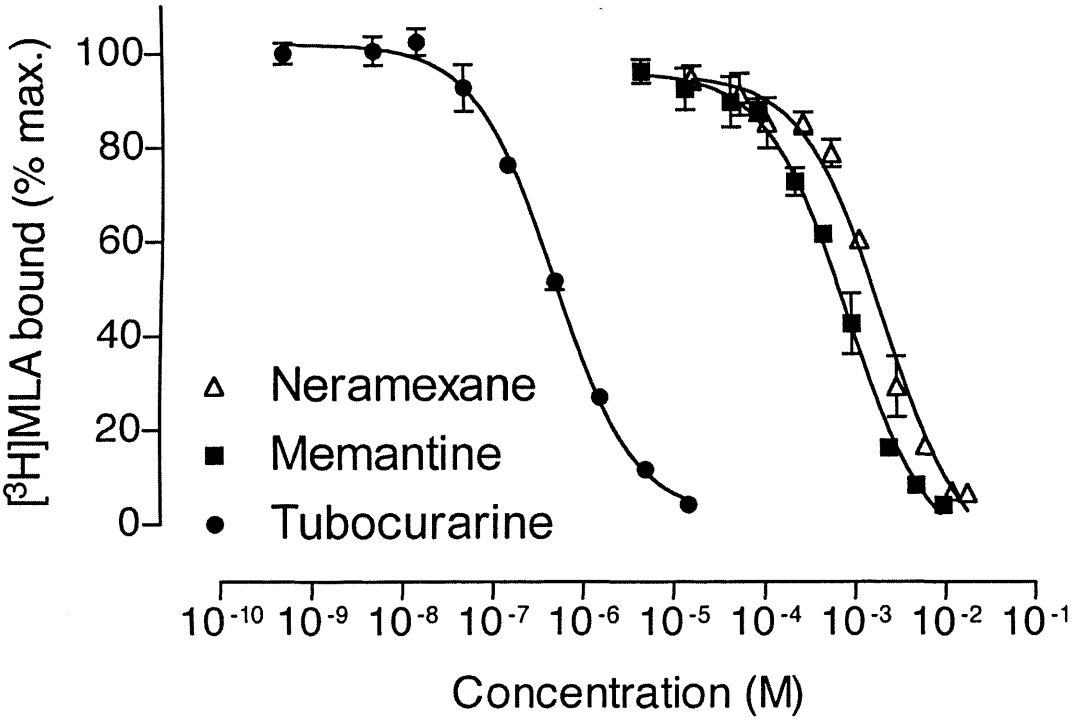

Figure 5.5 Competition radioligand binding to transfected mammalian cells. Cultured mammalian tsA201 cells were cotransfected with subunit chimaeras $\alpha9^{(L209)}$/5-HT_{3A} and $\alpha10^{(L206)}$/5-HT_{3A} (in which the extracellular N-terminal domain of the α9 or α10 subunits are fused to the transmembrane and intracellular domain of the mouse 5-HT_{3A} subunit). Competition-binding data with neramexane, memantine, and tubocurarine is presented as a percentage of [^{3}H]MLA binding obtained in the absence of competing ligand. The curves are from a single experiment but are typical of three independent experiments. Error bars = SEM and represent triplicate values.

binding indicated a substantially lower affinity (~7000-fold and ~700-fold, respectively). Moreover, no displacement of [^{3}H]MLA was observed at concentrations which gave full antagonist activity in oocytes. For comparison, competition binding was also performed with the nicotinic antagonist (+)-tubocurarine, which has previously been shown to displace [^{3}H]MLA binding in α9χα10χ nAChR expressing cells with high affinity (0.29 ± 0.09 μM; Baker *et al.*, 2004), a concentration comparable to the IC_{50} values for neramexane and memantine obtained in oocytes. It would appear, therefore, that the antagonist activity of neramexane and memantine is not due to competitive binding with the agonist-binding site of the α9α10 nAChR.

5.7.3 Discussion

Pharmacological data has been obtained which indicates that the block of acetylcholine-evoked responses of recombinant α9α10 nAChRs by neramexane and memantine is mediated via a non-competitive mechanism. The concentrations of neramexane and memantine required to effectively displace the high-affinity nicotinic radioligand [^{3}H]MLA were ~7000-fold and ~700-fold higher, respectively, than the IC_{50} values determined in *Xenopus* oocytes (Plazas *et al.*, 2007). The non-competitive mode of action of neramexane on the chimaeric α9α10 nAChR shown here (Figure 5.5) is supported by functional data from *Xenopus* oocytes expressing recombinant α9α10 nAChRs. At low micromolar concentrations of neramexane (3 μM) the maximal response to

acetylcholine is reduced and is not overcome by higher concentrations of agonist, as would be expected for non-competitive inhibition.

Neramexane is being developed as an NMDA receptor antagonist for use in therapeutic applications and is currently in phase II of clinical trials. As discussed above it was selected for study due to the similarity in effects to the already well-established NMDA receptor blocker memantine, which has been used clinically for over ten years. It has previously been established that neramexane blocks NMDA and $5HT_{3A}$ receptors with IC_{50} values in the low micro-molar range; 1μM (Parsons *et al.*, 1999a); and 2 μM (Rammes *et al.*, 2001), respectively. In this study (Plazas *et al.*, 2007), data has been obtained which demonstrates that neramexane also interacts with the α9α10 nAChR. Experiments conducted on rat inner hair cells have shown that neramexane can block acetylcholine-evoked responses with an IC_{50} value of 0.3 ± 0.08 μM, which is similar to its apparent affinity on recombinant α9α10 nAChRs reconstituted in oocytes (IC_{50} = 0.39 ± 0.03 μM). Since the sub-micromolar apparent affinity of neramexane on α9α10 nAChRs reported is higher than those found previously for the NMDA and 5-HT_{3A} receptor, it might be of therapeutic significance. The plasma concentrations achieved with neramexane at therapeutic doses is around 0.4-1 μM, which is similar to the IC_{50} value obtained for the α9α10 nAChR in oocytes and on rat inner ear cells, described above. Thus, there is a possibility that neramexane could lead to the reduction or loss of function of this nAChR within the inner ear when used clinically.

Chapter 6

Conclusions and summary

Chapter 6

Conclusions and summary

A series of nAChR subunit loop chimaeras has been constructed with the aim of investigating the influence of the nAChR and 5-HT_3R large intracellular loop domain upon various receptor properties. Work presented in this thesis has demonstrated that the M3-M4 intracellular loop domain exerts a dramatic influence on subunit folding and assembly and on receptor cell-surface expression, intracellular targeting and function.

The loop chimaeras created in this study contain a common extracellular domain (derived from the nAChR α7 subunit) and common transmembrane regions (derived from the 5-HT_{3A} subunit). As has been demonstrated previously, these features facilitate both detection of expressed subunit chimaeras by αBTX and efficient homomeric receptor assembly (Eiselé *et al.*, 1993; Cooper and Millar, 1998; Gee *et al.*, 2007). Consequently, all of these loop chimaeras would be expected to bind [^{125}I]αBTX unless subunit folding or assembly were disrupted by the intracellular loop domain. Interestingly, substantial differences in the levels of cell-surface [^{125}I]αBTX binding with different loop chimaeras were observed (Figure 3.3). These differences appear not to be a consequence of differences in

the level of expressed subunit protein, since loop chimaeras with high, low and intermediate levels of cell-surface [^{125}I]αBTX binding were detected in similar amounts by immunoprecipitation of FLAG-tagged subunit chimaeras (Figure 3.5). It seems reasonable to assume, therefore, that the variation in levels of cell-surface binding are a consequence of differences in the proportion of total subunit protein transported to the cell surface and that this is a consequence of differences in receptor trafficking caused by variation in the intracellular loop domains.

All loop chimaeras were also examined using radioligand binding on disrupted cells, thereby permitting detection of intracellular, as well as cell-surface, receptors. Whereas some loop chimaeras could not be detected on the cell surface, (or gave very low levels of cell surface radioligand binding), all of the intracellular loop chimaeras gave detectable levels of specific radioligand binding in disrupted cell preparations (Figure 3.4). It is likely that the differences in the level of [^{3}H]MLA binding reflect differences in the efficiency with which loop chimaeras are able to fold and oligomerise into a native conformation. Comparisons of the two sets of radioligand binding data indicate that intracellular loop domains influence both efficiency of subunit folding/assembly and also the proportion of correctly folded receptors which are transported to the cell surface. For example, the α5, α6 and α7 loop chimaeras have similar levels of [^{3}H]MLA binding in disrupted cells (Figure 3.4) but very different levels of cell-surface [^{125}I]αBTX binding (Figure 3.5).

It has been shown previously in this laboratory that a FLIPR-based assay, measuring agonist-induced changes in intracellular calcium, provides a convenient method by which to assess whether nAChR/5-HT_3R subunit chimaeras are able to generate functional receptors (Gee *et al.*, 2007). As expected, no evidence of functional expression was detected for loop chimaeras which failed to give cell-surface [^{125}I]αBTX binding. As has been demonstrated previously for the α7 loop chimaera (Gee *et al.*, 2007), clear evidence of functional expression was observed for the α3, α8, α10 and 5-HT_{3B} loop chimaeras. Interestingly, there was not a good correlation between those chimaeras which displayed high levels of cell-surface [^{125}I]αBTX binding and those for which clear evidence of functional expression could be detected. The α1 and α4 loop chimaeras, for example, give high levels of cell-surface [^{125}I]αBTX binding but no evidence of functional expression. The α3 and α10 loop chimaeras gave relatively low levels of cell-surface [^{125}I]αBTX binding, but clear evidence of functional expression. It appears, therefore, that the nAChR intracellular loop domain can also exert a profound influence upon the ability of subunits, once assembled, to generate functional receptors. Similar discrepancies between levels of radioligand binding and function have been reported in studies with other types of nAChR subunit chimaeras and with subunits altered by site-directed mutagenesis (García-Guzmán *et al.*, 1994; Valor *et al.*, 2002; Castelan *et al.*, 2007; Gee *et al.*, 2007).

Despite the well established evidence that the conductance of Cys-loop type ligand-gated ion channels is influenced by amino acids located within the second

transmembrane domain, there is now strong evidence to indicate that channel conductance is also influenced by other subunit domains, including the M3-M4 intracellular loop (Kelley *et al.*, 2003; Hales *et al.*, 2006; Gee *et al.*, 2007). Noise analysis of the loop chimaeras is entirely consistent with previous data implicating the intracellular loop in modulating channel conductance. It has been proposed that the influence of the intracellular loop domain is a consequence of positively charged amino acids (Kelley *et al.*, 2003; Hales *et al.*, 2006) and it has been demonstrated that the replacement of three arginine residues within the MA region of the 5-HT_{3A} subunit intracellular loop results in a dramatic increase in single channel conductance (Kelley *et al.*, 2003). Inspection of the MA region of the subunits examined in this study (α3, α7, α8 and α10) indicates that our findings are in general agreement with the proposal that positively charged amino acids in this region are important (Figure 4.10). It is possible, however, that charged amino acids other than the three arginines mutated by Kelley *et al.* are able to exert an additional influence on single channel conductance of the loop chimaeras. There appears to be a trend, whereby loop chimaeras containing more positively charged residues and/or fewer negatively charged residues display lower single-channel conductances (Figure 4.10). The number of positively charged residues is greater and the overall net charge is more positive in the MA region of the nAChR loop chimaera with the lowest conductance (α10) than in those with the highest conductance (α3, α7 and α8) although there appears to be no direct relationship between net charge and conductance as is observed for the M2 domain of the muscle nAChR (Imoto *et al.*, 1988).

The results provide evidence that the rate of receptor desensitisation is influenced by the M3-M4 intracellular domain. This is perhaps a surprising finding, given that residues within the M2 transmembrane domain of nAChRs have been shown to be important in determining rates of receptor desensitisation (Revah *et al.*, 1991). There is, however, evidence that subunit domains other than M2 can influence desensitisation. Recent studies with nAChR/5-HT_3R subunit chimaeras have demonstrated that the N-terminal extracellular domain can influence receptor desensitisation (Gee *et al.*, 2007). Taken together, these results indicate that receptor desensitisation can be influenced by a variety of subunit domains.

Use of nAChR/5-HT_3R subunit chimaeras has also enabled the pharmacological characterisation of α9α10 nAChRs. Expression of α9/5-HT_{3A} and α10/5-HT_{3A} subunit chimaeras circumvents problems associated with the inefficient folding and assembly of α9α10 nAChRs in mammalian heterologous expression systems. Competition radioligand binding studies have been employed to complement electrophysiological studies of α9α10 nAChRs conducted in Dr Belen Egoyhen's laboratory (Buenos Aires, Argentina) and have helped to determine whether these compounds are acting as either competitive or non-competitive antagonists.

In addition, preliminary studies with both nAChR/5-HT_3R chimaeras and intact nAChR subunits have been performed to examine the influence of co-expression on a recently identified transmembrane molecular chaperone protein RIC-3 and the intracellular protein rapsyn. RIC-3 was found to dramatically attenuate the

level of cell-surface loop chimaeric receptors. In addition, preliminary evidence was obtained concerning the ability of rapsyn to induce receptor clustering via interaction with the nAChR α1 loop domain.

Thus, in the course of this study, subunit chimaeras have been employed successfully to investigate the influence of specific protein domains upon receptor properties. Further studies, building on the work presented here, will in future help to contribute greater insights into the cell biological and biophysical properties of nAChRs and their relatives in health and disease.

In summary, the main focus of this thesis was to investigate the influence of the nAChR M3-M4 intracellular loop domain, upon various aspects of receptor folding, assembly, targeting and function. To examine the influence of the M3-M4 intracellular loop domain in isolation, a series of chimaeric receptors was created which differ only in their loop domain region. The chimaeric receptor constructs all shared a common N-terminal domain from the α7 nAChR subunit, and the four-transmembrane domains from the 5-HT_{3A}R subunit, facilitating homomeric assembly and expression in mammalian cell-lines. It was demonstrated that the large intracellular loop domain could dramatically influence cell-surface expression, targeting within the cell, and functional properties such as single-channel conductance and desensitisation.

References

References

Adams, P.R. (1981). Acetylcholine receptor kinetics. *Journal of Membrane Biology* 58, 161-174.

Alexander, S.P., Mathie, A., and Peters, J.A. (2007). Guide to Receptors and Channels, 2nd edition (2007 Revision). *British Journal of Pharmacology* 150 Suppl 1, S1.

Art, J.J., Fettiplace, R., and Fuchs, P.A. (1984). Synaptic hyperpolarization and inhibition of turtle cochlear hair cells. *Journal of Physiology* 356, 525-550.

Baker, E.R., Zwart, R., Sher, E., and Millar, N.S. (2004). Pharmacological properties of α9α10 nicotinic acetylcholine receptors revealed by heterologous expression of subunit chimeras. *Molecular Pharmacology* 65, 453-460.

Ballestero, J.A., Plazas, P.V., Kracun, S., Gómez-Casati, M.E., Taranda, J., Rothlin, C.V., Katz, E., Millar, N.S., and Elgoyhen, A.B. (2005). Effects of quinine, quinidine, and chloroqine on $\alpha 9\alpha 10$ nicotinic cholinergic receptors. *Molecular Pharmacology* 68, 822-829.

Bernard, C. (1850). Action de curare et de la nicotine sur le système nerveux et sur le système musculaires. *Comptes Rendus de la Société de Biologie* 2, 195.

Blount, P., and Merlie, J.P. (1989). Molecular basis of the two nonequivalent ligand binding sites of the muscle nicotinic acetylcholine receptor. *Neuron* 3, 349-357.

Blount, P., and Merlie, J.P. (1991). BIP associates with newly synthesized subunits of the mouse muscle nicotinic receptor. *Journal of Cell Biology* 113, 1125-1132.

Blount, P., Smith, M.M., and Merlie, J.P. (1990). Assembly intermediates of the mouse muscle nicotinic acetylcholine receptor in stably transfected fibroblasts. *Journal of Cell Biology* 111, 2601-2611.

Boorman, J.P.B., Groot-Kormelink, P.J., and Sivilotti, L.G. (2000). Stoichiometry of human recombinant neuronal nicotinic receptors containing the β3 subunit expressed in Xenopus oocytes. *Journal of Physiology* 529, 565-577.

Boulter, J., Connolly, J., Deneris, E., Goldman, D., Heinemann, S., and Patrick, J. (1987). Functional expression of two neuronal nicotinic acetylcholine receptors from cDNA clones identifies a gene family. *Proceedings of the National Academy of Sciences, USA* 84, 7763-7767.

Bourne, Y., Talley, T.T., Hansen, S.B., Taylor, P., and Marchot, P. (2005). Crystal structure of a Cbtx-AChBP complex reveals essential interactions between snake α-neurotoxins and nicotinic receptors. *EMBO Journal* 24, 1512-1522.

Boyd, G.W., Doward, A.I., Kirness, E.F., Millar, N.S., and Connolly, C.N. (2003). Cell surface expression of 5-hydroxytryptamine type 3 receptors is controlled by an endoplasmic reticulum retension signal. *Journal of Biological Chemistry* 278, 27681-27687.

Brejc, K., van Dijk, W.J., Klaassen, R.V., Schuurmans, M., van der Oost, J., Smit, A.B., and Sixma, T.K. (2001). Crystal structure of an ACh-binding protein reveals the ligand-binding domain of nicotinic receptors. *Nature* 411, 269-276.

Bresink, I., Benke, T.A., Collett, V.J., Seal, A.J., Parsons, C.G., Henley, J.M., and Collingridge, G.L. (1996). Effects of memantine on recombinant rat NMDA receptors expressed in HEK 293 cells. *British Journal of Pharmacology* 119, 195-204.

Brisson, A., and Unwin, P.N.T. (1985). Quaternary structure of the acetylcholine receptor. *Nature* 315, 474-477.

Britto, L.R., Hamassaki-Britto, D.E., Ferro, E.S., Keyser, K.T., Karten, H.J., and Lindstrom, J.M. (1992). Neurons of the chick brain and retina expressing both α-bungarotoxin-sensitive and α-bungarotoxin-insensitive nicotinic acetylcholine receptors: an immunohistochemical analysis. *Brain Research* 590, 193-200.

Brizzard, B.L., Chubet, R.G., and Vizard, D.L. (1994). Immunoaffinity purification of FLAG epitope-tagged bacterial alkaline phosphatase using a novel monoclonal antibody and peptide elution. *Biotechniques* 16, 730-735.

Bruses, J.L., Chauvet, N., and Rutishauser, U. (2001). Membrane lipid rafts are necessary for the maintenance of the (alpha)7 nicotinic acetylcholine receptor in somatic spines of ciliary neurons. *Journal of Neuroscience* 21, 504-512.

Buisson, B., and Bertrand, D. (1998). Open-channel blockers at the human alpha4beta2 neuronal nicotinic acetylcholine receptor. *Molecular Pharmacology* 53, 555-563.

Buisson, B., Gopalakrishnan, M., Arneric, S.P., Sullivan, J.P., and Bertrand, D. (1996). Human α4β2 neuronal nicotinic acetylcholine receptor in HEK 293 cells: a patch-clamp study. *Journal of Neuroscience* 16, 7880-7891.

Carbonetto, S.T., Fambrough, D.M., and Muller, K.J. (1978). Nonequivalence of α-bungarotoxin receptors and acetylcholine receptors in chick sympathetic neurons. *Proceedings of the National Academy of Sciences USA* 75, 1016-1020.

Castelan, F., Mulet, J., Aldea, M., Sala, S., Sala, F., and Criado, M. (2007). Cytoplasmic regions adjacent to the M3 and M4 transmembrane segments influence expression and function of alpha7 nicotinic acetylcholine receptors. A study with single amino acid mutants. *Journal of Neurochemistry* 100, 406-415.

Celie, P.H., Kasheverov, I.E., Mordvintsev, D.Y., Hogg, R.C., van Nierop, P., van Elk, R., van Rossum-Fikkert, S.E., Zhmak, M.N., Bertrand, D., Tsetlin, V., *et al.* (2005). Crystal structure of nicotinic acetylcholine receptor homolog AChBP in complex with an α-conotoxin PnIA variant. *Nature Structural and Molecular Biology* 12, 582-588.

Celie, P.H.N., van Rossum-Fikkert, S.E., van Dijk, W.J., Brejc, K., Smit, A.B., and Sixma, T.K. (2004). Nicotine and carbamylcholine binding to nicotinic acetylcholine receptors as studied in AChBP crystal structures. *Neuron* 41, 907-914.

Champtiaux, N., Gotti, C., Cordero-Erausquin, M., David, D.J., Przybylski, C., Lena, C., Clementi, F., Moretti, M., Rossi, F.M., Le Novere, N., *et al.* (2003). Subunit composition of functional nicotinic receptors in dopaminergic neurons investigated with knock-out mice. *Journal of Neuroscience* 23, 7820-7829.

Chang, C.C., and Lee, C.Y. (1963). Isolation of Neurotoxins from the Venom of Bungarus Multicinctus and Their Modes of Neuromuscular Blocking Action. *Archives Internationales de Pharmacodynamie et de Therapie* 144, 241-257.

Changeux, J.P., Kasai, M., and Lee, C.Y. (1970). Use of a snake venom toxin to characterize the cholinergic receptor protein. *Proceedings of the National Academy of Sciences USA* 67, 1241-1247.

Chen, H.S., Pellegrini, J.W., Aggarwal, S.K., Lei, S.Z., Warach, S., Jensen, F.E., and Lipton, S.A. (1992). Open-channel block of N-methyl-D-aspartate (NMDA) responses by memantine: therapeutic advantage against NMDA receptor-mediated neurotoxicity. *Journal of Neuroscience* 12, 4427-4436.

Cheng, A., Bollan, K.A., Greenwood, S.M., Irving, A.J., and Connolly, C.N. (2007). Differential subcellular localization of RIC-3 isoforms and their role in determining 5-HT3 receptor composition. *Journal of Biological Chemistry* 282, 26158-26166.

Cheng, A., McDonald, N.A., and Connolly, C.N. (2005). Cell surface expression of 5-hydroxytryptamine type 3 receptors is promoted by RIC-3. *Journal of Biological Chemistry* 280, 22502-22507.

Clarke, P.B.S., Schwartz, R.D., Paul, S.M., Pert, C.B., and Pert, A. (1985). Nicotinic binding in rat brain: autoradiographic comparison of [^{3}H]acetylcholine, [^{3}H]nicotine, and [^{125}I]-α-bungarotoxin. *Journal of Neuroscience* 5, 1307-1315.

Colquhoun, D., and Ogden, D.C. (1988). Activation of ion channels in the frog end-plate by high concentrations of acetylcholine. *Journal of Physiology* 395, 131-159.

Connolly, C.N., and Wafford, K.A. (2004). The Cys-loop superfamily of ligand-gated ion channels: the impact of receptor structure on function. *Biochemical Society Transactions* 32, 529-534.

Connolly, C.N., Wooltorton, J.R.A., Smart, T.G., and Moss, S.J. (1996). Subcellular localization of g-aminobutyric acid type A receptors is determined by receptor b subunits. *Proceedings of the National Academy of Sciences USA* 93, 9899-9904.

Connolly, J., Boulter, J., and Heinemann, S.F. (1992). α4-2 β2 and other nicotinic acetylcholine receptor subtypes as targets of psychoactive and addictive drugs. *British Journal of Pharmacology* 105, 657-666.

Conroy, W.G., and Berg, D.K. (1995). Neurons can maintain multiple classes of nicotinic acetylcholine receptors distinguished by different subunit compositions. *J Biol Chem* 270, 4424-4431.

Conroy, W.G., and Berg, D.K. (1998). Nicotinic receptor subtypes in the developing chick brain: appearance of a species containing the α4, β2 and α5 gene products. *Molecular Pharmacology* 53, 392-401.

Conroy, W.G., Vernallis, A.B., and Berg, D.K. (1992). The α5 gene product assembles with multiple acetylcholine receptor subunits to form distinctive receptor subtypes in brain. *Neuron* 9, 679-691.

Cooper, S.T., and Millar, N.S. (1997). Host cell-specific folding and assembly of the neuronal nicotinic acetylcholine receptor α7 subunit. *Journal of Neurochemistry* 68, 2140-2151.

Cooper, S.T., and Millar, N.S. (1998). Host cell-specific folding of the neuronal nicotinic receptor α8 subunit. *Journal of Neurochemistry* 70, 2585-2593.

Corringer, P.-J., Galzi, J.-L., Eliselé, J.-L., Bertrand, S., Changeux, J.-P., and Bertrand, D. (1995). Identification of a new component of the agonist binding site of the nicotinic α7 homooligomeric receptor. *Journal of Biological Chemistry* 270, 11749-11752.

Corringer, P.-J., Le Novère, N., and Changeux, J.-P. (2000). Nicotinic receptors at the amino acid level. *Annual Review of Pharmacology and Toxicology* 40, 431-458.

Corriveau, R.A., and Berg, D.K. (1993). Coexpression of multiple acetylcholine receptor genes in neurons: quantification of transcripts during development. *Journal of Neuroscience* 13, 2662-2671.

Couturier, S., Bertrand, D., Matter, J.M., Hernandez, M.C., Bertrand, S., Millar, N., Valera, S., Barkas, T., and Ballivet, M. (1990). A neuronal nicotinic acetylcholine receptor subunit (α7) is developmentally regulated and forms a homo-oligomeric channel blocked by α-BTX. *Neuron* 5, 847-856.

Cuevas, J., Roth, A.L., and Berg, D.K. (2000). Two distinct classes of functional α7-containing nicotinic receptor on rat superior cervical ganglion neurons. *Journal of Physiology* 525 Pt 3, 735-746.

Dale, H.H. (1914). The action of certain esters and ethers of choline, and their relation to muscarine. *Journal of Pharmacology and Experimental Therapeutics*, 147-190.

Dale, H.H., and Feldberg, W. (1934). The chemical transmitter of vagus effects to the stomach. *Journal of Physiology* 81, 320-334.

Dale, H.H., Feldberg, W., and Vogt, M. (1936). Release of acetylcholine at voluntary motor nerve endings. *Journal of Physiology* 86, 353-380.

Danysz, W., Parsons, C.G., Jirgensons, A., Kauss, V., and Tillner, J. (2002). Amino-alkyl-cyclohexanes as a novel class of uncompetitive NMDA receptor antagonists. *Current Pharmaceutical Design* 8, 835-843.

de Hoop, M.J., and Dotti, C.G. (1993). Membrane traffic in polarized neurons in culture. *Journal of Cell Science* Supplement 17, 85-92.

Dellisanti, C.D., Yao, Y., Stroud, J.C., Wang, Z.Z., and Chen, L. (2007). Crystal structure of the extracellular domain of nAChR α1 bound to α-bungarotoxin at 1.94 Å resolution. *Nature Neuroscience* 10, 953-962.

Dempster, J. (2001). The laboratory computer: a practical guide for physiologists and neuroscientists., 2nd Edition edn (London, Academic Press).

Deneris, E.S., Connolly, J., Boulter, J., Wada, E., Wada, K., Swanson, L.W., Patrick, J., and Heinemann, S. (1988). Primary structure and expression of β2: a novel subunit of neuronal nicotinic acetylcholine receptors. *Neuron* 1, 45-54.

DiPaola, M., Czajkowski, C., and Karlin, A. (1989). The sidedness of the COOH terminus of the acetylcholine receptor delta subunit. *Journal of Biological Chemistry* 264, 15457-15463.

Drisdel, R.C., Manzana, E., and Green, W.N. (2004). The role of palmitoylation in functional expression of nicotinic α7 receptors. *Journal of Neuroscience* 24, 10502-10510.

du Bois-Reymond, E. (1877). Gesammelte Abhandlung zur Allgemeinen Muskel- und Nervenphysiol. *Leipzig: Veit* II.

Duvoisin, R.M., Deneris, E.S., Patrick, J., and Heinemann, S. (1989). The functional diversity of the neuronal nicotinic acetylcholine receptors is increased by a novel subunit: β4. *Neuron* 3, 487-496.

Eiselé, J.-L., Bertrand, S., Galzi, J.-L., Devillers-Thiéry, A., Changeux, J.-P., and Bertrand, D. (1993). Chimaeric nicotinic-serotonergic receptor combines distinct ligand binding and channel specificities. *Nature* 366, 479-483.

Elgoyhen, A.B., Johnson, D.S., Boulter, J., Vetter, D.E., and Heinemann, S. (1994). α9: an acetylcholine receptor with novel pharmacological properties expressed in rat cochlear hair cells. *Cell* 18, 705-715.

Elgoyhen, A.B., Vetter, D.E., Katz, E., Rothlin, C.V., Heineman, S.F., and Boulter, J. (2001). α10: a determinant of nicotinic cholinergic receptor function in mammalian vestibular and cochlear mechanosensory hair cells. *Proceedings of the National Academy of Sciences USA* 98, 3501-3506.

Eusebi, F., Grassi, F., Nervi, C., Caporale, C., Adamo, S., Zani, B.M., and Molinaro, M. (1987). Acetylcholine may regulate its own nicotinic receptor-channel through the C-kinase system. *Proceedings of the Royal Society of London, Series B* 230, 355-365.

Feldberg, W., Fessard, A., and Nachmansohn, D. (1939). The cholinergic nature of the nerves to the electric organ of the Torpedo (Torpedo marmorata). *Journal of Physiology* 3P-4P.

Flores, C.M., DeCamp, R.M., Kilo, S., Rogers, S.W., and Hargreaves, K.M. (1996). Neuronal nicotinic receptor expression in sensory neurons of the rat trigeminal ganglion: demonstration of α3β4, a novel subtype in the mammalian nervous system. *Journal of Neuroscience* 16, 7892-7901.

Forsayeth, J.R., and Kobrin, E. (1997). Formation of oligomers containing the β3 and β4 subunits of the rat nicotinic receptor. *Journal of Neuroscience* 17, 1531-1538.

Froehner, S.C., Reiness, C.G., and Hall, Z.W. (1977). Subunit structure of the acetylcholine receptor from denervated rat skeletal muscle. *Journal of Biological Chemistry* 252, 8589-8596.

Fucile, S., Barabino, B., Palma, E., Grassi, F., Limatola, C., Mileo, A.M., Alemà, S., Ballivet, M., and Eusebi, F. (1997). α5 subunit forms functional α3β4α5 nAChRs in transfected human cells. *Neuroreport* 8, 2433-2436.

Gahring, L.C., and Rogers, S.W. (2005). Neuronal nicotinic acetylcholine receptor expression and function on nonneuronal cells. *AAPS Journal* 7, E885-894.

Gaimarri, A., Moretti, M., Riganti, L., Zanardi, A., Clementi, F., and Gotti, C. (2007). Regulation of neuronal nicotinic receptor traffic and expression. *Brain Research Reviews* 55, 134-143.

García-Guzmán, M., Sala, F., Sala, S., Campos-Caro, A., and Criado, M. (1994). Role of two acetylcholine receptor subunit domains in homomer formation and intersubunit recognition, as revealed by α3 and α7 subunit chimeras. *Biochemistry* 33, 15198-15203.

Gautam, M., Noakes, P.G., Mudd, J., Nichol, M., Chu, G.C., Sanes, J.R., and Merlie, J.P. (1995). Failure of postsynaptic specialization to develop at neuromuscular junctions of rapsyn-deficient mice. *Nature* 377, 232-236.

Gee, V.J., Kracun, S., Cooper, S.T., Gibb, A.J., and Millar, N.S. (2007). Identification of domains influencing assembly and ion channel properties in α7 nicotinic receptor and 5-HT(3) receptor subunit chimaeras. *British Journal of Pharmacology*.

Gerzanich, V., Anand, R., and Lindstrom, J. (1994). Homomers of α8 and α7 subunits of nicotinic receptors exhibit similar channels but contrasting binding site properties. *Molecular Pharmacology* 45, 212-220.

Gibson, R.E., O'Brien, R.D., Edelstein, S.J., and Thompson, W.R. (1976). Acetylcholine receptor oligomers from electroplax of Torpedo species. *Biochemistry* 15, 2377-2383.

Glushakov, A.V., Voytenko, L.P., Skok, M.V., and Skok, V. (2004). Distribution of neuronal nicotinic acetylcholine receptors containing different alpha-subunits in the submucosal plexus of the guinea-pig. *Autonomic Neuroscience* 110, 19-26.

Goldman, D., Deneris, E., Luyten, W., Kochhar, A., Patrick, J., and Heinemann, S. (1987). Members of a nicotinic acetylcholine receptor gene family are expressed in different regions of the mammalian central nervous system. *Cell* 48, 965-973.

Gomez-Casati, M.E., Fuchs, P.A., Elgoyhen, A.B., and Katz, E. (2005). Biophysical and pharmacological characterization of nicotinic cholinergic receptors in rat cochlear inner hair cells. *Journal of Physiology* 566, 103-118.

Gotti, C., Hanke, W., Maury, K., Moretti, M., Ballivet, M., Clementi, F., and Bertrand, D. (1994). Pharmacology and biophysical properties of α7 and α7-α8 α-bungarotoxin receptor subtypes immunopurified from the chick optic lobe. *European Journal of Neuroscience* 6, 1281-1291.

Gotti, C., Moretti, M., Gaimarri, A., Zanardi, A., Clementi, F., and Zoli, M. (2007). Heterogeneity and complexity of native brain nicotinic receptors. *Biochemical Pharmacology* 74, 1102-1111.

Green, W.N., and Claudio, T. (1993). Acetylcholine receptor assembly: subunit folding and oligomerization occur sequentially. *Cell* 74, 57-69.

Green, W.N., and Millar, N.S. (1995). Ion-channel assembly. *Trends in Neurosciences* 18, 280-287.

Green, W.N., and Wanamaker, C.P. (1997). The role of the cystine loop in acetylcholine receptor assembly. *Journal of Biological Chemistry* 272, 20945-20953.

Green, W.N., and Wanamaker, C.P. (1998). Formation of the nicotinic acetylcholine receptor binding sites. *Journal of Neuroscience* 18, 5555-5564.

Greene, L.A., Sytkowski, A.J., Vogel, Z., and Nirenberg, M.W. (1973). α-Bungarotoxin used as a probe for acetylcholine receptors of cultured neurones. *Nature* 243, 163-166.

Gu, Y., Forsayeth, J.R., Verrall, S., Yu, X.M., and Hall, Z.W. (1991). Assembly of the mammalian muscle acetylcholine receptor in transfected COS cells. *Journal of Cell Biology* 114, 799-807.

Hales, T.G., Dunlop, J.I., Deeb, T.Z., Carland, J.E., Kelley, S.P., Lambert, J.J., and Peters, J.A. (2006). Common determinants of single channel conductance within the large cytoplasmic loop of 5-hydroxytryptamine type 3 and alpha4beta2 nicotinic acetylcholine receptors. *Journal of Biological Chemistry* 281, 8062-8071.

Halevi, S., McKay, J., Palfreyman, M., Yassin, L., Eshel, M., Jorgensen, E.M., and Treinin, M. (2002). The *C.elegans ric-3* gene is required for maturation of nicotinic acetylcholine receptors. *EMBO Journal* 21, 1012-1020.

Halevi, S., Yassin, L., Eshel, M., Sala, F., Sala, S., Criado, M., and Treinin, M. (2003). Conservation within the RIC-3 gene family: effectors of mammalian nicotinic acetylcholine receptor expression. *Journal of Biological Chemistry* 278, 34411-34417.

Helenius, A., and Aebi, M. (2004). Roles of N-linked glycans in the endoplasmic reticulum. *Annual Review of Biochemistry* 73, 1019-1049.

Hiel, H., Elgoyhen, A.B., Drescher, D.G., and Morley, B.J. (1996). Expression of nicotinic acetylcholine receptor mRNA in the adult rat peripheral vestibular system. *Brain Research* 738, 347-352.

Hucho, F., Layer, P., Kiefer, H.R., and Bandini, G. (1976). Photoaffinity labeling and quaternary structure of the acetylcholine receptor from Torpedo californica. *Proceedings of the National Academy of Sciences USA* 73, 2624-2628.

Huebsch, K.A., and Maimone, M.M. (2003). Rapsyn-mediated clustering of acetylcholine receptor subunits requires the major cytoplasmic loop of the receptor subunits. *Journal of Neurobiology* 54, 486-501.

Huganir, R.L., and Greengard, P. (1983). cAMP-dependent protein kinase phosphorylates the nicotinic acetylcholine receptor. *Proceedings of the National Academy of Sciences USA* 80, 1130-1134.

Huganir, R.L., and Greengard, P. (1990). Regulation of neurotransmitter receptor desensitization by protein phosphorylation. *Neuron* 5, 555-567.

Huganir, R.L., Miles, K., and Greengard, P. (1984). Phosphorylation of the nicotinic acetylcholine receptor by an endogenous tyrosine-specific kinase. *Proceedings of the National Academy of Sciences USA* 81, 6968-6972.

Hunt, S., and Schmidt, J. (1978). Some observations on the binding patterns of αbungarotoxin in the central nervous system of the rat. *Brain Research* 157, 213-232.

Imoto, K., Busch, C., Sakmann, B., Mishina, M., Konno, T., Nakai, J., Bujo, H., Mori, Y., Fukuda, K., and Numa, S. (1988). Rings of negatively charged amino acids determine the acetylcholine receptor channel conductance. *Nature* 335, 645-648.

Ishii, M., and Kurachi, Y. (2006). Muscarinic acetylcholine receptors. *Current Pharmaceutical Design* 12, 3573-3581.

Jeanclos, E.M., Lin, L., Treuil, M.W., Rao, J., DeCoster, M.A., and Anand, R. (2001). The chaperone protein 14-3-3η interacts with the nicotinic acetylcholine receptor α4 subunit. *Journal of Biological Chemistry* 276, 28281-28290.

Jiang, M., and Chen, G. (2006). High Ca2+-phosphate transfection efficiency in low-density neuronal cultures. *Nature Protocols* 1, 695-700.

Jones, A.K., Davis, P., Hodgkin, J., and Sattelle, D.B. (2007). The nicotinic acetylcholine receptor gene family of the nematode *Caenorhabditis elegans*: an update on nomenclature. *Invertebrate Neuroscience* 7, 129-131.

Jung, T.T., Rhee, C.K., Lee, C.S., Park, Y.S., and Choi, D.C. (1993). Ototoxicity of salicylate, nonsteroidal antiinflammatory drugs, and quinine. *Otolaryngologic Clinics of North America* 26, 791-810.

Karlin, A. (2002). Emerging structure of the nicotinic acetylcholine receptors. *Nature Reviews Neuroscience* 3, 102-114.

Kassner, P.D., and Berg, D.K. (1997). Differences in the fate of neuronal acetylcholine receptor protein expressed in neurons and stably transfected cells. *Journal of Neurobiology* 33, 968-982.

Katz, B., and Miledi, R. (1977). Transmitter leakage from motor nerve endings. *Proceedings of the Royal Society of London, Series B* 196, 59-72.

Katz, E., Elgoyhen, A.B., Gomez-Casati, M.E., Knipper, M., Vetter, D.E., Fuchs, P.A., and Glowatzki, E. (2004). Developmental regulation of nicotinic synapses on cochlear inner hair cells. *Journal of Neuroscience* 24, 7814-7820.

Kelley, S.P., Dunlop, J.I., Kirkness, E.F., Lambert, J.J., and Peters, J.A. (2003). A cytoplasmic region determines single-channel conductance in 5-HT_3 receptors. *Nature* 424, 321-324.

Keyser, K.T., Britto, L.R., Schoepfer, R., Whiting, P., Cooper, J., Conroy, W., Brozozowska-Prechtl, A., Karten, H.J., and Lindstrom, J. (1993). Three subtypes of α-bungarotoxin-sensitive nicotinic acetylcholine receptors are expressed in chick retina. *Journal of Neuroscience* 13, 442-454.

Kühne, W. (1863). Uber die peripherischen Endorgane der motorischen Nerven, Mit 5 Tafeln. *Leipzig, W Engelmann.*

Langley, J.N. (1905). On the reaction of cells and of nerve-endings to certain poisons, chiefly as regards the reaction of striated muscle to nicotine and to curari. *Journal of Physiology* 33, 374-413.

Langley, J.N. (1906). On nerve endings and on excitable substances in cells. *Proceedings of the Royal Society of London, Series B* 78, 170-194.

Lansdell, S.J., Gee, V.J., Harkness, P.C., Doward, A.I., Baker, E.R., Gibb, A.J., and Millar, N.S. (2005). RIC-3 enhances functional expression of multiple nicotinic acetylcholine receptor subtypes in mammalian cells. *Molecular Pharmacology* 65, 1431-1438.

Lansdell, S.J., Schmitt, B., Betz, H., Sattelle, D.B., and Millar, N.S. (1997). Temperature-sensitive expression of Drosophila neuronal nicotinic acetylcholine receptors. *Journal of Neurochemistry* 68, 1812-1819.

Le Novère, N., and Changeux, J.-P. (1995). Molecular evolution of the nicotinic acetylcholine receptor: an example of multigene family in excitable cells. *Molecular Evolution* 40, 155-172.

Le Novère, N., Corringer, P.-J., and Changeux, J.-P. (2002). The diversity of subunit composition in nAChRs: evolutionary origins, physiologic and pharmacologic consequences. *Journal of Neurobiology* 53, 447-456.

Lee, C.Y., and Chang, C.C. (1966). Modes of actions of purified toxins from elapid venoms on neuromuscular transmission. *Memorias do Instituto Butantan* 33, 555-572.

Lester, H.A., Dibas, M.I., Dahan, D.S., Leite, J.F., and Dougherty, D.A. (2004). Cys-loop receptors: new twists and turns. *Trends in Neurosciences* 27, 329-336.

Lewis, T.M., Harkness, P.C., Sivilotti, L.G., Colquhoun, D., and Millar, N.S. (1997). The ion channel properties of a rat recombinant neuronal nicotinic receptor are dependent on the host cell type. *Journal of Physiology* 505, 299-306.

Linder, M.E., and Deschenes, R.J. (2007). Palmitoylation: policing protein stability and traffic. *Nature Reviews Molecular Cell Biology* 8, 74-84.

Lindstrom, J., Einarson, B., and Merlie, J. (1978). Immunization of rats with polypeptide chains from torpedo acetylcholine receptor causes an autoimmune response to receptors in rat muscle. *Proceedings of the National Academy of Sciences USA* 75, 769-773.

Lindstrom, J., Walter, B., and Einarson, B. (1979). Immunochemical similarities between subunits of acetylcholine receptors from Torpedo, Electrophorus, and mammalian muscle. *Biochemistry* 18, 4470-4480.

Lips, K.S., Pfeil, U., and Kummer, W. (2002). Coexpression of alpha9 and alpha10 nicotinic acetylcholine receptors in rat dorsal root ganglion neurons. *Neuroscience* 115, 1-5.

Loewi, O. (1921). Über humorale Übertragbarkeit der Herznervenwirkung. *Pflügers Archiv ges Physiol* 189, 239-242.

Love, R.A., and Stroud, R.M. (1986). The crystal structure of alpha-bungarotoxin at 2.5 A resolution: relation to solution structure and binding to acetylcholine receptor. *Protein Engineering* 1, 37-46.

Lukas, R.J., Changeux, J.-P., Le Novère, N., Albuquerque, E.X., Balfour, D.J.K., Berg, D.K., Bertrand, D., Chiappinelli, A.A., Clarke, P.B.S., Collins, A.C., *et al.* (1999). International union of pharmacology. XX. current status of the nomenclature for nicotinic acetylcholine receptors and their subunits. *Pharmacology Reviews* 51, 397-401.

Lustig, L.R., Peng, H., Hiel, H., Yamamoto, T., and Fuchs, P.A. (2001). Molecular cloning and mapping of the human nicotinic acetylcholine receptor a10 (CHRNA10). *Genomics* 73, 272-283.

Mandelzys, A., Pié, B., Deneris, E.S., and Cooper, E. (1994). The developmental increase in ACh current densities on rat sympathetic neurons correlates with changes in nicotinic ACh receptor a-subunit gene expression and occurs independent of innervation. *J Neurosci* 14, 2357-2364.

Margeta-Mitrovic, M., Jan, Y.N., and Jan, L.Y. (2000). A trafficking checkpoint controls GABA(B) receptor heterodimerization. *Neuron* 27, 97-106.

Marshall, L.M. (1981). Synaptic localization of alpha-bungarotoxin binding which blocks nicotinic transmission at frog sympathetic neurons. *Proceedings of the National Academy of Sciences USA* 78, 1948-1952.

Marubio, L.M., del Mar Arroyo-Jimenez, M., Cordero-Erausquin, M., Lena, C., Le Novere, N., de Kerchove d'Exaerde, A., Huchet, M., Damaj, M.I., and Changeux, J.P. (1999). Reduced antinociception in mice lacking neuronal nicotinic receptor subunits. *Nature* 398, 805-810.

Mays, R.W., Siemers, K.A., Fritz, B.A., Lowe, A.W., van Meer, G., and Nelson, W.J. (1995). Hierarchy of mechanisms involved in generating Na/K-ATPase polarity in MDCK epithelial cells. *Journal of Cell Biology* 130, 1105-1115.

McGehee, D.S., and Role, L.W. (1995). Physiological diversity of nicotinic acetylcholine receptors expressed by vertebrate neurons. *Annual Review of Physiology* 57, 521-546.

Mellman, I. (1995). Molecular sorting of membrane proteins in polarized and nonpolarized cells. *Cold Spring Harbor Symposium on Quantitaive Biology* 60, 745-752.

Merlie, J.P., and Lindstrom, J. (1983). Assembly in vivo of mouse muscle acetylcholine receptor: identification of an alpha subunit species that may be an assembly intermediate. *Cell* 34, 747-757.

Michelsen, K., Yuan, H., and Schwappach, B. (2005). Hide and run. Arginine-based endoplasmic-reticulum-sorting motifs in the assembly of heteromultimeric membrane proteins. *EMBO Reports* 6, 717-722.

Miledi, R., Molinoff, P., and Potter, L.T. (1971). Isolation of the cholinergic receptor protein of Torpedo electric tissue. *Nature* 229, 554-557.

Millar, N.S. (1999). Heterologous expression of mammalian and insect neuronal nicotinic acetylcholine receptors in cultured cell lines. *Biochemical Society Transactions* 27, 944-950.

Millar, N.S. (2003). Assembly and subunit diversity of nicotinic acetylcholine receptors. *Biochemical Society Transactions* 31, 869-874.

Millar, N.S. (2006). Ligand-gated ion channels. In Encyclopedia of Life Sciences (Chichester, John Wiley and Sons Ltd).

Millar, N.S. (2008). RIC-3: a nicotinic acetylcholine receptor chaperone. *British Journal of Pharmacology* In Press.

Millar, N.S., and Denholm, I. (2007). Nicotinic acetylcholine receptors: targets for commercially important insecticides. *Invertebrate Neuroscience* 7, 53-66.

Miller, K.G., Alfonso, A., Nguyen, M., Crowell, J.A., Johnson, C.D., and Rand, J.B. (1996). A genetic selection for Caenorhabditis elegans synaptic transmission mutants. *Proceedings of the National Academy of Sciences USA* 93, 12593-12598.

Mishina, M., Takai, T., Imoto, K., Noda, M., Takahashi, T., Numa, S., Methfessel, C., and Sakman, B. (1986). Molecular distinction between fetal and adult forms of muscle acetylcholine receptor. *Nature* 313, 364-369.

Miyazawa, A., Fujiyoshi, Y., and Unwin, N. (2003). Structure and gating mechanism of the acetylcholine receptor pore. *Nature* 423, 949-955.

Moroni, M., Zwart, R., Sher, E., Cassels, B.K., and Bermudez, I. (2006). α4β2 nicotinic receptors with high and low acetylcholine sensitivity: pharmacology, stoichiometry, and sensitivity to long-term exposure to nicotine. *Molecular Pharmacology* 70, 755-768.

Moss, S.J., and Henley, J.M. (2002). Receptor and Ion-Channel Trafficking: Cell Biology of Ligand-Gated and Voltage-Sensitive Ion Channels (Oxford Universiy Press).

Nasu-Nishimura, Y., Hurtado, D., Braud, S., Tang, T.T., Isaac, J.T., and Roche, K.W. (2006). Identification of an endoplasmic reticulum-retention motif in an intracellular loop of the kainate receptor subunit KA2. *Journal of Neuroscience* 26, 7014-7021.

Nelson, M.E., Kuryatov, A., Choi, C.H., Zhou, Y., and Lindstrom, J. (2003). Alternate stoichiometries of α4β2 nicotinic acetylcholine receptors. *Molecular Pharmacology* 63, 332-341.

Nelson, W.J., and Yeaman, C. (2001). Protein trafficking in the exocytic pathway of polarized epithelial cells. *Trends in Cell Biology* 11, 483-486.

Nguyen, M., Alfonso, A., Johnson, C.D., and Rand, J.B. (1995). Caenorhabditis elegans mutants resistant to inhibitors of acetylcholinesterase. *Genetics* 140, 527-535.

Noda, M., Takahashi, H., Tanabe, T., Toyosato, M., Furutani, Y., Hirose, T., Asai, M., Inayama, S., Miyata, T., and Numa, S. (1982). Primary structure of α-subunit precursor of Torpedo californica acetylcholine receptor deduced from cDNA sequence. *Nature* 299, 793-797.

Noda, M., Takahashi, H., Tanabe, T., Toyosato, M., Kikyotani, S., Furutani, Y., Hirose, T., Takashima, H., Inayama, S., Miyata, T., *et al.* (1983a). Structural homology of Torpedo californica acetylcholine receptor subunits. *Nature* 302, 528-532.

Noda, M., Takahashi, H., Tanabe, T., Toyosato, M., Kikyotani, S., Hirose, T., Asai, M., Takashima, H., Inayama, S., Miyata, T., *et al.* (1983b). Primary structures of β- and δ-subunit precursors of Torpedo californica acetylcholine receptor deduced from cDNA sequences. *Nature* 301, 251-255.

Oliver, D., Ludwig, J., Reisinger, E., Zoellner, W., Ruppersberg, J.P., and Fakler, B. (2001). Memantine inhibits efferent cholinergic transmission in the cochlea by blocking nicotinic acetylcholine receptors of outer hair cells. *Molecular Pharmacology* 60, 183-189.

Orr-Urtreger, A., Goldner, F.M., Saeki, M., Lorenzo, I., Goldberg, L., De Biasi, M., Dani, J.A., Patrick, J.W., and Beaudet, A.L. (1997). Mice deficient in the α7 neuronal nicotinic acetylcholine receptor lack α-bungarotoxin binding sites and hippocampal fast nicotinic currents. *Journal of Neuroscience* 17, 9165-9171.

Ortells, M.O., and Lunt, G.G. (1995). Evolutionary history of the ligand-gated ion-channel superfamily of receptors. *Trends in Neurosciences* 18, 121-127.

Palma, E., Bertrand, S., Binzoni, T., and Bertrand, D. (1996). Neuronal nicotinic α7 receptor expressed in *Xenopus* oocytes presents five putative binding sites for methyllycaconitine. *Journal of Physiology* 491, 151-161.

Palma, E., Maggi, L., Barabino, B., Eusebi, F., and Ballivet, M. (1999). Nicotinic acetylcholine receptors assembled from the α7 and β3 subunits. *Journal of Biological Chemistry* 274, 18335-18340.

Papke, R.L., Boulter, J., Patrick, J., and Heinemann, S. (1989). Single-channel currents of rat neuronal nicotinic acetylcholine receptors expressed in Xenopus oocytes. *Neuron* 3, 589-596.

Parsons, C.G., Danysz, W., Bartmann, A., Spielmanns, P., Frankiewicz, T., Hesselink, M., Eilbacher, B., and Quack, G. (1999a). Amino-alkyl-cyclohexanes are novel uncompetitive NMDA receptor antagonists with strong voltage-dependency and fast blocking kinetics: in vitro and in vivo characterization. *Neuropharmacology* 38, 85-108.

Parsons, C.G., Danysz, W., and Quack, G. (1998). Glutamate in CNS disorders as a target for drug development: an update. *Drug News and Perspectives* 11, 523-569.

Parsons, C.G., Danysz, W., and Quack, G. (1999b). Memantine is a clinically well tolerated N-methyl-D-aspartate (NMDA) receptor antagonist--a review of preclinical data. *Neuropharmacology* 38, 735-767.

Parsons, C.G., Gruner, R., Rozental, J., Millar, J., and Lodge, D. (1993). Patch clamp studies on the kinetics and selectivity of N-methyl-D-aspartate receptor antagonism by memantine (1-amino-3,5-dimethyladamantan). *Neuropharmacology* 32, 1337-1350.

Paterson, D., and Nordberg, A. (2000). Neuronal nicotinic receptors in the human brain. *Progress in Neurobiology* 61, 75-111.

Patrick, J., and Stallcup, B. (1977a). α-Bungarotoxin binding and cholinergic receptor function on a rat sympathetic nerve line. *Journal of Biological Chemistry* 252, 8629-8633.

Patrick, J., and Stallcup, W.B. (1977b). Immunological distinction between acetylcholine receptor and the alpha-bungarotoxin-binding component on sympathetic neurons. *Proceedings of the National Academy of Sciences USA* 74, 4689-4692.

Pedersen, S.E., and Cohen, J.B. (1990). d-Tubocurarine binding sites are located at α-γ and α-δ subunit interfaces of the nicotinic acetylcholine receptor. *Proceedings of the National Academy of Sciences USA* 87, 2785-2789.

Peng, H.B., and Froehner, S.C. (1985). Association of the postsynaptic 43K protein with newly formed acetylcholine receptor clusters in cultured muscle cells. *Journal of Cell Biology* 100, 1698-1705.

Peper, K., Bradley, R.J., and Dreyer, F. (1982). The acetylcholine receptor at the neuromuscular junction. *Physiological Reviews* 62, 1271-1340.

Peters, J.A., Hales, T.G., and Lambert, J.J. (2005). Molecular determinants of single-channel conductance and ion selectivity in the Cys-loop family: insights from the 5-HT3 receptor. *Trends in Pharmacological Sciences* 26, 587-594.

Picciotto, M.R., Zoli, M., Lena, C., Bessis, A., Lallemand, Y., Le Novere, N., Vincent, P., Pich, E.M., Brulet, P., and Changeux, J.P. (1995). Abnormal avoidance learning in mice lacking functional high-affinity nicotine receptor in the brain. *Nature* 374, 65-67.

Plazas, P.V., Katz, E., Gomez-Casati, M.E., Bouzat, C., and Elgoyhen, A.B. (2005). Stoichiometry of the α9α10 nicotinic cholinergic receptor. *Journal of Neuroscience* 25, 10905-10912.

Plazas, P.V., Savino, J., Kracun, S., Gomez-Casati, M.E., Katz, E., Parsons, C.G., Millar, N.S., and Elgoyhen, A.B. (2007). Inhibition of the alpha9alpha10 nicotinic cholinergic receptor by neramexane, an open channel blocker of N-methyl-d-aspartate receptors. *European Journal of Pharmacology.*

Quik, M., and Geertsen, S. (1988). Neuronal nicotinic α-bungarotoxin sites. *Canadian Journal of Physiology and Pharmacology* 66, 971-979.

Raftery, M.A., Hunkapiller, M.W., Strader, C.D., and Hood, L.E. (1980). Acetylcholine receptor: complex of homologous subunits. *Science* 208, 1454-1456.

Raleigh, W. (1596). The discovery of the large, rich and beautiful empire of Guiana.

Rammes, G., Rupprecht, R., Ferrari, U., Zieglgansberger, W., and Parsons, C.G. (2001). The N-methyl-D-aspartate receptor channel blockers memantine, MRZ 2/579 and other amino-alkyl-cyclohexanes antagonise 5-HT(3) receptor currents in cultured HEK-293 and N1E-115 cell systems in a non-competitive manner. *Neuroscience Letters* 306, 81-84.

Rangwala, F., Drisdel, R.C., Rakhilin, S., Ko, E., Atluri, P., Harkins, A.B., Fox, A.P., Salman, S.B., and Green, W.N. (1997). Neuronal α-bungarotoxin receptors differ structurally from other nicotinic acetylcholine receptors. *Journal of Neuroscience* 17, 8201-8212.

Resh, M.D. (2006). Palmitoylation of ligands, receptors, and intracellular signaling molecules. *Science Signal Transduction Knowledge Environment* 2006, re14.

Revah, F., Bertrand, D., Galzi, J.L., Devillers-Thiery, A., Mulle, C., Hussy, N., Bertrand, S., Ballivet, M., and Changeux, J.P. (1991). Mutations in the channel domain alter desensitization of a neuronal nicotinic receptor. *Nature* 353, 846-849.

Reynolds, J.A., and Karlin, A. (1978). Molecular weight in detergent solution of acetylcholine receptor from Torpedo californica. *Biochemistry* 17, 2035-2038.

Rothlin, C.V., Katz, E., Verbitsky, M., and Elgoyhen, A.B. (1999). The α9 nicotinic acetylcholine receptor shares pharmacological properties with type A γ-aminobutyric acid, glycine, and type 3 serotonin receptors. *Molecular Pharmacology* 55, 248-254.

Rust, G., Burgunder, J.M., Lauterburg, T.E., and Cachelin, A.B. (1994). Expression of neuronal nicotinic acetylcholine receptor subunit genes in the rat autonomic nervous system. *European Journal of Neuroscience* 6, 478-485.

Sakmann, B., and Neher, E. (1984). Patch clamp techniques for studying ionic channels in excitable membranes. *Annual Review of Physiology* 46, 455-472.

Salaün, C., Gould, G.W., and Chamberlain, L.H. (2005). The SNARE proteins SNAP-25 and SNAP-23 display different affinities for lipid rafts in PC12 cells. Regulation by distinct cysteine-rich domains. *Journal of Biological Chemistry* 280, 1236-1240.

Schoepfer, R., Conroy, W.G., Whiting, P., Gore, M., and Lindstrom, J. (1990). Brain α-bungarotoxin binding protein cDNAs and mAbs reveal subtypes of this branch of the ligand-gated ion channel gene superfamily. *Neuron* 5, 35-48.

Schuetze, S.M., and Role, L.W. (1987). Developmental regulation of nicotinic acetylcholine receptors. *Annual Review of Neuroscience* 10, 403-457.

Scott, D.B., Blanpied, T.A., Swanson, G.T., Zhang, C., and Ehlers, M.D. (2001). An NMDA receptor ER retention signal regulated by phosphorylation and alternative splicing. *Journal of Neuroscience* 21, 3063-3072.

Sealock, R. (1982). Visualization at the mouse neuromuscular junction of a submembrane structure in common with Torpedo postsynaptic membranes. *Journal of Neuroscience* 2, 918-923.

Séguéla, P., Wadiche, J., Dineley-Miller, K., Dani, J.A., and Patrick, J.W. (1993). Molecular cloning, functional properties, and distribution of rat brain α7: a nicotinic cation channel highly permeable to calcium. *Journal of Neuroscience* 13, 596-604.

Servent, D., Winckler-Dietrich, V., Hu, H.Y., Kessler, P., Drevet, P., Bertrand, D., and Menez, A. (1997). Only snake curaremimetic toxins with a fifth disulfide bond have high affinity for the neuronal alpha7 nicotinic receptor. *Journal of Biological Chemistry* 272, 24279-24286.

Severance, E.G., Zhang, H., Cruz, Y., Pakhlevaniants, S., Hadley, S.H., Amin, J., Wecker, L., Reed, C., and Cuevas, J. (2004). The α7 nicotinic acetylcholine receptor subunit exists in two isoforms that contribute to functional ligand-gated ion channels. *Molecular Pharmacology* 66, 420-429.

Sine, S.M. (2002). The nicotinic receptor ligand binding domain. *Journal of Neurobiology* 53, 431-446.

Sine, S.M., and Engel, A.G. (2006). Recent advances in Cys-loop receptor structure and function. *Nature* 440, 448-455.

Sine, S.M., Ohno, K., Bouzat, C., Auerbach, A., Milone, M., Pruitt, J.N., and Engel, A.G. (1995). Mutation of the acetylcholine receptor α subunit causes a slow-channel myasthenic syndrome by enhancing agonist binding affinity. *Neuron* 15, 229-239.

Standley, S., Roche, K.W., McCallum, J., Sans, N., and Wenthold, R.J. (2000). PDZ domain suppression of an ER retention signal in NMDA receptr NR1 splice variants. *Neuron* 28, 887-889.

Swanson, L.W., Simmons, D.M., Whiting, P.J., and Lindstrom, J. (1987). Immunohistochemical localization of neuronal nicotinic receptors in the rodent central nervous system. *Journal of Neuroscience* 7, 3334-3342.

Swope, S.L., Moss, S.J., Raymond, L.A., and Huganir, R.L. (1999). Regulation of ligand-gated ion channels by protein phosphorylation. *Advances in Second Messenger and Phosphoprotein Research* 33, 49-78.

Takai, T., Noda, M., Mishina, M., Shimizu, S., Furutani, Y., Kayano, T., Ikeda, T., Kubo, T., Takahashi, H., Takahashi, T., *et al.* (1985). Cloning, sequencing and expression of cDNA for a novel subunit of acetylcholine receptor from calf muscle. *Nature* 315, 761-764.

Toyoshima, C., and Unwin, N. (1988). Ion channel of acetylcholine receptor reconstructed from images of postsynaptic membranes. *Nature* 336, 247-250.

Traynelis, S.F., and Jaramillo, F. (1998). Getting the most out of noise in the central nervous system. *Trends in Neurosceinces* 21, 137-145.

Ulens, C., Hogg, R.C., Celie, P.H., Bertrand, D., Tsetlin, V., Smit, A.B., and Sixma, T.K. (2006). Structural determinants of selective a-conotoxin binding to a nicotinic acetylcholine receptor homolog AChBP. *Proceedings of the National Academy of Sciences USA* 103, 3615-3620.

Unwin, N. (1993). Nicotinic acetylcholine receptor at 9 Å resolution. *Journal of Molecular Biology* 229, 1101-1124.

Unwin, N. (2005). Refined structure of the nicotinic acetylcholine receptor at 4Å resolution. *Journal of Molecular Biology* 346, 967-989.

Vailati, S., Moretti, M., Balestra, B., McIntosh, M., Clementi, F., and Gotti, C. (2000). β3 subunit is present in different nicotinic receptor subtypes in chick retina. *European Journal of Pharmacology* 393, 23-30.

Valor, L.M., Mulet, J., Sala, F., Ballesta, J.J., and Criado, M. (2002). Role of the large cytoplasmic loop of the α7 neuronal nicotinic acetylcholine receptor subunit in the receptor expression and function. *Biochemistry* 41, 7931-7938.

van Beest, M., Robben, J.H., Savelkoul, P.J., Hendriks, G., Devonald, M.A., Konings, I.B., Lagendijk, A.K., Karet, F., and Deen, P.M. (2006). Polarisation, key to good localisation. *Biochimica et Biophysica Acta* 1758, 1126-1133.

Verbitsky, M., Rothlin, C.V., Katz, E., and Elgoyhen, A.B. (2000). Mixed nicotinic-muscarinic properties of the α9 nicotinic cholinergic receptor. *Neuropharmacology* 39, 2515-2524.

Vernallis, A.B., Conroy, W.G., and Berg, D.K. (1993). Neurons assemble acetylcholine receptors with as many as three kinds of subunits while maintaining subunit segregation among receptor subtypes. *Neuron* 10, 451-464.

Vetter, D.E., Liberman, M.C., Mann, J., Barhanin, J., Boulter, J., Brown, M.C., Saffiote-Kolman, J., Heinemann, S.F., and Elgoyhen, A.B. (1999). Role of alpha9 nicotinic ACh receptor subunits in the development and function of cochlear efferent innervation. *Neuron* 23, 93-103.

Vincler, M., Wittenauer, S., Parker, R., Ellison, M., Olivera, B.M., and McIntosh, J.M. (2006). Molecular mechanism for analgesia involving specific antagonism of alpha9alpha10 nicotinic acetylcholine receptors. *Proceedings of the National Academy of Sciences USA* 103, 17880-17884.

von Humboldt, A. (1808). Observations on the Electric Eel of the New World. *Beobacht Zool vergleich Anat* 2, 49-123.

von Humboldt, A., and Bonpland, A. (1807). Voyage aux régions equinoxiales du Nouveau-Continent. *Relation historique du voyage* 2.

Vulpian, E.F. (1866). Lecons sur la Physiologie Generale et Comparee du Systeme Nerveux. *Bailliere, Paris.*

Wada, K., Ballivet, M., Boulter, J., Connolly, J., Wada, E., Deneris, E.S., Swanson, L.W., Heinemann, S., and Patrick, J. (1988). Functional expression of a new pharmacological subtype of brain nicotinic acetylcholine receptor. *Science* 240, 330-334.

Wanamaker, C.P., Christianson, J.C., and Green, W.N. (2003). Regulation of nicotinic acetylcholine receptor assembly. *Annals of the New York Academy of Sciences* 998, 66-80.

Wanamaker, C.P., and Green, W.N. (2005). N-linked glycosylation is required for nicotinic receptor assembly but not for subunit associations with calnexin. *Journal of Biological Chemistry* 280, 33800-33810.

Wang, H., Yu, M., Ochani, M., Amella, C.A., Tanovic, M., Susarla, S., Li, J.H., Wang, H., Yang, H., Ulloa, L., *et al.* (2003). Nicotinic acetylcholine receptor α7 subunit is an essential regulator of inflammation. *Nature* 421, 384-388.

Waterton, C. (1879). Wanderings in South America. *London: Macmillan Co.*

Wiesner, A., and Fuhrer, C. (2006). Regulation of nicotinic acetylcholine receptors by tyrosine kinases in the peripheral and central nervous system: same players, different roles. *Cellular and Molecular Life Sciences* 63, 2818-2828.

Williams, B.M., Temburni, M.K., Levey, M.S., Bertrand, S., Bertrand, D., and Jacob, M.H. (1998). The long internal loop of the α3 subunit targets nAChRs to subdomains within individual synapses on neurones *in vivo*. *Nature Neuroscience* 1, 557-562.

Williams, M.E., Burton, B., Urrutia, A., Shcherbatko, A., Chavez-Noriega, L.E., Cohen, C.J., and Aiyar, J. (2005). Ric-3 promotes functional expression of the nicotinic acetylcholine receptor a7 subunit in mammalian cells. *Journal of Biological Chemistry* 280, 1257-1263.

Witzemann, V. (2006). Development of the neuromuscular junction. *Cell and Tissue Research* 326, 263-271.

Xu, J., Zhu, Y., and Heinemann, S.F. (2006). Identification of sequence motifs that target neuronal nicotinic receptors to dendrites and axons. *Journal of Neuroscience* 26, 9780-9793.

Yu, C.R., and Role, L.W. (1998). Functional contribution of the α7 subunit to multiple subtypes of nicotinic receptors in embryonic chick sympathetic neurones. *Journal of Physiology* 509 (Pt 3), 651-665.

Zerangue, N., Schwappach, B., Jan, Y.N., and Jan, L.Y. (1999). A new ER trafficking signal regulates the subunit stoichiometry of plasma membrane K_{ATP} channels. *Neuron* 22, 537-548.

Zoli, M., Lena, C., Picciotto, M.R., and Changeux, J.P. (1998). Identification of four classes of brain nicotinic receptors using β2 mutant mice. *Journal of Neuroscience* 18, 4461-4472.

Zoli, M., Moretti, M., Zanardi, A., McIntosh, J.M., Clementi, F., and Gotti, C. (2002). Identification of the nicotinic receptor subtypes expressed on dopaminergic terminals in the rat striatum. *Journal of Neuroscience* 22, 8785-8789.

Zwart, R., and Vijverberg, H.P.M. (1998). Four pharmacologically distinct subtypes of α4β2 nicotinic acetylcholine receptor expressed in Xenopus laevis oocytes. *Molecular Pharmacology* 54, 1124-1131.